Structural and Biophysical Characterisation of the small GTPase Rab6a and its Effectors BicaudalD2, $p150_{glued}$ and PIST

Dissertation

zur Erlangung des akademischen Grades
eines Doktor der Naturwissenschaften
der Fakultät für Chemie der Universität Dortmund

angefertigt am Max-Planck-Institut für molekulare Physiologie
Dortmund

vorgelegt von
Dipl. Biotechnologe Tim Bergbrede
Porta Westfalica

November 2006

Die vorliegende Arbeit wurde in der Zeit von Mai 2003 bis November 2006 am Max-Planck-Institut für molekulare Physiologie in Dortmund unter der Anleitung von Prof. Dr. Roger S. Goody und Dr. Kirill Alexandrov durchgeführt

1. Gutachter : Prof. Dr. R.S. Goody
2. Gutachter : Prof. Dr. R. Winter

1 INTRODUCTION

1.1 Small G-proteins

The basic processes of life, such as gene expression, structural reorganisation or transport depend upon complex interactions of multiple factors and therefore require tight temporal and spatial control. The living cell constitutes a complex environment in which these processes occur, in particular with the increased complexity of evolutionary advanced biological systems. Small guanyl-nucleotide binding proteins (small G-proteins) of the Ras-superfamily are central regulators of diverse cellular processes. Today more than 170 members of this family of GTP-hydrolases have been identified and subclassified into the Ras, Rho, Rab, Arf and G_{α} families [(1)] (Fig.1). The superfamily derives its name from Ras (rat sarcoma) proteins that were first identified as oncogens in their mutationally activated forms *H-Ras*, *K-Ras* and *N-Ras* [(2)]. Different members of the Ras-superfamily have been found to regulate such widespread functions as intracellular signalling (Ras [(3)]), cell stress responses (Rho [(4)]), cytoskeletal remodelling (Arf [(5)]), ion channel gating (G_{α} [(6)]), nuclear transport (Ran [(7)]) and vesicle transport (Rab [(8)]). Despite their different functions small G-proteins share common features such as a low molecular weight of 20 to 40 kDa, sequence conservation of 30-50% as well as post-translational modification throughout the superfamily. The defining structural element of all Ras-related proteins is the structurally and functionally conserved catalytic G-domain that binds and hydrolyses guanine triphosphate (GTP) to diphosphate (GDP) [(9)]. The alteration between GTP- and GDP-bound conformations define the active and inactive state of the protein respectively. Upon binding of GTP two otherwise unstructured regions of the G-domain, called switch I and switch II, become structurally ordered to form a platform to bind down-stream effectors [(10,11)]. After GTP hydrolysis the reversion of this conformational change dissolves the effector binding interface, however the diphosphate product remains tightly bound to the G-domain. As small G-proteins show only poor intrinsic GTPase activity (t½ ≈ 0.5-5h [(**12**)]), the change from the active to the inactive state is assisted by regulatory proteins of two different categories. Guanine nucleotide exchange factors (GEFs) facilitate the release of GDP from the protein, and subsequent binding of GTP. GTPase activating protein domains (GAPs) promote GTPase deactivation by accelerating the low intrinsic GTPase activity.

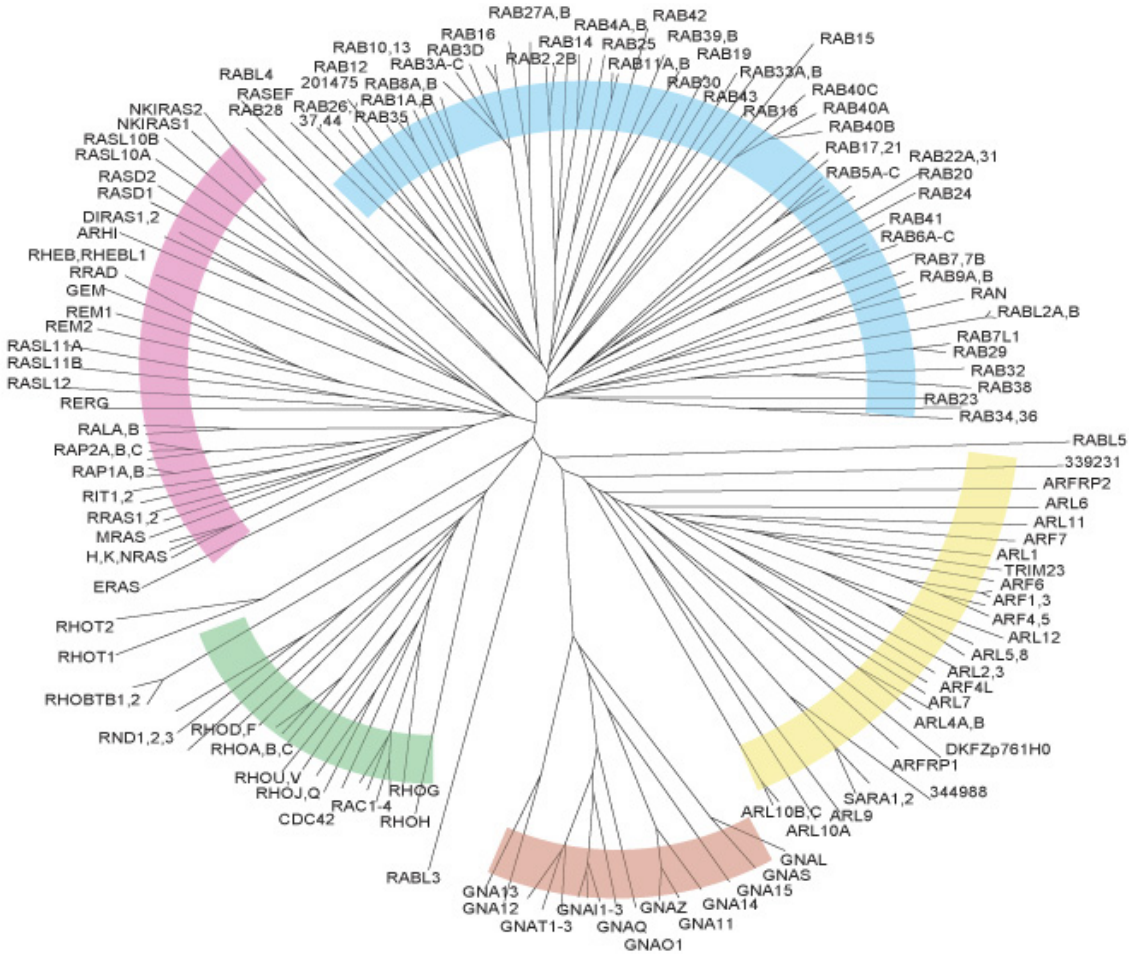

Fig.1 Unrooted phylogenetic dendrogram of the human family of small Ras-like GTPases from [1]. Branch lengths are directly proportional to the number of differences between sequences compared. Analysis based on the program *ClustalW*.

1.2 Rab proteins

Biosynthesis as well as catabolic breakdown of organic compounds occurs in a series of enzymatic reactions. To adapt to the sequential processing steps, eukaryotic cells have developed a network of membrane bordered compartments with a high degree of specialization. Transfer between the differentiated compartments as well as exo- and endocytosis require tightly regulated mechanisms of membrane transport. Spatial specificity of these transport processes relies on the interactions of RabGTPases and their specific effectors, whereas temporal specificity is mediated by nucleotide-state dependent conformational changes.

In 1980 Novick and co-workers first described mutations in the gene *Sec4* that led to blocked vesicle secretion in temperature-sensitive strains of the yeast *Saccharomyces cerevisiae*[13]. Mutational analysis showed that the corresponding gene product is a Ras-like small GTPase and suggested a cyclical mechanism for the regulation of vesicle trafficking in yeast [14]. Subsequently, another yeast gene *Ypt1p* was identified as a small GTPase essential for vesicle trafficking between the endoplasmatic reticulum (ER) and post-Golgi cisternae [15,16]. In higher eukaryotes small GTPases homologous to *Sec4* and *Ytp1p* were first isolated from rat brain, coining the name of the family (*Ras-like protein from rat brain*) [17]. Today, more than 60 members of this largest subfamily of Ras related small GTPases have been identified in humans. They share 54-71% sequence identity to their eleven homologs in yeast, which are still called Ypt/Sec proteins [1,8].

Rab proteins share a high degree of conservation throughout evolution; however, their number has increased from the lower eukaryotes (e.g. yeast) to more complex organisms such as plants and vertebrates. For many subfamilies of the Rab GTPases a gene duplication seems to have occurred quite recently in evolution. The resulting isoforms share 75-95% sequence homology and sometimes overlap in their function [18]. While some Rab proteins have been found to act in specialized processes in differentiated tissues, others are expressed ubiquitously. Rab proteins localise to distinct compartments and act in specific transport steps (Fig.2).

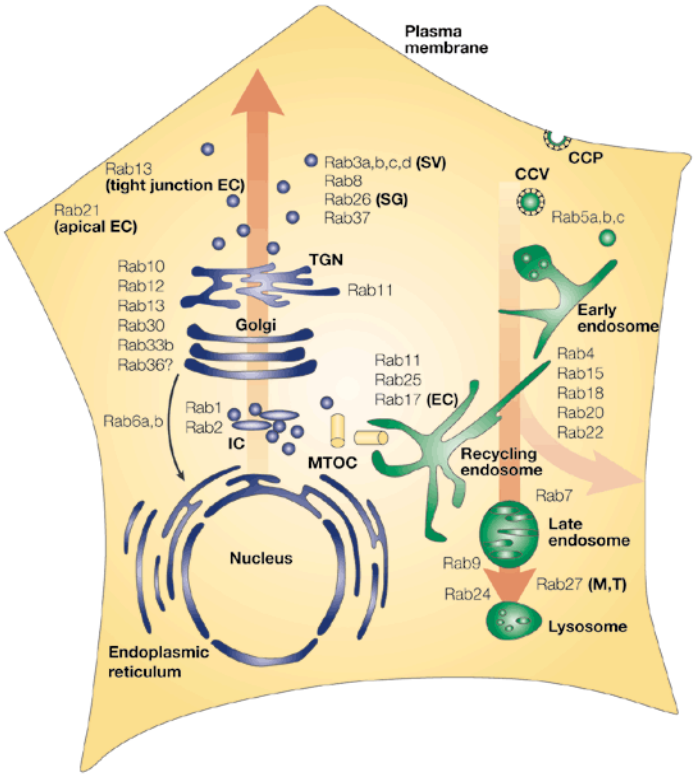

Fig.2 Schematic representation of the cellular localization of different RabGTPases in the mammalian cell, from [8].

To fulfil their biological function Rabs, like all other Ras-like GTPases (except Rad and Ran) must reversibly attache to cellular membranes. This is accomplished via the posttranslational addition of lipid moieties[19]. In the case of Rab proteins GGTase-II (RabGGTase or geranylgeranyltransferase type II [20,21]) catalyses the formation of a stable thioether bond between two C-terminal cysteins and two geranylgeranyl moieties. Together with farnesyltransferase (FTase) and GGTase-I, which modify Ras and Rho/Rac respectively, GGtase-II is a member of the family of protein prenyltransferases [22,23]. The signal motif for geranylgeranylation in Rab proteins is heterogenic (CXC, CC, CCX, CCXX or CCXXX) but usually comprises two cystein residues both of which become modified by the specific RabGGTase-II [24,25]. In addition to this lipid modification further posttranslational modifications of Rabs, such as phosphorylation (Rab1a, Rab4a) or methyl esterification, have been observed [26,27,28]. Unlike other the prenyltransferases, GGTase-II does not directly interact with its protein substrate, but requires a protein chaperone named REP (Rab escort protein) [29,30]. The newly synthesised Rab protein in its GDP bound state is recognized by REP through interaction with hydrophobic residues in the hypervariable C-terminal part of the Rab [31,32,33]. RabGGTase binds to the binary REP:Rab complex and catalyses the attachment two geranylgeranyl moieties to the C-terminal cysteins of the Rab[34,35,36]. Addition of the second GGPP moiety to Rab triggers dissociation of the RabGGTase from the REP:Rab complex and the otherwise insoluble geranylgeranylated Rab protein is delivered to the membrane by REP [37,38].

As expected for all Ras related proteins, Rabs shuttle between two structurally distinct conformations, depending on their nucleotide state (Fig. 3). Adopting either the GDP-bound 'off' or the GTP-bound 'on' conformation, the function of Rab proteins in vesicular trafficking is that of a molecular switch. The tight temporal control required for co-ordinated vesicular transport is maintained mainly through two classes of Rab regulators, guanine nucleotide-exchange factors (GEFs) and GTPase-activating protein domains (GAPs). While in the active state, Rabs are membrane-bound and associated to their specific effectors, whereas in the inactive state a guanine nucleotide-dissociation inhibitor (GDI) extracts the Rab protein from the acceptor membrane to build a cytosolic pool of the GTPase and recycle it back to the donor compartment[39]. The combination of the cycling between membrane association / cytosolic localization and the coupled nucleotide states is termed the Rab cycle.

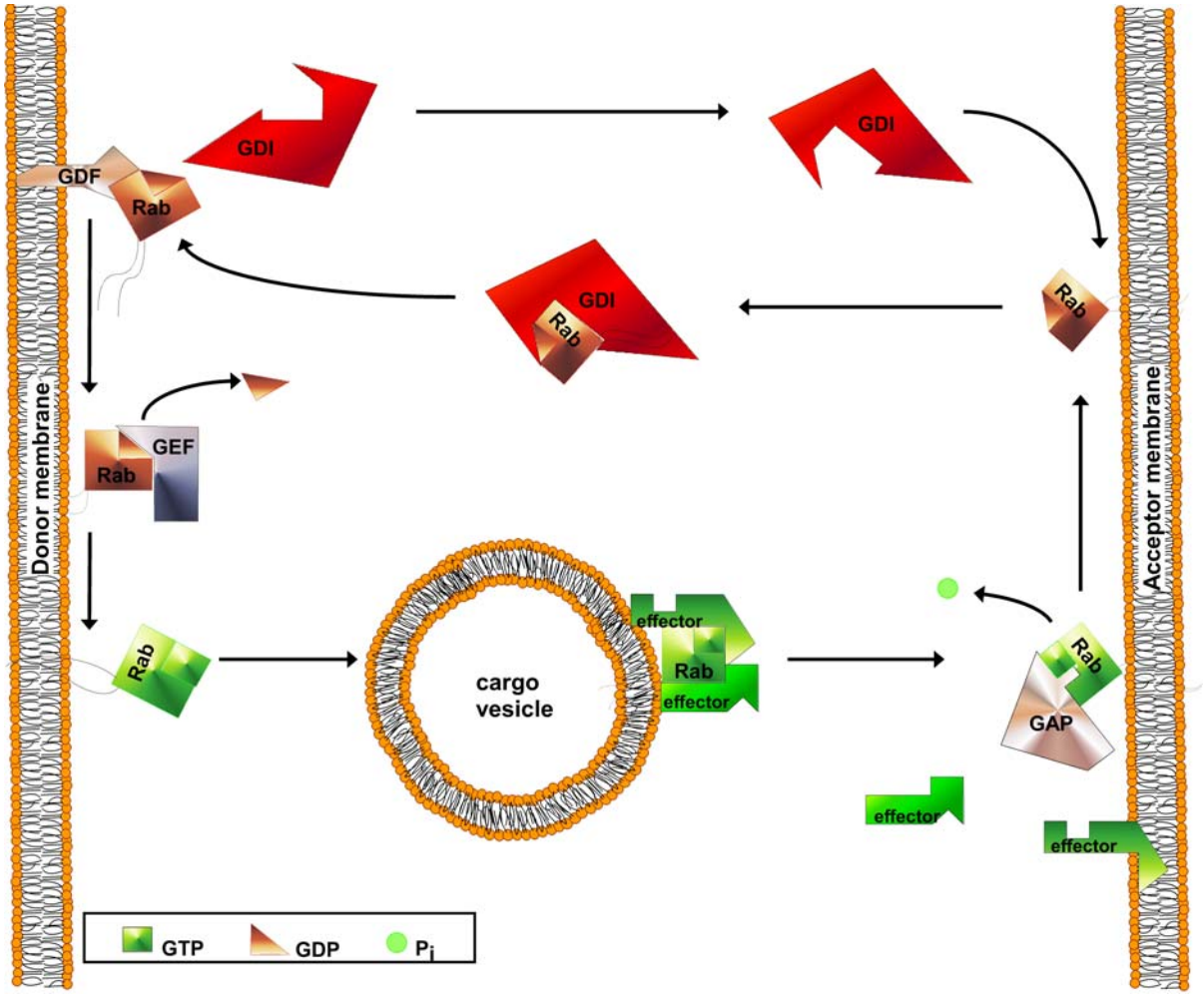

Fig.3 The Rab-Cycle. See text for a detailed description. Rab(GTP) green; Rab(GDP) red; GEF: guanine nucleotide-exchange factor; GAP: GTPase-activating protein domain; GDI: guanine nucleotide-dissociation inhibitor; GDF: GDI-displacement factor.

1.3 *Rab-Cycle*

As a initial means to control the activity of the Ras-like GTPase, Rab subfamily specific GEFs catalyse the exchange of GDP for GTP [40,41,42,43]. It is assumed that induction of the active state of the Rab can be directly linked to the recruitment of its effectors. Indeed, studies on Ypt7p and Rab5 gave evidence of the coupling of nucleotide exchange and effector interaction, which might be a common theme among Rab proteins [44,45].

A second class of regulatory proteins is required to bring the Rab back to its inactive state, facilitating an exact timing of the duration of Rab activity [46]. RabGAP domain containing proteins stimulate the hydrolysis of GTP; however, *in vitro* they appear to be more promiscuous acting on several Rab proteins [47,48]. It has been suggested that RabGAPs might act on all those Rabs with a shared subcellular localization, thus introducing spatial specificity. However, for the Rab5 subfamily of RabGTPases, recent studies determined specific activity of a GAP domain protein, by showing that overexpression of RabGAP-5 results in a loss of the Rab5-specific interaction with the effector EEA1 [49]. Still, since the human genome contains at least 52 potential RabGAPs, assigning specific Rab - GAP interactions remains a complex task [50].

A mechanism apparently counteracting inactivation has been suggested based on findings that Rab proteins in complex with their effectors sometimes display even lower hydrolytic activity [51]. Stabilizing the active conformation of the Rab may be a way to stabilize the Rab-effector complex for the time required to exert its physiological function.

After vesicle fusion, Guanine nucleotide-dissociation inhibitor proteins extract GDP-bound Rab proteins from acceptor membranes to recycle them back to their donor compartment. Structurally unrelated GDIs have been found for Rab- [52] and RhoGTPases [53]. While in yeast only one gene of GDI1/Sec19 has been identified [54], analysis of mouse and rat genomes suggest that these contain up to five RabGDI isoforms [55]. So far, three different isoforms (α, β, γ) of ~80% sequence identity have been isolated [56], which appear to have some functional specificity for particular Rabs [57,58]. The GDIs display stretches of high sequence homology with, and have a similar fold to, REP. However, GDI is not recognized by RabGGTase and only binds prenylated Rabs with high affinity [59]. This is consistant with the two main functions of RabGDI. When bound to inactive Rab in the cytosol, GDI prevents reactivation of the Rab by inhibiting nucleotide exchange [60]. How RabGDI exerts its crucial function in extracting geranylgeranylated Rab from cellular membranes is still not completely understood. Additional recycling factors, such as the heat shock protein (HSP) complex may play a role in Rab extraction. Hsp90 and Hsc70, which have been shown to be crucial for membrane extraction of Rab3a. However, it seems that the driving force of the extraction is at least in part based on the high affinity binding of the RabGDI to the prenylated C-terminus of the Rab [61].

After extraction and shuttling through the cytosol, GDI delivers Rab back to its donor membrane, ensuring a continuous cycling of the GTPase [62]. This is believed to involve some sort of membrane acceptor that helps to release the otherwise tightly bound GDI into the cytosol[60]. The localization of a Rab on a particular compartment seems to depend upon the presence of a GDF (GDI-displacement factor) termed receptor [63]. The yeast-interacting proteins (Yips) and their mammalian analogs, prenylated Rab-acceptor proteins (PRA), have been suggested to fulfil a role as GDFs, based on the finding that human Yip3p (PRA-1) is able to dissociate a stable Rab:RabGDI complex and to specifically recruit Rabs [64]. Since additional experiments showed that Yips are able to interact with themselves as well as with other components of the vesicular transport machinery without GDF activity, it appears more likely that this class of proteins plays a broader role in trafficking than simply that of a GDF[65,63,66,67].

1.4 Structure and Function of RabGTPases

Rab proteins are more distantly related to other small GTPases of the Ras superfamily, sharing an overall homology of no more than 30%. Least conserved are the hypervariable N- and C-teminal parts of the protein, flanking a more conserved core that lies between residues Lys5 and Arg164 (counting based on H-Ras p21). The overall topological order of secondary structure elements is conserved for all small GTPases [68,69,70]. It consists of a central β-sheet, built with five parallel and one anti-parallel β-strand, surrounded by five α-helices and connecting loops [71]. While usually α-helices and β-sheets are the most conserved structural elements within a given class of proteins, for the family of small GTPases the loop regions display the highest degree of sequence conservation. NMR studies with members of all the subfamilies of the Ras superfamily of GTPases identified a number of highly conserved sequence motifs responsible for binding the guanine bases and the β- and γ-phosphates. These elements compose the functional core of the molecular switch mechanism, called the guaninenucleotide-binding domain (G-domain) (Fig.4).

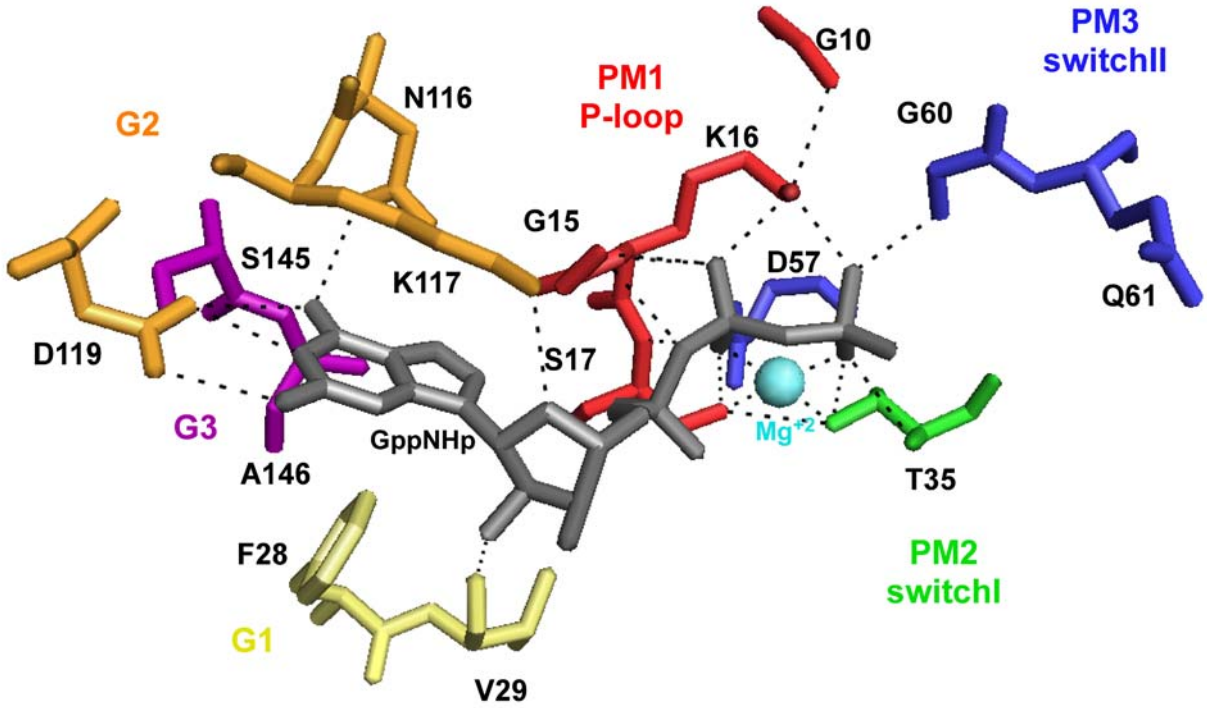

Fig.4 Stick representation of conserved catalytic residues of the G-domain. Colour coding of single residues according to their localization in the different conserved sequence motifs: PM1 (red), G1 (yellow), PM2 (green), PM3 (blue), G2 (orange), G3 (purple). Polar contacts between nucleotide (grey), Mg^{+2} (cyan sphere) and single amino acids are displayed as dashed lines.

Interactions of residues of this G-domain with a Mg^{2+} ion and the γ-phosphate induces rigidity in the so-called effector loop (L2) and a region following the DxxGQ motif (PM3), whereas cleavage of the γ-phosphate destabilizes these regions. Measurements using NMR, EPR or FTIR identified these two switch regions as the

part of the GTPase displaying the highest degree of structural flexibility [72,73]. A nucleotide state dependent movement between two defined positions of switchII has been observed by monitoring the relative position of Tyr32 to the γ-phosphate group [10]. Whereas switchI and switchII undergo dramatic structural changes, the G1 region (also called the P-loop) is not affected by the hydrolysis of GTP.

The main factor mediating specificity for guanine nucleotides, has been determined to be the H-bond between the highly conserved Asp119 in G2 and the guanine base[74]. Two other highly conserved residues have been shown to be indispensable for GTP hydrolysis. Gln61 and Glu63 act as the activating species for a nucleophilic in-line attack on the γ-phosphate by a conserved water molecule. Reorientation of Gln61 is essential and the rate limiting step for hydrolysis [75]. The nucleophilic displacement is facilitated by hydrogen bonds from Tyr35, Gly60 and Lys16 to the γ-phosphate [69].

Experiments using yeast and mammalian cells over-expressing a hydrolysis deficient mutant of a Rab protein provided evidence that GTP-hydrolysis is not required for interaction with downstream effectors, but rather for Rab recycling [76].

Comprehensive sequence analysis of small GTPases determined five sequence motifs that are specific for the entire Rab family (RabF, Rab family motif) and four motifs specific for particular subfamilies (RabSF, Rab subfamily motif) [77] (Fig.5). All five RabF motifs are located surrounding the switchI and switchII region, whereas the RabSF motifs form two distinct surfaces (1st: RabSF1, 3 and 4, 2nd: RabSF2) on opposite sides of the protein. It has been suggested that effectors bind to RabF sites to distinguish the nucleotide state of the Rab, while binding to different combinations of RabSFs from the two sites might be a means to guarantee specificity of the interaction. This idea is supported by the recently solved structure of the Rab3a:Rabphilin-3a complex [78].

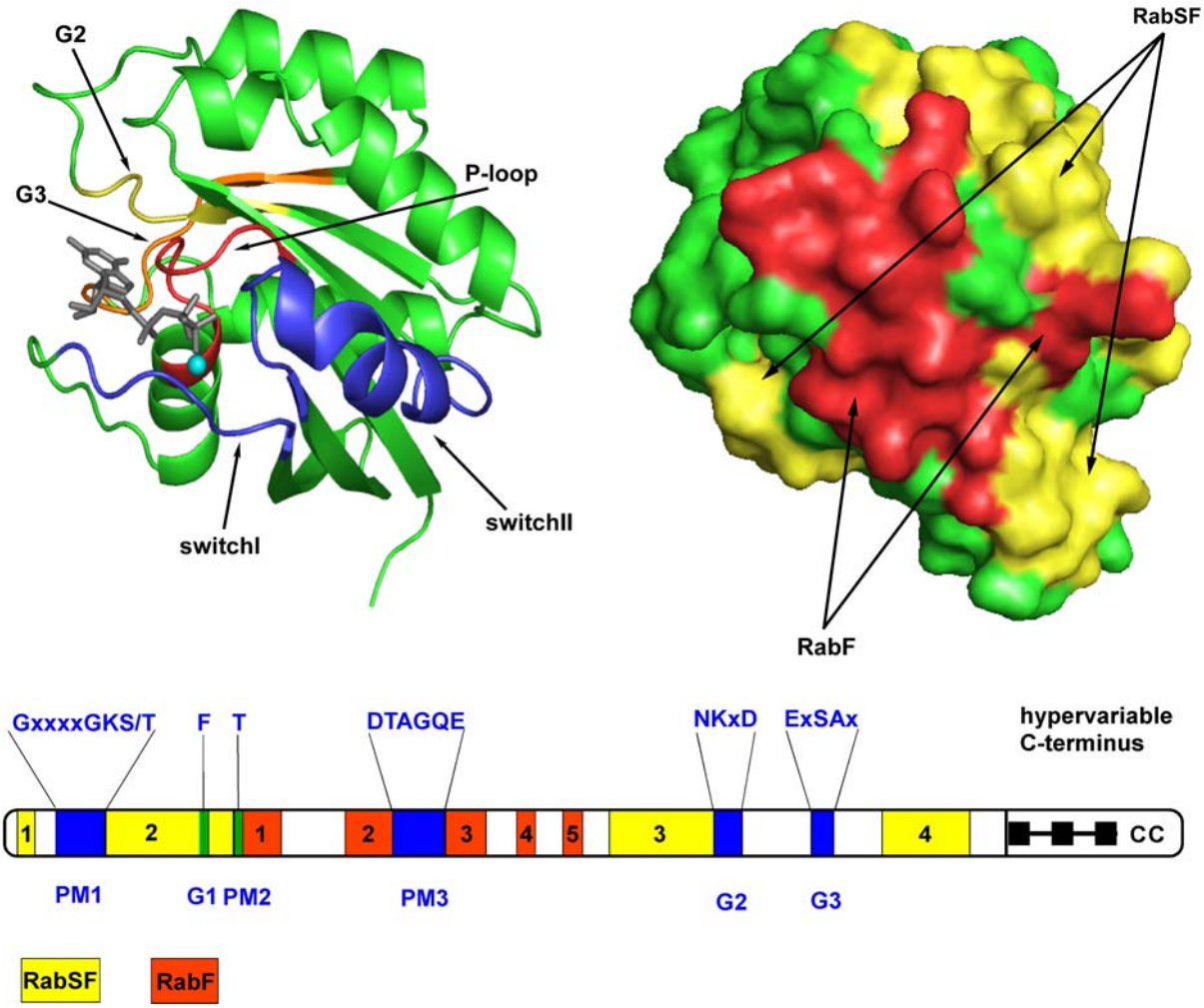

Fig.5 ***Top left*** ribbon representation of Rab3a (PDB 3RABA) with bound nucleotide as a grey stick model and Mg^{+2} a as cyan sphere. Conserved structural elements are indicated with arrows and highlighted in blue (switch I & II), red (P-loop), yellow (G2) and orange (G3). ***Top right*** Surface representation of Rab3a indicating the localization of two distinct RabF sites (red) and three RabSF interfaces (yellow). ***Bottom*** Cartoon representation displaying the arrangement of conserved sequence motifs (blue), RabF (red) and RabSF(yellow) of Rab proteins, form [79,80].

One of the major protein:protein contacts in the Rab3a:Rabphilin-3a complex is formed by an invariant hydrophobic triad (Phe59, Trp76, Tyr91) of Rab3A, which contacts a complementary interaction epitope on the surface of Rabphilin-3A. While the hydrophobic interface of the RabSF motifs is a common feature, the conformation of the hydrophobic triad changes dramatically among different RabGTPases [81]. Thus, structural plasticity of this element may introduce a specificity factor to the effector binding platform.

1.5 Vesicular Transport

Transport of biomolecules between subcellular compartments as well as exo- and endocytosis require tightly regulated mechanisms to control membrane turnover.
A crucial event, which follows from the interaction of the RabGTPase with vesicle tethering complexes, is the mutual recognition of vesicular v-SNARES and target t-SNARES that brings membranes in sufficient proximity for lipid mixing to occure. The conserved membrane proteins Syntaxin 1A, Synaptobrevin II and SNAP-25B (SNAP: soluble NSF-attachment Protein, NSF: N-ethyl-maleimide-sensitive factor) assemble spontaneously to form the stable four-helical coiled-coil bundle of the SNARE. Progressive 'zipping' of the *trans*-SNAREs is believed to convey mechanical force through the trans-membrane regions of the SNAREs, which brings the vesicle and target membrane closer together, leading to the formation of a pore in the membranes [82]. While for some time the fusion event was thought to be exclusively SNARE-driven, and indeed purified SNAREs alone can act as a minimal fusion machinery *in-vitro* [83,84], it has become apparent that additional factors are required to ensure specificity as well as a physiologically relevant efficiency [85,86]. The SNARE complex as the key component of the docking/fusion machinery interacts with a number of regulators including RabGTPases (Fig.6). The nucleotide cycling of RabGTPases mediates the temporal specificity of vesicular transport, whereas directionality relies on interactions of the Rab with its specific effectors.
According to the current model, vesicular transport can be divided into five steps. The first is the formation of the budding vesicle at the donor membrane. This is followed by movement of the vesicle through the cytosol, membrane remodelling and then docking to and fusion with the acceptor compartment. In the firststep at the donor compartment Rab proteins have been shown to be involved in two aspects of vesicle formation. The first is a regulatory function in cargo sequestration via their respective effectors. This has been demonstrated for Rab5, Rab9 and Rab11. While the adaptor-dependent assembly of clathrin-coated pits is supported by the Rab5-GDI complex [87], Rab9 effector TIP47 has been shown to retrieve the mannose-6-phosphate receptor into budding vesicles [88]. Rab11 via its effector Rabphilin11 interacts with Sec13, a component of the COPII coat complex (coatomer protein) at the Golgi [89]. The second function for Rab proteins in vesicle formation has been suggested for Rab1 and its effector p115, which appear to effectively program budding vesicles by recruiting proteins essential for later docking and fusion. In the second step, following dissociation from the donor membrane, the vesicle is actively transported through the cytosol via Rab-mediated interactions with kinesin- or dyneine-like motor-proteins that confer actively directed transport along the cytoskeleton[90]. Several RabGTPases have been implicated in this process. A prominent example is the interaction of Rab27a and its putative effector effector melanophilin with MyosinVa[91]. Activity of this complex appears to

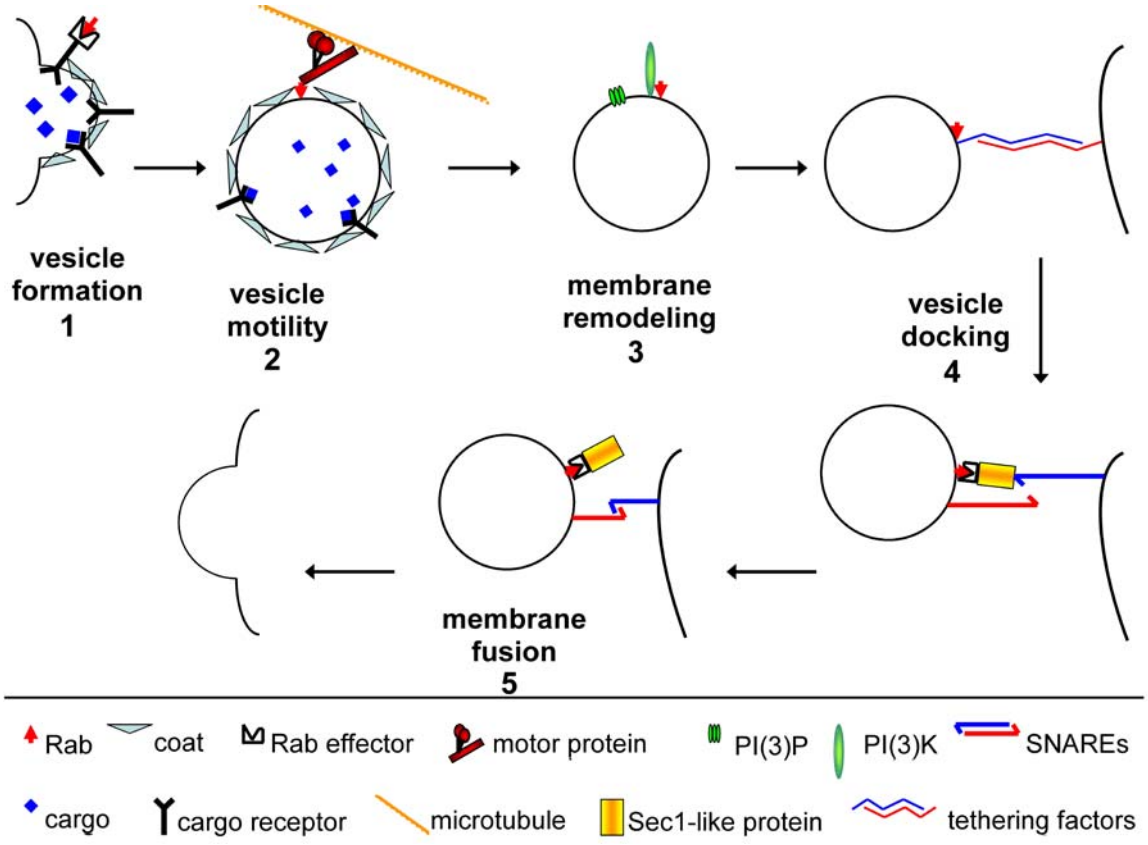

Fig.6 Functions of RabGTPases in vesicular trafficking. Shown are the five steps of vesicle trafficking: Vesicle formation or budding, vesicle transport along the cytoskeleton, membrane remodelling, docking or tethering of the vesicle and fusion of the two membranes. See text for a detailed description.

tether melanosomes to the actin cytoskeleton of melanocytes, which is required for normal skin and hair pigmentation [92,93]. Mutations in Rab27a or Myosin Va lead to disorders of pigmentation and accompanied severe immunological or neurological defects, resulting in the rare inherited Griscelli syndrome type II or I respectively [94,95,96,97].

An example of membrane remodelling, as the third step in vesicular transport, is the activity of Rab5. Rab5 and its effector PI(3)K (phosphoinositide 3-kinase) have been linked to the generation of a molecular homing machinery for later docking and fusion. Rab5 seems to recruit PI(3)K, thus causing a local increase in the concentration of PI(3)P. This in turn leads to an active remodelling of the membrane, since PI(3)P-rich domains are targeted by the protein EEA1, which acts in tethering of vesicles to the target membrane [98,99,100].

The interaction of Rab proteins with soluble tethering factors precedes the actual docking and fusion events. Tethering factors that have so far been shown to bind RabGTPases fall into two classes: either large oligomeric complexes (COG, HOPS, Exocyst, TRAPP); or homodimeric coiled-coil domain effectors (EEA1, Uso1p, p115) [101,102]. Interactions with a class of evolutionary conserved protein components of the docking/fusion machinery led to the suggestion that tethering

factors might initiate these processes directly or indirectly [8]. However, exact functions of these protein factors have not yet been determined.

1.6 Retrograde Transport

In order to prevent depletion, resident proteins such as components of the sorting or processing machinery must be retrieved from the acceptor membranes and returned to their donor compartments to maintain a dynamic equilibrium. Whereas in anterograde transport cargo proteins travel from the ER through the Golgi apparatus and towards the plasma membrane, retrograde transport is the counterbalancing flow of materials to ensure stable membrane turnover. In retrograde trafficking three distinct transport steps have been defined: The first step includes transport from the endosomal elements to the trans-Golgi network (TGN). Intra Golgi trafficking defines the second part and Golgi to ER vesicle movement marks the final step of retrograde transport [103] (Fig.7). Two transport routes for proteins from the endosomal elements to the TGN have been identified. A well studied example for transport of a cargo protein by the first rout is the cation-independent mannose-6-phosphate receptor. This interacts with the Rab9 effector TIP47 [104], on its way to the TGN via the late endosomal elements.
Although some findings suggest an involvement of Rab11, the exact mechanisms underlying a second, direct route bypassing the late endosomes, remain ambiguous [105]. In either case, it has become apparent that docking to TGN membranes requires the activity of Rab6 [106]. Rab6 is associated with the TGN and late Golgi membranes where it interacts with the GARP (Golgi-associated retrograde protein) complex. GARP in turn forms a tethering complex with the t-SNARE Tlg1p, which has been shown to mediate the recruitment of endosomatic vesicles onto late Golgi compartments [107,108].
Intra-Golgi trafficking, as the second step in retrograde transport, is required to maintain the structure of the Golgi apparatus and to counteract maturation of the Golgi cisternae or the depletion of processing/sorting enzymes [109]. In *S.cerevisiae*, intra-Golgi retrograde trafficking was associated with the Ypt1p controlled Sec34p-Sec35p protein complex [110]. This putative tethering factor was shown to interact with the t-SNARE Sed5p and components of the COPI coat complex. In mammals the COG (conserved oligomeric Golgi) complex, an eight protein complex containing three homologs of Sec34p-Sec35p (subunits COG-4, -6, -8), has been suggested to fulfil a similar role [111].
For the final retrograde trafficking step from the Golgi apparatus to the ER a COPI-dependent and a COPI-independent transport route have been described. The former is controlled through the small GTPase Arf1, which initiates formation of COPI coated vesicles. A KDEL-receptor mediates the retrieval of KDEL-bearing luminal proteins into these COPI vesicles [112]. The mechanisms underlying COPI-independent Golgi to ER transport remain elusive. Recently Rab6 has emerged as a key regulator of biosynthesis and endocytosis, linking vesicle movement along the cytoskeleton and membrane recycling through retrograde transport.

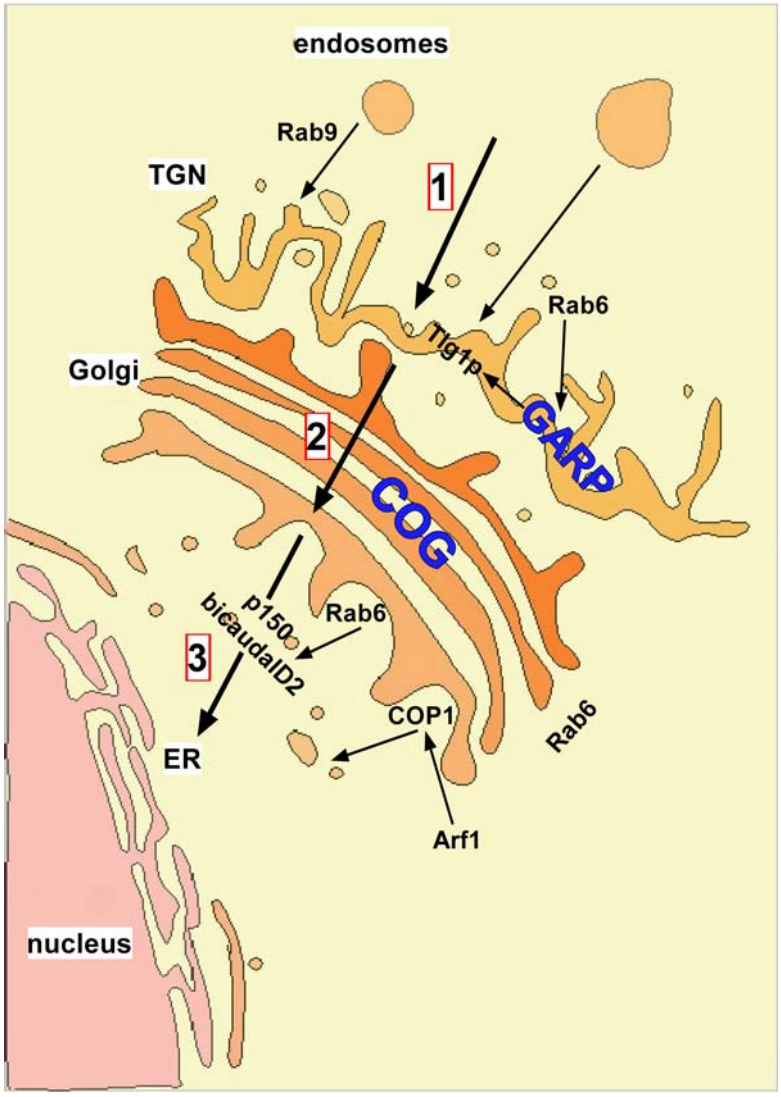

Fig.7 Retrograde transport route from cell periphery to the nucleus. The three steps of retrograde transport: 1) Endosomal elements to trans-Golgi network (TGN) trafficking. Controlled by Rab9 and Rab6 via Golgi-associated retrograde protein (GARP) and the t-SNARE Tlg1p; 2) Intra Golgi transport. Mediated by the conserved oligomeric Golgi (COG) complex and controlled by Rab6; 3) Transport from the Golgi to the ER. Mediated by Afr1 via COP1 vesicles or by Rab6 via interaction with p150 and bicaudalD2.

The final part of retrograde transport appears to require Rab6-controlled transport along microtubules [113,114,115]. An early example of Rab6 interacting with a member of the kinesin-/dynein-like motor-protein family, was the characterisation of the Rab6 effector rabkinesin6 (RAB6-KIFL, MKlp2 or KIF20A) [116]. Rabkinesin6 plays a role in mitosis, during which it is greatly up-regulated [117,118]. A more general role for Rab6 in retrograde trafficking has been suggested based on various findings, associating this GTPase with dynein/dynactin mediated vesicle transport between the cell periphery and the ER [119]. Interactions of Rab6 with the actin cytoskeleton have been shown to occur either directly with the $p150^{glued}$ (p150) subunit of dynactin or via the homodimeric coiled-coil protein BicaudalD2 (BicD2), which in turn binds to the dynamitin (p50) subunit of the dynactin complex [120,121].

1.7 Rab effector interactions

The transduction of the Rab-mediated signal in transport processes is carried out through downstream effector proteins. Earlier models of Rab function proposed that a particular Rab protein controls one distinct trafficking step. However, a number of examples suggests that a single Rab can regulate many different aspects of vesicular transport (see 1.6). For instance chromatography of bovine brain extract on a Rab5•GTPγS-column yielded a library of 20 different proteins interacting either directly or indirectly with this GTPase. The identified set included components of the docking and the fusion machinery (EEA1, rabaptin-5) as well as proteins with established nuclear functions (APPL1/DIP3α) [98,122,123]. In contrast to their upstream regulators, most Rab downstream effectors display little or no homology. As in the example of rabaptin-5 and its interaction with Rab5 and Rab4 [124,125], it was shown that in some cases a single protein can harbour more than one Rab effector domain. Such multivalent effectors are believed to link different transport processes.

Most, if not all of the functions of the cytoskeletal motor protein dynein in transport require the activity of the multi-subunit protein complex dynactin (for reviews see [126,127]). Dynactin is recruited to specific sites on organelle membranes in a controlled fashion [128] and Rab GTPases are considered to be possible mediators of dynactin recruitment. The interaction of Rab27a and its effector melanophilin (see 1.5) gave a clear example that Rab-controlled transport and movement along the cytoskeleton can be linked [93]. Rab6 may play a role in dynactin recruitment as Hoogenraad and co-workers identified the $p150_{glued}$ subunit of dynactin and a TGN resident protein named bicaudalD as Rab6a-effectors[121]. Another Rab6a-effector, BicaudalD, is a representative of the recently emerging class of Rab effectors named Golgins that, although not sequence homologous, share cellular location and have some common functions.

1.8 Rab6

Two distinct Rab6-coding genes located on chromosome 11 [129] and chromosome 3 [130] encode the two members of the Rab6 subfamily of small RabGTPases, called Rab6A and Rab6B respectively. Both proteins share 91% sequence identity with substitutions mainly in their hypervariable C-terminal region. However, Rab6B is tissue- and celltype-specific, being expressed primarily in the brain, while Rab6A is ubiquitously expressed. Rab6A is composed of 208 amino acids and has a molecular mass of 23.6kDa[131]. One peculiarity of Rab6A is its alternative splicing and the incorporation of either one of two exons of its gene that leads to the generation of a functionally distinct isoform called Rab6A'. It was suggested that a gene duplication late in evolution yielded these two exons and as a consequence resulted in the two human isoforms of Rab6A, since only one homolog of Rab6 can be found in yeast (Ypt6, [132]) as well as in *Plasmodium falciparum* [133]. The two isoforms of Rab6A deviate only in three amino acids flanking the switch II region, V62 → I62, T87 → A87 and V88 → A88 (6A → 6A'). In particular the surface exposed residue A87 (T87) [134] was shown to be important for effector binding, since its mutation in Rab6a leads to loss of interaction with rabkinesin6 [135]. It is still a matter of debate whether Rab6A and Rab6A' overlap in their function. Just like Rab6B, which also contains a threonine at position 87, both Rab6A isoforms associate with the Golgi and appear to act in retrograde trafficking [136,137]. Early studies showed that over-expression of a GTP-locked mutant of Rab6A, but not of Rab6A', leads to a microtubule-dependent redistribution of Golgi proteins into the ER [131]. This led to a model of Rab6A function that suggested a spatial separation of the two isoforms, with Rab6A regulating Golgi to ER transport and Rab6A' acting in transport processes from the endosomes to the Golgi [113]. However, this model could not be confirmed and in a revised model both isoforms function as sequential regulators of retrograde trafficking, with Rab6A acting predominantly in recycling proteins from the TGN directly to the ER, bypassing the Golgi-stacks [138]. Nevertheless, studies which knocked down Rab6A function, led to a revaluating of the relevance of Rab6A' in retrograde trafficking. Goud and co-workers suggested a model in which Rab6A' is the main regulator of retrograde trafficking, whereas Rab6A regulates the function of the Golgi-localized Rab33b [139] in compensating loss of Rab6A' function [140]. Given the spatial distribution of Rab6A function throughout the cytosol and its interactions with components of the cytoskeleton [120] the effective impact of the Rab6A isoform in vesicular trafficking in general and in retrograde transport in particular requires further investigation.

1.9 Golgins as Rab6 effectors

Unlike the ER, the different cisternae of the Golgi apparatus do not fuse, but assemble to form a polarized membrane structure. The first clues on how this structure is maintained came from early electron microscopic observations of protein bridges linking the adjacent Golgi stacks [141,142]. In fact, detergent extracts of the Golgi apparatus gave evidence of a protein exoskeleton defining the morphology and structure of this organelle [143]. A class of Golgi-localized coiled-coil proteins, termed Golgins, has emerged as RabGTPase effectors that function in membrane tethering and fusion as well as for the structural organization of Golgi stacks. Golgins associate with Golgi membranes either via trans-membrane domains (Giantin), a myristylated GRASP-adaptor domain (Golgi reassembly stacking protein) (golgin-45, GM130) or through recruitment by small GTPases (Rab, Arf, Arl) (for review see [144]. Golgins bind RabGTPases via their coiled-coil domains, however a particular Golgin might bind to different Rabs. For example GM130[145] has been observed to interact with Rab1, Rab2 and Rab33b. Analysing earlier findings regarding the interaction of Rab6 with the dynein motor complex, Barr and co-workers found that Rab6 indeed binds to the Golgins BicaudalD1 and D2 as well as to $p150^{glued}$ and to the p50 subunit of dynactin and dynamitin [120]. As an aspect of Rab6 regulatory function in microtubule-dependent retrograde trafficking, Rab6 laden membranes have proven sufficient to recruit the dynein motor complex *in vitro* and *in vivo*. Furthermore, the positioning of the Golgi in the pericentriolar region of the cell is known to be dynein-dependent. In the context of these findings, it appears that Rab6 regulates the linking and tethering of vesicles and the TGN to the cytoskeleton via its effectors and the dynein/dynactin complex. Thus, extending its field of action from regulating retrograde transport only, it has been suggested that Rab6 might be a component of the search/capture system of microtubules, to collect Golgi membranes to the correct cellular position.

1.9.1 BicaudalD2

BicaudalD2 is one of two isoforms of an evolutionary conserved Golgi-resident coiled-coil protein. Its mammalian homolog consists of 824 amino acids with a calculated mass of 93.5kDa. BicaudalD was initially identified as a component of the dynein pathway in *Drosophila* [146]. It has been shown to interact with Rab6 via a C-terminal coiled-coil domain [147], while an N-terminal coiled-coil domain has been associated with inducing microtubule minus end directed transport [121,148]. Interestingly, dynein recruitment by full length BicaudalD2 is reduced, compared with that of the N-terminal domain alone. Further studies showed the N- and the C-terminal domain can interact with each other, suggesting an intramolecular regulatory function for the C-terminal coiled-coil domain. The model suggests that only when the C-teminal domain is bound to Rab6 (i.e. to the cargo vesicle), does the N-terminal domain become available for interaction with the dynein motor. Apart form this assumed function as a bivalent linker molecule, more recent models suggest a regulatory role for bicaudalD2. Evidence for such a role is based on the finding that BicaudalD2 is specific for dynactin and the dynein motor, whereas p150 is able to interact with kinesin-II [149], switching of dynactin between the kinesin and the dynein motor complexes appears feasible.

1.9.2 PIST

PIST, also known as GOPc, FIG or CAL, was originally described as an interaction partner of the small GTPase TC10 (PDZ-domain protein interacting specifically with TC10) [150]. The protein is expressed in many tissues and may fulfil different functionalities depending on the molecular context. However, all of these functions seem to be connected with the Golgi, to which PIST is associated by binding to the Q-SNARE syntaxin-6 [151]. The protein has a calculated mass of 49.7kDa and comprises two putative coiled-coil domains separated by a leucine-zipper. The C-terminal coiled-coil domain is required for Golgi localization, while the N-terminal coiled-coil domain was shown to be necessary for Rab6 binding in yeast two-hybrid screens by Barr and co-workers (Max-Planck Institute, Martinsried). PIST has been found to bind to CALEB/NGC a member of the EGF protein family that is expressed in the nervous system [152]. More general, tissue independent, interactions of PIST led to a proposed model for its downstream function. Transmembrane proteins like the cystic fibrosis transmembrane conductance regulator (CFTR) or the frizzled proteins bind to the PDZ-domain of PIST and this interaction is important for their transport toward the plasma membrane [153,154] Similarly, the somatostatin receptor subtype-5 (SSTR5) contains a PDZ-ligand motif and is retained within the Golgi via interaction with PIST, which is important for its sorting back to the plasma

membrane [155]. Hence, it has been proposed that PIST might be a general sorting molecule for a variety of transmembrane proteins. A recent study describing interactions of PIST with the Rho effector Rhotekin is another element of crosstalk among the family of small GTPases via this Rab6 effector [156].

1.10 Coiled-coil protein domains

The first example of a coiled-coil domain protein was proposed in 1953 as a model of the intermediate filament protein α-keratin [157]. Coiled-coils are formed of right-handed α-helices, twisted counterclockwise around one another to form a left-handed supercoil structure (Fig.8). A characteristic determinant of all left-handed coiled-coils is the seven amino acid repeat pattern (heptad) of primarily apolar residues that form the oligomeric interface. While in a regular α-helix 3.6 aminoacid residues constitute one full turn, the left-handed coiled-coil is somewhat distorted, which leads to one turn every 3.5 residues. Hence, the heptad repeat occurs every two turns [158,159]. Contrariwise, an eleven residue periodicity (undecat repeat) gives rise to a right-handed coiled-coil [160]. Coiled-coils are found as homo- or heterotypic arrangements of two to five parallel or antiparallel α-helices. The latter is typically found in intrachain helix-loop-helix motifs. The residues of the heptad repeat of one chain are commonly denoted $(a\text{-}b\text{-}c\text{-}d\text{-}e\text{-}f\text{-}g)_n$ and for the other, interacting chain $(a'\text{-}b'\text{-}c'\text{-}d'\text{-}e'\text{-}f'\text{-}g')_n$. The 'Peptide Velcro hypothesis' (PV hypothesis) defined three requirements for the formation of a parallel left-handed coiled-coil [161] (Fig.8). Firstly, the heptad periodicity must be given with apolar (hydrophobic, Leu, Val, Ile) residues in the first (a) and fourth (d) position. Secondly, residues in positions e and g must be charged (hydrophilic, Glu, Lys) [162]. Finally, the remaining residues b, c and f must be hydrophilic, because they are solvent exposed [163]. The driving force of coiled-coil formation is the stable 'knobs-into-holes' packing of apolar sidechains from one helix into the hydrophobic core of the other helix [164], which is accounted for by the first criterion of the PV hypothesis. However, ~20% of residues in the a and d position were found to be polar [165]. Pairing specificity is greatly influenced by electrostatic interactions between positions g of one heptad repeat and e' of the next heptad.

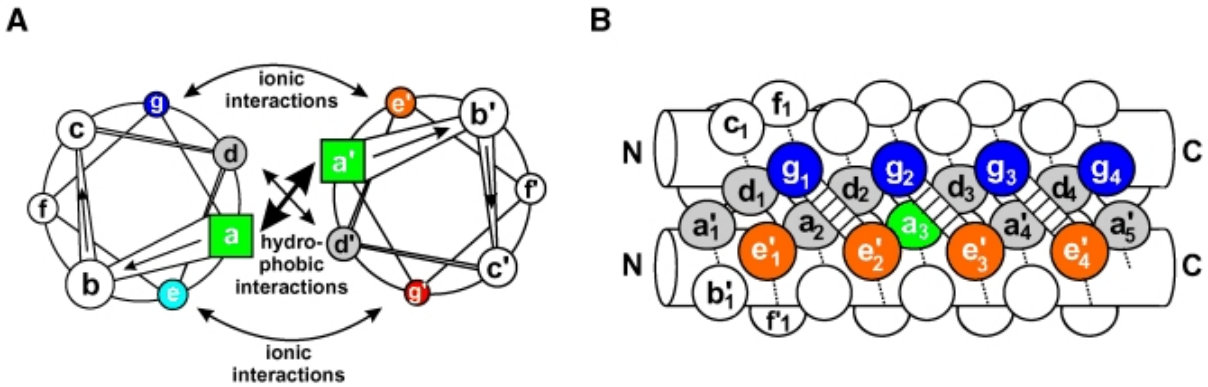

Fig.8 Schematic representation of a parallel dimeric coiled-coil[166]. *Left* The helical wheel diagram looks down the axis of the α-helices from N- to C-terminus. *Right* a side view of the coiled-coil. Residues are labelled a-g in one helix and a'-g' in the other. Hydrophilic interactions (g-e' and g'-e) within the heptad repeat and hydrophobic interactions of the core (a-a' and d-d') are shown.

These residues must be of opposite charge in heterodimers and of the same charge in homodimers. It is still a matter of debate whether or not 'trigger sequences' are required for a sequence of heptad repeats to fall into a coiled-coil structure [167,166].

Whereas coiled-coils were initially thought to be rigid structures, it has become apparent that breaks in the periodicity of the heptad can introduce an element of structural flexibility. The two most prominent breaks in periodicity are called *stutter* and *stammer*. A stutter represents a three residue deletion (= four residue insertion), which has to be compensated by an underwinding of the supercoil. Stammers represent a four residue deletion (= three residue insertion) that is compensated for by an underwinding of the supercoil. The combination of stability with structural variability makes coiled-coils versatile functional entities. Consequently, they can be found in a wide variety of proteins with very different functionalities. Examples include all three motor protein types (myosins, kinesins, dyneins), transcription factors, viral capsid proteins and the SNARE complex. In fact, conserved residues within the SNARE coiled-coil complex has given rise to a new terminology for the denotation of these structures. Target SNAREs contain a conserved Glu (Q) residue and hence are called Q-SNAREs. The analogous position (d) in synaptobrevin is a conserved Arg residue, determining the R-SNARE. Coiled-coil protein domains have been found in Rab effectors [168,169]. Moreover, through the identification of Golgins (see 1.9) as Rab effectors a family of coiled-coil domain proteins has become associated with membrane tethering and fusion in vesicular transport. For the putative Rab6a effectors bicaudalD2, PIST and p150 predicted coiled-coil domains were suggested to be crucial for the interaction with the GTPase [170,171]

2 AIMS OF THE PROJECT

Small GTPases of the Rab family are essential regulators in the vesicular transport in eukaryotic cell. Their function as molecular switch is based on the transition between two distinct conformations that results from hydrolysis and exchange of the bound GTP. The GTP-dependent interaction with a variety of specific effector proteins is the underlying principle for temporal control and spatial specificity of the Rab-controlled transport pathways.

Although the basic molecular mechanism of the transition between the active and the inactive conformations of a Rab can be inferred from studies on other GTPases, little is known about the origin of the great heterogeneity in the intrinsic rates of catalysis among Rab proteins. Although RabGTPases are a very homogeneous family, their effector molecules display little or no similarity with each other. The fact that, in the activated conformation, RabGTPase can specifically interact with several effectors raises a question of the structural mechanisms and the thermodynamics of the Rab:effector interaction.

This project aimed to address these questions by analysing the mammalian GTPase Rab6a that functions as a regulator of microtubule-dependent retrograde vesicle trafficking. The proteins BicaudalD2, $p150_{glued}$ and PIST, which had been identified as putative effectors of Rab6a, provide a convenient model system to study RabGTPase:effector interactions. A combination of biochemical, biophysical and structure analysis methods is used to gain an insight into the mechanism of GTP hydrolysis and to characterise the Rab6a:effector interactions that are required in order to facilitate the specific transport step.

3 MATERIALS AND METHODS

3.1 Materials

3.1.1 Chemicals

All chemicals were purchased from the following companies with the highest purity available.

Table of the most frequently used chemicals

Supplier	Compound
Applichem Darmstadt, Germany	acrylamid/bis-acrylamide (37.5:1, 30 %), methanol, guanidiniumHCl, ammoniumsulfate
Gerbu Gaiberg, Germany	dithioerythritol (DTT), sodium dodecyl sulfate (SDS), N-(2-hydroxyethyl)piperazine-N'-(2-ethanesulfonic acid) (HEPES), ethylenediaminetetraacetic acid (EDTA), glycerol, imidazol, isopropyl-β-D-thiogalactopyranoside (IPTG)
Hampton Research, Laguna Niguel, CA, USA	crystallization screens, additive and detergent screens
JT Baker Deventer, NL	acetonitrile, ethanol, 2-propanol, acetone, urea, dipotassium hydrogenphosphate, potassium dihydrogenphosphate, potassium hydroxide, hydrochloric acid, sodium chloride, potassium chloride
Merck Darmstadt, Germany	ammonium persulfate (APS), sodium hydroxide
Roth Karlsruhe, Germany	3-[(3-Cholamidopropyl)dimethylammonio]-1-propanesulfonate (CHAPS), CTAB, Tris(hydroxymethyl) aminomethan (Tris) TECEP
Serva Heidelberg, Germany	*N*,*N*,*N´*,*N´*-tetramethylethylendiamine (TEMED), bromphenol blue, Coomassie brilliant blue R250, Triton X-100, ampicillin (Amp), DMSO, β-mercaptoethanol
Sigma Taufkirchen, Germany	sinapinic acid, ethidium bromide, bovine serum albumin (BSA), trifluoracetic acid (TFA), agarose, phenylmethylsulfonylfluoride (PMSF), lithium chloride, GTP, GDP, GppNHp
Bio-Rad München, Germany	BRADFORD reagent, Gel Filtration Standard
Fermentas, St. Leon-Roth, Germany	dNTPs
Fluka BioChimika	TCEP

3.1.2 Nucleotides and Nucleotide Analogs

Guanosindiphosphat (GDP) and guanosintriphosphat (GTP), as well as the non-hydrolysable GTP-analog guanosin-5'-O-(β,γ-imidodiphoshpat) (GppNHp) were purchased from Sigma-Aldrich (Taufkirchen) with a purity of >95 %. Fluorescently labeled *N*-methylanthaniloyl-GppNHp (mant-GppNHp) was synthesized by S. Gentz (AG Goody).

3.1.3 Enzymes

Table of the used enzymes

Supplier	Enzyme
Roche (Mannheim, Germany)	RNase A, alkaline phosphatase, High Fidelity Expand polymerase, trypsin, elastase
Fermentas (St. Leon-Rot, Germany)	restriction enzymes, Generuler 1 kb DNA standard
New England Biolabs (Beverly, USA)	restriction enzymes, T4 DNA-Ligase
Amersham Biosciences (Freiburg, Germany)	LMW-Standard
GeneCraft (Lüdinghausen, Germany)	BioTherme polymerase

3.1.4 Software and Databases

Basic Local Alignment Search Tool (*BLAST*): [172]
ClustalX 1.8.1 Multiple Sequence Alignment Program: [173]
The *ExPASy* (Expert Protein Analysis System) proteomics server from the Swiss Institute of Bioinformatics (SIB): [174]
*Generunne*r 3.05 (Hastings Software Inc.)
MultAlign DNA sequence alignement tool: [175]
Multicoil program described in: [176]
Origin 7.0 OriginLab Corporation (Northampton, USA)
Paircoil program described in: [177,176]
PAWS Genomic Solutions (Huntingdon, UK)
The Protein Data Bank (*PDB*): [178]
PyMol DeLano Scientific LLC. (San Francisco, USA)
WinCoot 0.0.25 (CCP4 Program Suite)

3.1.5 Buffers and Bacterial Growth Media

Luria-Bertani medium (LB): 10 g tryptone, 5 g yeast extract, 10 g NaCl added to 950 mL ddH_2O

M9 minimal medium: 7.5 g $Na_2HPO_4 \bullet 2H_2O$, 3 g KH_2PO_4, 0.5 g NaCl, 0.25 g $MgSO_4 \bullet 7H_2O$, 0.14g $CaCl_2 \bullet 2H_2O$, to 1 L ddH_2O + 10 mL trace element solution

Trace element solution: 9 mL 10 x solution 1, 10 mL solution 2, 81 mL ddH_2O

solution 1 (x 10): 500 mg EDTA, 200 mg $Fe(III)SO_4 \bullet 7H_2O$, 90 mL dd$H_2O$

solution 2: 100 mg $ZnSO_4 \bullet 7H_2O$, 30 mg $MnCl_2$, 300 mg H_3BO_3, 200 mg $CoCl_2 \bullet 6H_2O$, 10 mg $CuCl_2 \bullet 2H_2O$, 20 mg NiCl2$\bullet 6H_2O$, 30 mg $Na_2MoO_4 \bullet 2H_2O$, 1000 mL ddH_2O

LB-ampicillin agar: 10 g tryptone, 5 g yeast extract, 10 g NaCl, 20 g agar, ddH_2O to 1 L. 50 mg / L ampicillin are filter-sterilized and added to the agar after autoclaving and cooling to 55°C.

3.1.6 Bacterial Strains

BL21-CodonPlus(DE3)-RIL strain: *E. coli* B F– *ompT hsdS*(r_B– m_B–) *dcm*+ Tet^r *gal l* (DE3) *endA* Hte *[argU ileY leuW* Cam^r] (Stratagene, La Jolla, USA)

3.1.7 Expression Vectors and Oligonucleotides

pET containing TEV-protease cleavage site for removal of amino terminal His_6-tag (**179**)

pGATEV containing TEV-protease cleavage site for removal of amino terminal His_6- and GST-tag (**180**).

pIF-1 pET-15b-based, comprises TEV-protease recognition-site for removal of N-terminal His_6-tag and fragment of the *E. coli* initiation factor-1(IF1) (**181**).

Table of oligonucleotide primers used in the PCR reactions

name	sequence
Rab6A_F	TTTTTTTTTCATATGTCCACGGGCGGAGACTTCGGG
Quick_Rab6aQL_F	GTCCTGTCTTCGTCTCTTACTTACTAACTGTAT
Quick_Rab6aQL_R	ATAGGATTAGTAAGTAAGAGACGAAGACAGGAC
Rab6A_D22_R	ATCGGCCTCGAGTCATTCTCTGCTTCTGTCCTGTGTGCTTTCCA
Rab6a_D27_R	AAAACTCGAGTTACTGTGTGCTTTCCATTCCCGGCAA
bicD2mini_F	TTTTTTTTTCATATGTCCGTGGCCCTTGCCACCCTG
bicD2mini_R	ATCAAGAATTCCTACAGGCTCGGT
PIST-F	TTTTTTTTTCATATGTCGGCGGGCGGTCCA
PIST-R	ATCGCCCTCGAGTTAATAAGATTTTTTATGATACAGAGTGTG
PIST_IF_F	TTTTTTCAGGGCGCCATGGCGGCGGGCGGTCCATGCCCAGCAGC
PIST_IF_R	TTTTTTCTCGAGTCAATAAGATTTTTTATGATACAGAGTGTGC
p150_F	TTTTTTCAGGGCGCCATGGCGTCAGCAGGTGAGCTGAGCAG
p150_R	TTTTTTCTCGAGTCACTCATCAATGGTGCTCTCTGCCTG
PIST-sq(493-513)	GCACAACTTGAAGCTGAAGTG
Rab6aCORE_F	TTTTTTTCATATGAAATTCAAGCTGGTGTTC
Rab6aCORE_R	ATGTTTCTCGAGTTACAAAGCTGCTGCT
PISTcc1_F	TTTTTTTCATATGTCCATGTTCCGGTGG
Pistcc1_R	ATGTTTCTCGAGTTAAAGCTGCAGCTG
bicD2_miniCORE_F	TTT TTT TCA TAT GAA GAG CAA GTA TGA G
bicD2_miniCORE_R	ATG TTT CTC GAG TTA CAG CAG CGA GTT CAG
bicD2_miniCd10_R	ATG TTT CTC GAG TTA GGC GGC TTT GGC ACG
PISTcc1CORE_F	TTT TTT TCA TAT GCA AAT CAA CCA CAA GC
PIST2cc_R	ATG TTT CTC GAG TTA ATA TAC TTC AGC CT
p150cc_F	TTTTTTTCATATGTTGAAGAAGTCACTCAAGATTAAGGGAGAG
p150cc_R_	ATGTTTCTCGAGTTAGTCAGCCTGGAGTGCATCCATTGT

3.1.8 Accession Numbers of Rab6a and Rab6a - Effectors

DEFINITION: RAB6A protein [Homo sapiens].
ACCESSION: AAH68486
VERSION: AAH68486.1 GI:46249771

DEFINITION: bicaudal D homolog 2 isoform 1 [Homo sapiens].
ACCESSION: NP_001003800
VERSION: NP_001003800.1 GI:51479166

DEFINITION: Dynactin-1 (150 kDa dynein-associated polypeptide) (p150-glued) [Homo sapiens]
ACCESSION: Q14203
VERSION: Q14203 GI:17375490

DEFINITION: PIST [Homo sapiens].
ACCESSION: AAG00572
VERSION: AAG00572.1 GI:9837431

3.2 General instrumentation

Protein purifications were typically carried out on either Pharmacia Biotech GradiFrac system or Äkta prime system (GE Healthcare, Uppsala, Sweden) with REC 112 recorder. Centrifugation was performed using Eppendorf 5415C/D benchtop centrifuges (Eppendorf, Cologne, Germany) or an Avanti J20-XP Centrifuge from Beckman Coulter (Palo Alto, CA, USA). For preparative ultracentrifugation a Beckmann Optima L-70K centrifuge was used. SDS-PAGE was performed using the Biorad Mini-Protean II system. Measurements of the pH were performed using a pH-meter 761 from Calimatic Knick (Berlin, Germany). Deionized water (ddH2O) was produced by an apparatus from Millipore (Eschborn, Germany). Dialysis tubes were from Schleicher and Schuell (Dassel, Germany). For concentration of proteins various devices from Millipore (Eschborn, Germany) were used.
Electroporation cuvettes from BioRad (München) and precision balance METTLER PM 480 Delta Range Mettler-Toledo-GmbH (Giessen) were used. The LS 55 Luminescence fluorescene fotospectrometer was supplied by Perkin Elmer (Wellesley, USA). MALDI-TOF-mass spectrometry was done on a Voyager system from Applied Biosystems (USA). A Stopped Flow Multi-Mixing Spectrofluorimeter SF-61MX with IS-2 Rapid Kinetics High Tech Scientific (Salisbury, UK) was used. Isothermal titration calorimetry was done using a VP-ITC and ThermoVac system from MicroCal (Northampton, USA). Ultrasonic bath Sonorex Super RK 103 H Bandelin (Berlin) was used for degassing of buffers and solutions. UV-Visible-spectrometer DU 640 Beckman Coulter (USA) was used for absorbance and fluorescence measurements. HPLC 600S controller with 626 pump system, autosampler (717plus) absorbance (2487 Dual λ Absorbance) and fluorescence (2475 Multi λ Fluorescence) detectors was supplied by Waters (Milford, Massachusetts, USA). Protein and DNA concentration determination was carried out using a Nanodrop system from peQLab Biotechnology. Infors-HT shakers (Infors AG, Bottmingen CH) were used for aeration and temperature control of bacterial cultures.

3.2.1 Chromatography Columns and Matrices

Matrix Materials

DEAE-Sepharose Amersham Biosciences (Freiburg)
HiTrap SP Amersham Biosciences (Freiburg)
Ni-NTA Sephadex-superflow Qiagen (Hilden)
GSH Superflow (Matrix) Amersham Biosciences (Freiburg)

Columns

HiTrap crude FF Amersham Biosciences (Freiburg)
Hypersil-C18 25/4,6 (HPLC) Bischoff (Leonberg)
NAP-5 (gelfiltration) Amersham Biosciences (Freiburg)
Q-Sepharose (matrix) Amersham Biosciences (Freiburg)
Superdex 75 16/60 (gelfiltration) Amersham Biosciences (Freiburg)
Superdex 75 HR10/30 (gelfiltration) Amersham Biosciences (Freiburg)
Superdex 200 16/60 (gelfiltration) Amersham Biosciences (Freiburg)
Superdex 200 HR10/30 (gelfiltration) Amersham Biosciences (Freiburg)

3.3 Molecular Biological Methods

3.3.1 Agarose Gelelectrophoresis

Purification and analysis of DNA-fragments was carried out using an agarose concentration between 0.8 and 1.2 % (w/v), depending on the size of the DNA fragment. The required amount of agarose was solubilized by heating in TAE buffer with added ethidium bromide at a final concentration of 0.5 µg/mL. The gel was poured into the flatbed gel casting equipment and allowed to polymerize. Samples were prepared with 1/6th volume equivalent DNA loading buffer and the gels were run at 10 V/cm, immersed in TAE-buffer, until fragment separation was complete. For detection of the DNA and documentation a UV-transluminating system with attached digitalcamera was used at a wavelength of 312 nm. A DNA-molecular weight standard (DNA Ladder, New England Biolabs (Beverly, USA)) was used for determination of the DNA-fragment size.

- TAE buffer: 200 mM Tris/acetat pH 8.0, 5 mM EDTA
- Sample buffer: 0,25% (w/v) bromphenol blue, 30% (v/v) glycerin

3.3.2 Preparation of Plasmid DNA

Plasmid DNA was purified using the plasmid mini-prep kit (peQLab Biotechnology GmbH) as following the instrtuctions of the supplier: A single bacterial colony was used to seed 4 mL of LB medium containing the appropriate antibiotic(s) and the culture grown overnight (10 - 12 h) at 37° C. Cells were harvested by centrifugation at 5000 g for 5 min and lysed by alkaline/SDS treatment. Precipitated chromosomal DNA, lipids and proteins were removed by centrifugation and the supernatant was loaded on a silica spin column. Following a washing step, the plasmid DNA was eluted using 40 µL sterile buffer (10 mM TrisHCl pH 8.0) or deionized water.

3.3.3 PCR

3.3.3.1 Preparative PCR

DNA amplification was carried out with polymerase chain reaction (PCR), as described in [182]. A 50 µL reaction mixture typically contained 1 - 10 ng of plasmid template DNA, 10 pM of upstream and downstream primers, 100 µM of dNTP mix, 2-3 units of Expand High Fidelity Polymerase mix (Roche Diagnostics) as well as the corresponding reaction buffer and salts. The PCRreaction was carried out in a MJ Research PTC-200. A denaturation step for 1 min at 96° C was followed by annealing for 30 sec at 50 - 70° C depending on primer length and GC content. Extension occurred at 72°C during a period of 1 - 4 min, depending on the length of the DNA fragment. In general, 15 - 25 cycles of the above temperature profil were sufficient for efficient amplification. Prior to further use, excess salts and buffer was

removed from the PCR sample using the Cycle-Pure Kit from peQLab Biotechnology GmbH.

3.3.3.2 Colony PCR Screen

Single colonies were picked from an agar plate and resuspended in 50 µl of sterile ddH_2O in a PCR test tube using sterile eppendorf filter tips. After replicating the selected colonies by streaking of the cell suspension onto a new agar plate containing the required antibiotics, the samples were heated to 90°C for 5 min. 5 µL of this suspension were mixed with 5 µL of PCR mix, containing 100 µM of each dNTP, 5 pmol of each primer, 1 unit of BioTherm polymerase (Gene Craft) in the corresponding buffer. The PCR reactions were carried out as follows: 25 cycles of denaturation for 30 sec at 96°C, annealing for 30 sec at 50 - 70°C, and primer extension for 1 - 4 min at 72°C. The PCR products were analyzed by agarose gel electrophoresis.

3.3.3.3 Mutagenesis of Rab6a

For site-directed insertion of point-mutations into the sequence of Rab6a coding expression vectors the QuikChange Site-Directed Mutagenesis Kit (Stratagene, La Jolla, USA) was used. To reduce background of parental plasmid DNA, samples underwent alkaline treatment before following the instructions of the supplier. For the alkaline treatment, 1 - 5 µg plasmid DNA in 40 µL ddH_2O were incubated for 15 min at 37°C together with 10 µL of a mixture of 1 M NaOH / 1 mM EDTA. The reaction was neutralized with 5 µL 3 M sodium acetate (pH 4.8) and the DNA precipitated by addition of 150 µL ice-cold ethanol. After centrifugation for 10 min at 4°C the supernatant was removed and the pellet washed with 150 µL 70 % ethanol (v/v). Following centrifugation for 3 min the supernatant was removed, residual ethanol allowed to evaporate and the DNA recovered by addition of 20 µL ddH_2O.

3.3.4 Restriction enzyme digestion

Restriction digests of DNA fragments were performed using enzymes and buffers from New England Biolabs (Beverly, USA) or Fermentas (St. Leon-Rot, Germany) as recommended by the manufacturers. The reaction mixture was incubated at the appropriate temperature, according to the used enzyme, stopped by addition of DNA loading buffer after 2 - 3 h. Fragments produced by restriction enzyme digestion were separated using agarose gel electrophoresis, which was followed by purification using the Gel Extraction Kit from Qiagen.

3.3.5 Ligation

For ligation 50 - 100 ng of linear plasmid DNA was mixed with a 5 - 10 fold molar excess of fragment DNA, 5 U T4-DNA Ligase (Fermentas) and appropriate buffer in a total volume of 10 µL. Ligation was performed for 2 - 3 h at roomtemperature.

3.3.6 Sequenzing of DNA constructs

Sequencing of the cloned DNA fragments using the BigDyeDesoxy terminator cycle sequencing kit and an ABI Prism 373XL machine (Applied Biosystems, Weiterstadt, Germany) was carried out by R. Anders (ZE Biotechnologie). The sequencing reactions contained 0.5 - 1 µg plasmid DNA, 3 pmol of the corresponding primers, and 4 µL BigDye termination mix in a final volume of 10 µL. 25 cycles of a temperature profil were performed with the following parameters: Denaturation for 30 sec at 96°C (1 min for the first cycle), annealing for 1 min at 50°C, and primer extension for 4 min at 60°C.

3.3.7 Preparation and transformation of competent cells

For preparation of electrocompetent cells [183] 1 L of LB medium was inoculated with an aliquot of an overnight culture of the desired *E.coli* strain, to an OD_{600} of 0.05. Cells possessing antibiotic resistance genes (e.g. BL21(DE3) codon plus RIL) were grown in the presence of the corresponding antibiotic. The culture was grown at 37°C on a shaker, to reach a final OD_{600} of 0.8. Following this the culture was incubated on ice for 20 min, transferred to sterile centrifugation vessels and centrifuged for 10 min at 4°C and 2000 g. After decanting of the supernatant, the bacterial cell pellet was gently resuspended in 5 mL of ice-cold sterile 0.125 % (w/v) yeast extract, 0.25 % (w/v) tryptone, 10 % (v/v) glycerol (GYT) and recentrifuged as described above. Cells were resuspended in a final volume of 1 mL GYT, dispensed in 50 µL aliquots, shock frozen in liquid nitrogen and stored at -80°C.
For transformation, ~1 ng of DNA was added to the thawed cell suspension in a chilled electroporation cuvette on ice. Electrotransformation was carried out by applying a high voltage pulse using the *E.coli* Pulser from Biorad at 25 µF, 200 Ω and 2.5 kV. 1 mL of LB medium was added to the cell suspension and the culture incubated at 37°C for 45 min. Transformed cells were selected on agar plates containing the corresponding antibiotics.

3.3.8 DNA Purification

3.3.8.1 Products of Restriction Enzyme Digest

DNA fragments produced by restriction enzyme digestion were purified via preparative agarose gel electrophoresis. A Generuler 1 kb DNA ladder (Fermentas) was used as a molecular weight standard. The band of interest was excised and

extracted from the gel using a gel extraction kit from Qiagen according to the instructions of the manufacturer.

3.3.8.2 DNA Fragments from PCR

DNA fragments produced in polymerase chain reactions were freed from excess salts, primers and buffer components using the Cycle Pure Kit from peQLab Biotechnology GmbH (Erlangen, Germany), following instructions of the supplier.

3.4 Protein Expression

All constructs of Rab6a and the effectors bicaudalD2, PIST and p150 were recombinantly expressed using vectors based on the T7-polymerase expression system under the control of the IPTG-inducible lacUV5-promotor [179]. The bacterial expression strain *E.coli* BL21 (DE3) *RIL* contains an additional plasmid coding for tRNAs with triplet codons for arginine for arginine (R), isoleucine (I) and leucine (L) that are rare in *E.coli*.

3.4.1 Rab6a

For expression of Rab6a 3 L LB-medium containing 125 mg/mL ampicillin was inoculated with an aliquot of an overnight culture to an OD_{600} of ~0.05. The culture was incubated in flasks with baffles in a shaker at 37°C and 100 rpm till the OD_{600} reached ~0.6. For induction of the recombinant over-expression, IPTG was added to the culture to a final concentration of 0.4 mM. The culture was further incubated at 30°C and 130 rpm, before harvesting the cells 5 - 6 h after induction, by centrifugation for 40 min at 4200 g and 4°C. The bacterial pellet was washed once by resuspension with ice-cold PBS buffer followed by another 20 min centrifugation. Finaly, the pellet was frozen and stored at -80°C.

PBS buffer: 10 mM Na_2HPO_4, 2 mM KH_2PO_4, 140 mM NaCl, 3 mM KCl, pH adjusted to 7.4 with HCl

3.4.2 Effectors

For expression of Rab6a-effectors 5 L cultures were grown and the above procedure adjusted as described in the following: After addition of IPTG the culture was further incubated over night at 18°C and 130 rpm, before harvesting the cells 10 - 15 h post induction. The bacterial pellet was washed once with ice-cold PBS buffer containing the protease inhibitor PMSF at a concentration of 1 mM.

3.4.3 Uniformly ^{15}N-labelled Proteins for NMR

For NMR spectroscopic measurements uniformly ^{15}N-labelled proteins were recombinantly expressed in 1 L cultures using M9 minimal medium with added glucose (10 mg/mL), $^{15}NH_4Cl$ (1 mg/mL) as the isotope source, 100 mg/mL ampicillin and trace element additions (3.1.4). The procedure described above was adjusted to the slower growth of the bacterial culture in minimal medium as follows: The culture was inoculated with an aliquot of an overnight culture to an OD_{600} of ~0.1 and grown at 37°C on a shaker at 100 rpm to an OD_{600} of ~0.8. Recombinant expression was induced by addition of 0.6 mM IPTG and, following this, the culture was further grown overnight (12 - 15 h) at 21°C and 130 rpm.

3.5 Analytical Methods

3.5.1 Denaturing SDS-PAGE [184]

Typically 5 % stacking and 15 % resolving SDS-PAGE gels were used for the analysis of proteins in a mass range of 12 to 65 kDa. Protein samples were prepared by mixing with an equal amount of SDS-PAGE sample buffer (2x) and heating for 5 min at 95° C. Gels were run at ca. 10 V/cm until the bromphenol blue front had entered the buffer solution. The proteins were subsequently stained using a solution of Coomassie brilliant blue. A molecular weight standard was used for comparative analysis of the proteins.

stacking gel: 5 % acrylamid/bis-acrylamid (37.5:1), 125 mM TrisHCl pH 6.8, 0.06 % (w/v) SDS, 50 µL 10 % (w/v) APS and 5 µL TEMED in 10 ml gel solution to start polymerization

stacking gel buffer: 0.5 M TrisHCl pH 6.8, 0,4 % (w/v) SDS

resolving gel: 15 % acrylamid/bis-acrylamid (37.5:1), 375 mM TrisHCl pH 8.8, 0.1% (w/v) SDS, 50 µL 10 % (w/v) APS and 5 µL TEMED in 10 ml gel solution

resolving gel buffer: 1.5 M TrisHCl pH 8.8, 0.4 % SDS (w/v) SDS

SDS-sample buffer: 100 mM TrisHCl pH 6.8, 20 % (v/v) glycerol, 2 % (w/v) SDS, 0.1 % (w/v) bromphenol blue, 200 mM (v/v) β-mercaptoethanol

low molecular weight standard (Amersham Biosciences): phosphorylase b (94 kDa), bovine serumalbumin (66 kDa), ovalbumin (45 kDa), carboanhydrase (30 kDa), trypsininhibitor (20,1 kDa), α-lactalbumin (14,4 kDa).

running buffer: 250 mM Tris-base, 2 M glycine, 1 % (w/v) SDS

Coomassie stain: 0.1 % (w/v) Coomassie blue R250, 40 % (v/v) ethanol, 10 % (v/v) acetic acid

destain solution: 10 % (v/v) ethanol, 5 % (v/v) acetic acid

3.5.2 Protein Concentration Determination

3.5.2.1 Based on Bradford Assay[185]

The method makes use of the absorbance shift in the dye Coomassie blue when bound to arginine and hydrophobic amino acid residues of a protein. 1 - 10 µL protein solution (0.1-1 mg/ml) was mixed with ddH_2O to give a total volume of 100 µL. After addition of 900 µL Bradford reagent, the mixture was incubated at room temperature for 10 min. Following this, the extinction at 595 nm was measured and the protein concentration determined by correlation to a BSA calibration curve.

3.5.2.2 Protein Concentration Based on Absorption at 280 nm

The method makes use of the absorbance of aromatic amino acid sidechains at 280 nm. For a protein of known calculated mass and extinction coefficient ε_λ, the protein concentration of a sample can be determined from its extinction, following the *Lambert-Beer-law*:

$$c = E_\lambda / \varepsilon_\lambda \times l$$

Where c the concentration of the sample, E_λ is the extinction and l the pathlength of the light.

Following the instructions of the supplier a NanoDrop machine (peQLab Biotechnology) was used to determine protein concentrations. Molecular weights and extinction coefficients of proteins were calculated using the *ProtParam* tool of the *ExPASy* bioinformatics server[186].

3.5.3 MALDI-TOF-mass spectrometry

MALDI spectra were recorded on a Voyager-DE Pro Biospectrometry workstation from Applied Biosystems (Weiterstadt, Germany). Protein samples were desalted using small GF spin columns (Quiagen, Hilden, Germany) and mixed with an equal volume of sample matrix (10 mg/ml sinapinic acid and 0.1 % (v/v) TFA in water / acetonitril (1:1)). The mixture was quickly spotted on a MALDI sample plate, air-dried and spectra were measured with the following device settings: acceleration voltage = 25 kV, grid voltage = 93 %, extraction delay time = 750 ns and guide wire = 0.3 %. The laser intensity was manually adjusted during the measurements in order to obtain an optimal signal to noise ratio. Calibrations were carried out using a protein mixture of defined molecular mass (Sigma). Spectra recording and data evaluation was performed using the supplied Voyager software package.

3.5.3.1 Extraction of Whole Protein Bands from SDS-PAGE Gels

The extraction procedure for whole proteins from SDS-PAGE gels for analysis by MALDI-MS was adapted from Cohen and Chait[187]. The band of interest was excised from the gel and completely destained in a large volume of acetic acide / ethanol (0.1:1). After crushing the gel in an eppendorf tube, ~ 30 - 40 µL MALDI-MS matrix solution is added to cover the pieces. The tube is closed and vortexed at room temperature for 2 h. Crystallisation of the matrix was induced by leaving open the tube for 1 -2 h with vortexing. 1 µL of the crystal-containing supernatant was immediately analysed by MS, while the sample was closed and left vortexing for further extraction. Samples of the sample were analysed after extraction for 4 - 12 h, until the obtained signal to noise ratio was sufficient.

3.5.4 LC-ESI-MS

Liquide chromatography in combination with electronspray ionisation mass spectrometry (LC-ESI-MS) analysis was performed on an Agilent 1100 series chromatography system (Hewlett Packard) equipped with an LCQ electrospray mass spectrometer (Finnigan, San Jose, USA) using Jupiter C4 columns (5 µm, 15 x 0.46 cm, 300 Å pore-size) from Phenomenex (Aschaffenburg, Germany). For LC-separations a gradient of buffer B (0.1 % formic acid in acetonitrile) in buffer A (0.1 % formic acid in water) with a constant flow-rate of 1 ml/min was employed. Upon sample injection, a ratio of 20 % buffer B was kept constant for 2 min. Elution was achieved using a linear gradient of 20-50 % buffer B in buffer A over 13 min followed by a steep gradient (50-90 % buffer B) over 3 min. The column was extensively flushed for at least 10 min with 95 % buffer B. Data evaluation and deconvolution was carried out using the Xcalibur software package.

3.5.5 Analytical reversed-phase HPLC

For analysis of the nucleotide bound to the GTPase, the progress of nucleotide exchange or nucleotide hydrolysis, analytical reversed-phase high performance liquide chromatography was performed. A Waters 600 chromatography instrument equipped with a Waters 2475 fluorescence detector and a Waters 2487 absorbance detector (Waters, Milford, MA, USA) was used with a Hypersil-C18 column (5 µm, 12 x 0.5 cm,) from Phenomenex (Aschaffenburg, Germany). GTP, GppNHp and GDP were separated using an isocratic elution method with a flowrate of 1.5 mL/min. Nucleotides were detected at an absorption wavelength of 254 nm.
Mant-GppNHp and mant-GDP were eluted with a linear gradient of buffer B in buffer A at a flow rate of 1.5 mL/min. The column was equilibrated with 5 % buffer B in buffer A. Upon sample injection individual components eluted upon a linear gradient (30-70 % buffer B) over 20 min. Afterwards the column was flushed for at least 5 min with 100 % buffer B in order to elute hydrophobic compounds. For detection, the nucleotides were excited at 356 nm and fluorescence was detected at 448 nm. Data analysis was carried out using the Empower software package provided by Waters.

- *isocratic buffer*: 100 mM KP_i pH 6.5, 10 mM TBAB, 10% acetonitril
- *buffer A*: 50 mM KP_i pH 6,5
- *buffer B*: 70 % acetonitril in ddH_2O

3.5.6 Analytical Gel-Filtration (GF)

Analytical size-exclusion chromatography was carried out using a HPLC 600S controller with 626 pump system, autosampler (717plus) absorbance (2487 Dual λ Absorbance) and fluorescence (2475 Multi λ Fluorescence) detectors supplied by Waters (Milford, Massachusetts, USA). Pre-equilibrated Superdex 75 HR10/30 and 200 HR10/30 gelfiltration columns were used, depending on the calculated molecular weight of the analysed protein. The molecular weight of the protein was determined by correlating the corresponding elution volume with a calibration calibration curve that was based on proteins of known size.

- *protein standard*: Gel Filtration Standard #151-1901 (BioRad, München) + albumin (61 kDa) and chymotrypsinogen A (25 kDa)

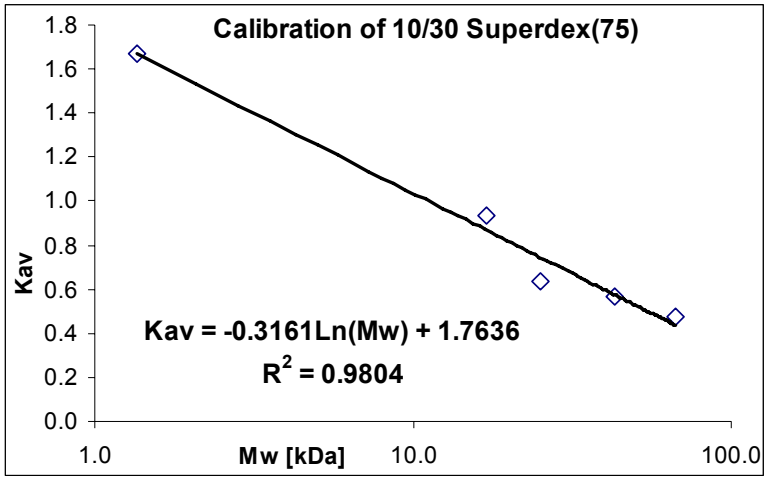

V_0= 7 mL, V_t = 26 mL
Flowrate: 0.5 mL/min

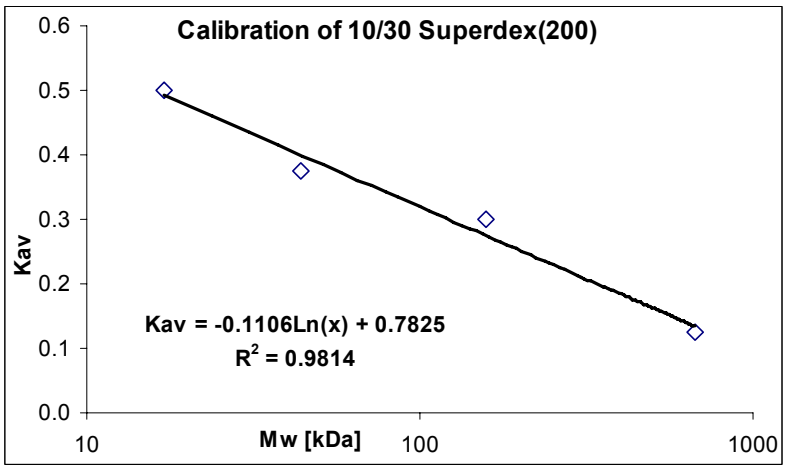

V_0= 7 mL, V_t = 26 mL
Flowrate: 0.5 mL/min

From: $$K_{av} = \frac{V_e - V_0}{V_t - V_0},$$

where V_0 is the dead volume, V_t is the total volume and V_e is the elution volume of the protein, the molecular weight M_w can becalculated, following the equation:

$$M_w = e^{-\frac{(K_{av} - B)}{A}}$$

3.6 Protein-Biochemical Methods

3.6.1 Protein Purification

All chromatographic purification methods were carried out on Äkta FPLC or Waters HPLC systems, at 4°C using filtered buffers.

3.6.1.1 Rab6a

The bakterial pellet was thawed and resuspended in lysis buffer befor breaking the cells by two passages through a microfluidizer (Microfluidics Corporation) at 4°C and 950 kPa. The lysate was cleared from the cell debris by centrifugation (40 min at 45000×g and 4°C) and consecutive filtration of the supernatant. After addition of 5 mM imidazole, the lysate was loaded onto 5 mL Ni-HisTrap FF crude affinity chromatography column equilibrated with buffer A. The column was washed with buffer A until the detector signal at 280 nm returned to baseline. Proteins unspecificly bound to the column matrix were eluted with 5 % buffer B. His_6-tagged protein was eluted in 50 column volumes with a linaer gradient from 5 to 40% buffer B. Target protein containing fractions were identified by SDS-PAGE, pooled and the total amount of protein determined by a Bradford assay. For removal of the affinity tag, TEV protease was added to the protein sample typically at a 1:30 molar ratio, before overnight dialysis at 4°C in dialysis buffer. TEV protease and His_6-tag were removed by passing the dialysed sample over a Ni-HisTrap FF crude affinity chromatography column. The flowthrough was analysed for protein content and tag-cleavage by SDS-PAGE, before concentrating the sample via membranfiltration.
Size-exclusion chromatography on a Superdex(75) 26/60 column at a flowrate of 3 mL/min GFC buffer was used as a final purification step to ensure homogeneity and to desalt the protein sample. Fractions containing the target protein were identified by SDS-PAGE, the pooled sample was concentrated by membrane filtration and aliquots shock-frozen in liquid nitrogen before storing at -80°C.

- *lysis buffer*: 0.5× PBS 10 mM Na_2HPO_4, 2 mM KH_2PO_4, 140 mM NaCl, 3 mM KCl, pH adjusted to 7.4 with HCl, 2 mM β-mercapto ethanol, 1 mM PMSF
- *buffer A*: 50 mM TrisHCl pH 7.5, 300 mM LiCl, 2 mM β-mercapto ethanol
- *buffer B*: as buffer A + 500 mM imidazole
- *dialysis buffer*: 30 mM TrisHCl pH 7.5, 150 mM LiCl, 2 mM β-mercapto ethanol
- *GFC buffer*: 30 mM TrisHCl pH 7.5, 50 mM LiCl, 5 mM DTT, 1 mM $MgCl_2$ and 100 µM GTP

3.6.1.2 Rab6a-Effectors

For purification of effector constructs containing a His_6- or His_6-fusion tag, the procedure described above was adjusted as follows:
In addition to PMSF the protease inhibitor mixture CLAP was added to the cell suspension before lysis. After washing the loaded Ni-HisTrap FF crude affinity chromatography column with buffer A, an additional washing step with 6 column volumes of wash buffer containing 0.5 % (w/v) CHAPS was applied. After this the column was washed with buffer A until the detector signal at 280 nm returned to baseline, prior to removal of unspecific bound protein by washing the column with 5% buffer B. While all constructs of PIST and p150 were TEV digested, no protease was added to the overnight dialysis in the case of $_{GST}$bicD2_mini and the protein further purified containing His_6-GST-tag. Size-exclusion chromatography was carried out as described above using either Superdex(75) or Superdex(200) preparative scale columns, according to the molecular mass of the purified protein.

- *lysis buffer*: 0.5× PBS 5 mM Na_2HPO_4, 1 mM KH_2PO_4, 70 mM NaCl, 1.5 mM KCl, pH adjusted to 7.4 with HCl, 2 mM β-mercapto ethanol, 1 mM PMSF, CLAP: (chymostatin, leupeptin, antipain, pepstatin A in DMSO) at 5 µg/mL final concentration
- *buffer A*: 50 mM TrisHCl pH 7.5, 300 mM LiCl, 2 mM β-mercapto ethanol
- *buffer B*: as buffer A + 500 mM imidazole
- *wash buffer*: 50 mM TrisHCl pH 7.5, 300 mM LiCl, 2 mM β-mercapto ethanol, 0.5 % (w/v) CHAPS
- *dialysis buffer*: 30 mM TrisHCl pH 7.5, 150 mM LiCl, 2 mM β-mercapto ethanol
- *GFC buffer*: 30 mM TrisHCl pH 7.5, 40 mM LiCl, 4 % (v/v) glycerol, 5 mM DTT,

3.6.2 Affinity Matrix Binding Assay [188]

24 nmol $_{GST}$bicD2_mini was incubated on a shaker for 30 min at 4°C with 300 µL Glutathion Sepharose 4Fast Flow matrix (Amersham Bioscience) that had been equilibrated with buffer, in a total volume of 1 mL. After washing the matrix with 5 mL buffer, Rab6a was added in a molar ratio of 0.5 and the sample incubated for 1 h under the above conditions. Following this, unbound protein was washed off the matrix with 5 x 2 mL buffer. The GSH-matrix was mixed with SDS-sample buffer, heated to 95°C for 5 min and the supernatant analysed by SDS-PAGE. To check for unspecific binding, Rab6a alone was incubated with the matrix and the sample analysed following the procedure described above.

- *buffer*: 50 mM TrisHCl pH 7.5, 100 mM LiCl, 4 % (v/v) glycerol, 2 mM β-mercapto ethanol, 1 mM $MgCl_2$, 100 µM nucleotide (GTP or GDP)

3.6.3 Preparation of Rab6a-Effector Complexes

For preparation of Rab6a-effector complexes with p150 or PIST, 400 µM of the GTPase were mixed with 200 µM of the effector protein, 10 mM $MgCl_2$ and 1 mM GTP. The sample s were incubated for 1 h on ice before separating the newly formed complex from excess Rab6a and nucleotide by size-exclusion chromatography using a Superdex(200) gelfiltration column. Complex containing fractions were identified by SDS-PAGE, the pooled sample was concentrated by membrane filtration and aliquots shock-frozen in liquid nitrogen before storing at -80°C.

- *GFC buffer*: 30 mM TrisHCl pH 7.5, 80 mM LiCl, 2 % (v/v) glycerol, 5 mM DTT

3.6.3.1 Preparation of the Rab6aΔ27:bicD2_mini complex

For preparation of the Rab6aΔ27:bicD2_mini complex, the GST-tagged minimal Rab6a-binding domain of bicaudalD2 was incubated with GSH-sepharose for 1 h at 4°C on a shaker. 10 µM GTP was added before mixing with Rab6aΔ27 and further incubation for 1 h. After this, the slurry was poured into a column and unbound protein removed by washing with 3 column volumes of buffer. Following addition of 1 mM GTP the complex was TEV digested using the protease at 1:20 molar ratio at 4°C overnight (10 - 12 h) on a shaker. The flow-through was then loaded on a Superdex(75) gelfiltration column, using size-exclusion chromatography for separation of the newly formed complex from TEV protease, unbound protein and excess nucleotide. Rab6aΔ27:bicD2_mini containing fractions were identified by SDS-PAGE and pooled. The sample was concentrated by membrane filtration and, after addition of GTP to a final concentration of 1 mM, the aliquots shock-frozen in liquid nitrogen before storing at -80°C.

- *wash buffer*: 30 mM TrisHCl pH 7.5, 50 mM LiCl, 2 % glycerol (v/v), 5 mM DTT,
- *GFC buffer*: 30 mM TrisHCl pH 7.5, 50 mM LiCl, 5 mM DTT, 10 µM GTP

3.6.4 Nucleotide Exchange

Rab6a was purified in a 1:1 stoichiometric complex with a nucleotide (90% GTP, 10% GDP).

For the preparation of Rab6a●GDP, a sample of freshly purified Rab6a was incubated at room temperature in the presence of 10 mM $MgCl_2$. Hydrolysis of GTP by Rab6a was monitored by HPLC (5.5.5) until no more GTP was detected in the sample (~10 d). Precipitated protein and excess magnesium was removed by centrifugation and gelfiltration using a pre-equilibrated NAP-5 column.

- *GFC buffer*: 30 mM TrisHCl pH 7.5, 50 mM LiCl, 5 mM DTT, 1 mM $MgCl_2$

For exchange of the nucleotide to the unhydrolysable analog GppNHp or the fluorescent analogs mant-GTP, mant-GDP and mant-GppNHp two different methods were used.

3.6.4.1 EDTA-Method

The method exploits the increased nucleotide dissociation from the GTPase upon complexation of the magnesium ion through addition of EDTA. In the presence of a high molar excess of the new nucleotide, magnesium is re-added and the complex of protein and nucleotide stabilised. EDTA was added to the protein solution to a concentration of 10 mM and the sample incubated at room temperature for 1 h. Free nucleotide and magnesium were removed by gelfiltration using a NAP-5 column, pre-equilibrated with buffer A. The above procedure was repeated once. The new nucleotide was added to the sample at a 25-fold molar excess, before incubation for 2 h at room temperature. After addition of 20 mM $MgCl_2$, excess nucleotide and EDTA were removed by gelfiltration using a NAP-5 column, pre-equilibrated with buffer B. Nucleotide exchange was monitored via HPLC as described in 5.5.5.

- *buffer A*: 50 mM TrisHCl pH 7.5, 100 mM LiCl 10 mM EDTA, 2 mM β-mercapto ethanol
- *buffer B*: 50 mM TrisHCl pH 7.5, 100 mM LiCl, 10 mM $MgCl_2$, 2 mM β-mercapto ethanol

3.6.4.2 Enzymatic Degradation using Alkaline Phosphatase [189]

Enzymatic degradation of GTP and GDP by alkaline phosphatase was applied for exchange of the Rab6a-bound nucleotide to the non-hydrolysable nucleotide analogs GppNHp and mant-GppNHp.

The protein sample was brought into NE buffer by gelfiltration using a pre-equilibrated NAP-5 column. Dissociation of nucleotide from the protein is increased through the presence of $(NH_4)_2SO_4$, the nucleotide analog was used at a 5-fold molar excess and digest of the free GTP started by addition of 5 U/mg alkaline phosphatase. Samples were incubated at room temperature and the nucleotide exchange monitored by HPLC-analysis. After completion of the exchange reaction (~24 h) 10 mM $MgCl_2$ was added and excess nucleotide and guanosine removed by gelfiltration using a NAP-5 column pre-equilibrated with buffer B.

- *NE buffer*: 50 mM TrisHCl pH 8.5, 200 mM $(NH_4)_2SO_4$, 5 mM DTT, 10 µM $ZnCl_2$
- *buffer B*: 50 mM TrisHCl pH 7.5, 100 mM LiCl, 10 mM $MgCl_2$, 2 mM β-mercapto ethanol

3.6.5 Limited Proteolysis of Proteins

For the limited proteolysis of proteins, dilutions of trypsin (1 mg/mL in 10 mM HCl) and of elastase (1 mg/mL in 1 M TrisHCl pH 8.5) were used in varying concentrations, depending on the digested protein. Usually 20 µg of the protein under investigation was added to the reaction mixture. The digests were carried out at room temperature and samples taken for analysis at varying times during the incubation. The digest reaction in the samples was stopped either by addition of an equal volume of SDS-sample buffer, when preparing the sample for SDS-PAGE, or by addition of 2 mM PMSF, when preparing the sample for MALDI-MS.

- *digest reaction mixture*:
  5 µL 1 M NH_4HCO_3 pH 8.5
  10 µL protein solution
  1 µL enzyme solution to 50 µL with ddH_2O

3.7 Biophysical Methods

Fluorescence measurements were obtained with a LS-55 Luminescence Spectrometer (Perkin Elmer). Measurements were carried out in 1 ml quartz cuvettes (Hellma) with continuous stirring and thermostated at 25°C. Stopped-flow measurements were performed on an Applied Photophysics SX.18MV-R apparatus (Surrey, UK) at 25°C or 4°C.

3.7.1 Nucleotide Dissociation Assay

Steady-state fluorescence measurements for monitoring the spontaneous nucleotide dissociation of Rab6a were performed in 50 mM HEPES pH 7.5, 150 mM LiCl, 10 mM $MgCl_2$, 5 mM DTT and 3 % glycerol. 100 µM GDP was added to the degassed buffer and incubated for 5 min at 25° C. The excitation and emission monochromators were set to 295 nm and 448 nm, respectively. 200 nM Rab6a●mantGDP was then added to the cuvette and the fluorescence signal was monitored over a time of 21 h. The change in fluorescence was plotted as a function of the time and corrected for unspecific fluorescence. The data was fitted to the following equation using Origin 7.0 (MicroCal, Northampton, USA):

$$Y = Y_{\infty} + Ae^{-k_1 t} \qquad [1]$$

where Y is the observed fluorescence, Y_{∞} is the fluorescence at t = ∞, A is the signal amplitude, t is the time, and k_1 yields the rate constant, which equals k_{off} for dissociation of the used nucleotide.

Kinetics of ligand dissociation (190)

The dissociation rate constant (k_1) of a labeled ligand (L*, mantGDP) from its complex (PL*) can be determined by displacing it with an unlabeled ligand (L, GDP). The simplest model that describes both reactions is:

$$PL^* \underset{k_{-1}}{\overset{k_1}{\rightleftharpoons}} L^* + P + L \underset{k_{-2}}{\overset{k_2}{\rightleftharpoons}} P\,L$$

The disappearance of PL* can then be described by

$$\frac{d[PL^*]}{dt} = k_{-1}[L^*][P] - k_1[PL^*] \qquad [2]$$

In the present case both labeled and unlabeled ligand interact with the protein in a similar manner and that the rate constants describing the association and

dissociation reaction are in the same order of magnitude (i.e. $k_1 \sim k_2$ and $k_{-1} \sim k_{-2}$). If the concentration of the components is chosen such that $[L^*] \sim [P] << [L]$, then the association rate of the unlabeled competitor L with the free protein is significantly faster than the reassociation of the labeled ligand L^* (i.e. $k_{-2}[L] >> k_{-1}[L^*][P]$. This would make the dissociation of PL^* quasi irreversible. Under such conditions the concentration of free (unbound) protein P is very low ([P] → 0) and the term $k_{-1}[L^*][P]$ is negligible, which will give:

$$\frac{d[PL^*]}{dt} = -k_1[PL^*] \qquad [3]$$

and upon integration: $[PL^*] = [PL^*]_0 e^{-k_1 t}$ [4].

3.7.2 Transient Kinetics (stopped-flow)

To determine the rates for association (k_{on}) and for dissociation (k_{off}) of Rab6a with its effectors a Spectrofluorimeter SF-61MX with IS-2 Rapid Kinetics (High Tech Scientific) was used. Measurements were carried out at 4°C and 25°C in degassed buffer containing 50 mM TrisHCl pH 7.5, 80 mM LiCl, 2 mM $MgCl_2$ and 5 mM DTT. In the applied rapid mixing device the two components under investigation are kept in separate reservoir-syringes. Through application of a pressure impulse (4 bar) on the pistons of the syringes, equal volumes of the two interaction partners are rapidly injected into a mixing chamber. Then, the homogeneous sample enters the measuring cuvette and the volume that is displaced from the measuring cuvette fills a stop-syringe. Complete filling of the stop-syringe leads to a stop of the sample flow and simultaneously triggers the start of the signal detection. The detection delay that follows from this method is ~5 ms. The fluorescence signal of the mant-group at 448 nm caused by FRET resulting from the excitation of the tryptophans in the two proteins at 295 nm, was monitored. To improve the signal to noise ratio, data from eight to twelve single measurements was averaged and used for further analysis.

For the chosen experimental set-up, with [Rab6a●mantGppNHp] << [effector], association can be considered a pseudo-first order reaction and the fluorescence signal can be analysed by fitting to a single exponential equation (3.7.1).

Plotting the observed rate constants of the single exponential fit against the corresponding concentrations of the effector yields a linear relation. The rate of association (k_{on}) can be derived from the slope of the straight line, while the dissociation rate (k_{off}) results from the intercept with the ordinate. Based on k_{on} and k_{off}, the dissociation constant (K_d) for the interaction of Rab6a with its effector follows from:

$$K_d = \frac{k_{off}}{k_{on}}$$

3.7.3 GTPase Activity Assay

GTPase hydrolysis was assayed as a function of time by HPLC as described previously [34,12]. The excess GTP form the storage buffer of the protein sample was removed by passing it over a NAP-5 column (Amersham Biosciences) equilibrated with a buffer containing 50 mM TrisHCl pH 7.5, 100 mM LiCl and 5 mM DTT. The hydrolysis reaction was started by addition of 10 mM $MgCl_2$ at 25°C, and 20 µL samples were withdrawn at appropriate time intervals and analysed by HPLC chromatography.

3.7.4 Isothermal Titration Calorymetry (ITC)[191]

ITC was used as a quantitative approach to determine thermodynamic properties of Rab6a - effector interactions, which are characterized by the free energy (ΔG), enthalpy (ΔH), entropy (ΔS), association constant (K_a) and stoichiometry. All measurements were carried out in 30 mM HEPES pH 7.5, 80 mM, 5 mM DTT, 1 mM $MgCl_2$ and 100 µM nucleotide (GTP or GDP), using a VP-ITC and thermovac system (MicroCal) at 25°C. Samples in syringe and cell were extensively dialysed in the same batch of buffer, before determining their protein concentration by Bradford assay and via absorption at 280 nm (5.5.2.1 and 5.5.2.2). All samples were degassed for at least 10 min at 25°C prior to the experiment.

The time-dependent input of power that is required to maintain equal temperatures between a sample cell in which two binding partners associate and a reference cell is monitored. Heat that is absorbed or generated during a titration is proportional to the fraction of bound interaction partner. Assuming one binding site for the interaction, the heat generated by addition of the binding partner can be calculated from the equation:

$$Q = \frac{V_0 \Delta H_b [M]_t K_a [L]}{(1 + K_a [L])} \qquad [1]$$

where V_0 is the volume of the cell, ΔH_b is the enthalpy of binding per mole of titrated binding partner, $[M]_t$ is the total concentration of protein provided in the cell including free and bound fractions, K_a is the binding constant and [L] is the concentration of the free binding partner. For binding of a protein L to its interaction partner, the association constant is defined as:

K_a = [occupied binding sites] / [free binding sites] [L]

The acquired data was corrected for the increase in volume and for the heat generated through dilution of the titrated binding partner, which were determined in separate control experiments.
The change in the free enthalpy is defined as:

$$\Delta G = -RT \ln K_a = \Delta H - T\Delta S \qquad [2]$$

where ΔH and $T\Delta S$ is the change in enthalpy and entropy respectively, assuming a single binding site. ΔH, K_a and the stoichiometry n of the interaction were determined directly from the experiment. To do so equation 1 is represented in terms of the binding constant and total ligand concentration $[L]_t$ to obtain the quadratic:

$$Q = (n[M]_t \Delta H V_0)/2 \; \{1 + [L]_t/(n[M]_t) + 1/(nK_a[M]_t) - [(1 + [L]_t/(n[M]_t) + 1/(nK_a[M]_t)) - 4[L]_t/(n[M]_t)]^{1/2}\} \qquad [3]$$

ΔH, K_a and n are then optimized using the standard Marquardt method with routines provided in the ORIGIN 7.0 software (MicroCal).

3.8 Structure-Analysis Methods

3.8.1 Crystallographic Methods

3.8.1.1 Protein crystallisation

As with small molecules, proteins are crystallised from oversaturated solutions. These solutions are thermodynamical instable systems that, through generation of a solid phase, make the transition to a stable system. In an ideal case the solid phase is composed of a single crystal, however, more often many small crystals, crystalline agglomerates or amorphous precipitates are observed. In contrast to salt crystals, electrostact attraction of the charged ions is lacking in a protein crystal and the the main forces between the protein molecules are the weaker hydrogen bonds. Furthermore, protein molecules are not rigid, their conformation and surface charge distribution change with temperature, pH and ionic strength of the solution. Flexibility of protein domains hinders ordered packing of the molecules in a crystal, which is why proteins need to be engineered in almost all cases. Crystallisation of Rab6a was performed using micro seeds of crushed crystals in the hanging-drop vapour diffusion method at 293 K. Protein solution is mixed with an equal volume of reservoir solution. Crystals appeared 2 days after micro seeding. Soaking of the crystal in cryoprotection solution prior to cooling in a 100 K nitrogen gas stream was not necessary, due to the used crystallisation conditions.
Diffraction data was recorded using a copper rotating-anode (Enraf-Nonius, Belft) at a wavelength 1.54 Å. An Osmic mirror (OSMIC, Auburn Hills, USA) was used for focusing and a MAR345 phosphor plate detector was utilized for data recording. The obtained data was used for determination of the crystal space group, while high resolution data was recorded during analysis of the crystals at the ESRF beamline ID 14-3 (λ = 0.931 Å).

3.8.1.2 X-ray Crystallography

X-ray beams diffract at the electron sheaths of the protein molecules in the periodical arrangement of the crystal. Constructive interference of the diffracted beams generates a two dimensional diffraction pattern of symmetrically arranged dots on the detector plate. The symmetry of the reflexes correlates to the symmetry of the crystal, while the intensity of the reflexes is a function of atom type and spatial distribution of the atoms in the crystal. Constructive interference only occurs, if the retardation of two x-rays that are reflected from two neighbouring crystal lattices is an integer multiple of the x-ray's wavelength, as described in *Bragg's Law*:

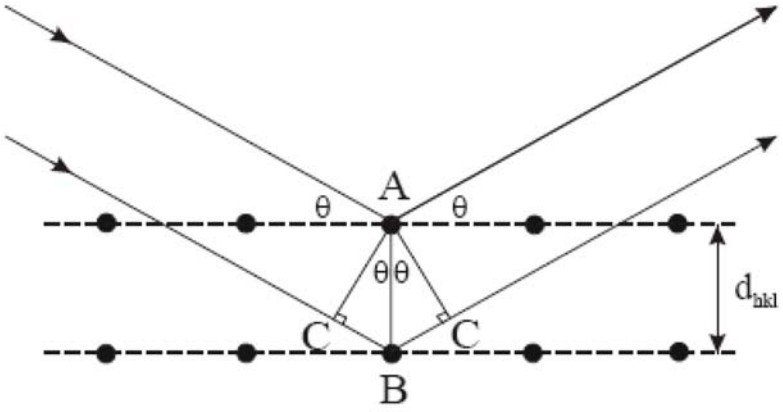

Geometric construction of *Bragg's law*.

$$2 \times d_{hkl} \times \sin\Theta = n \times \lambda \qquad [1]$$

Where d_{hkl} is the distance between crystal lattices, Θ is the scattering angel, n an integer and λ the wavelength of the x-ray radiation.

Bragg's law allows determination of the unit cell dimensions and the symmetry of the crystal. However, for the determination the intensity of reflexes, the diffracted x-rays must be analysed as a simple wave function expressed by the Fourier transformation:

$$f(x) = F \cos 2\pi (hx + \alpha) \qquad [2]$$

or

$$f(x) = F \sin 2\pi (hx + \alpha) \qquad [3]$$

F: amplitude
h: frequency
α: phase

The detected reflexes represent the sum of many diffracted x-rays. Hence, the x-ray that falls onto the detector, as the sum of all contributions coming from all atoms in the unit cell, is more accurately represented by a Fourier series:

$$F_{hkl} = fA + fB + ... + fN' \qquad [4]$$

F_{hkl}: structure factor of reflex hkl
fA: structure factor of atom A
fB: structure factor of atom B
:
fN': structure factor of atom N'

In case the phase information is known, the electron density allocation can be calculated from the intensity of the reflexes through a Fourier transformation. However, only intensities are measured in an x-ray experiment from which structure amplitudes can be calculated, while phase information remains elusive. Various

methods can be employed to obtain the required phase information. In this study the molecular replacement[192] approach was used. For this method, a known structure model of a highly homologous protein is placed in the unit cell of the unknown structure. Through rotation and translation the search model is optimised to fit the position and orientation of the unknown structure. When the search model is placed in the unitcell with sufficient similarity to the unknown structure, the diffraction pattern of the crystal can be approximated with a calculated diffraction pattern of the model and the missing phase information can be deduced.
Molecular replacement for the structure determination of Rab6a was carried out with the program AmoRe [193]. The search model was calculated with the program MODELLER [194] using Rab6●GDP from *P. falciparum* (1D5C) as a template. Refinement was performed using the programs CNS [195] and REFMAC5 [196]. The programs O and PyMOL were used for the model building in maps.

3.8.2 NMR-Spectroscopy[197,198]

In a magnetic field certain magnetic nuclei, such as ^{1}H, ^{13}C, ^{15}N or ^{31}P can adopt nuclear spin states of different energy depending on the strength of the magnetic field and and the gyromagnetic ratio (γ). The gyromagnetic ratio is a characteristic value for each nucleus and is related to its spin angular moment $\vec{J}$ and the torsion moment $\vec{\mu}$ via:

$$\vec{\mu} = \gamma \times \vec{J} = \gamma \times \hbar\sqrt{I(I+1)}$$

$\vec{\mu}$: torsion moment; $\vec{J}$: spin angular moment; γ: gyromagnetic ratio; $\hbar$: Planck's constant; I: spin quantum number

By application of a radio-frequency radiation puls the magnetic nuclei in the magnetic field can be induced to flip between the adopted spin states. The chemical environment of a particular magnetic nucleus in a molecule determines its nuclear magnetic resonance (NMR) properties, namely the energy differences between the orientations and thus the frequency at which the nucleus absorbs energy (its resonance frequency). The measure of this is the chemical shift, given in parts per million (p.p.m.) relative to a reference compound. Magnetic nuclei are affected by each other as well as the applied field, both through chemical bonds (spin-spin coupling) and over long distances (dipole-dipole coupling). This can be exploited to assign resonance signals to particular nuclei in a structure and derive constraints for the distances separating them.

The high spatial proton density in many biomolecules makes ^{1}H-NMR an extremely rich source of structural information on proteins. The same properties make it difficult to extract this abundant structural information from recalcitrant biomolecular samples. Uniform isotopic labelling of macromolecules, where $^{2}H_2O$, $^{15}NH_4Cl$ or ^{13}C-glucose are employed, can result in increased resolution and sensitivity and in reduced complexity of NMR spectra [199].

In heteronuclear single quantum correlation (HSQC), the obtained spectrum has two axes, a proton axis (^{1}H) and a heteronucleus axis (^{15}N). ^{15}N-HSQC experiments are very frequently recorded experiments in protein NMR. Each residue of the protein (except proline) has an amide proton attached to a nitrogen in the peptide bond. If the protein is folded, the peaks are usually well dispersed, and most of the individual peaks can be distinguished. The number of peaks in the spectrum should match the number of residues in the protein, (plus the sidechains that contain nitrogen bound protons).

While it is not possible to assign which peaks correspond to a particular residue in a protein by the HSQC spectrum alone, the HSQC experiment is a useful tool for detecting interactions with ligands, such as other proteins. By comparing the HSQC spectrum of the free protein with the one bound to the ligand, it is possible to find

the changes in the chemical shifts of the peaks, which are most likely to occur in the binding interface.

All NMR experiments were carried out on a Varian Inova 600 spectrometer. Typically, Varian-NMR puls sequences of 2048 x 2048 transients were recorded to obtain $^{1}H/^{15}N$-HSQC-spectra of the different proteins at 27°C. Following transformation of the data to the Bruker format, spectra were analysed using the program Aurelia.

- *^{1}H-NMR buffer*: 20 mM Kp_i pH 6.4, 20 mM LiCl, 5 mM DTT, 0.5 mM $MgCl_2$
- *$^{1}H/^{15}N$-NMR buffer*: 10 mM TrisHCl pH 6.2, 10 mM LiCl, 5 mM DTT, 0.5 mM $MgCl_2$, 8 % D_2O (+ 20 µM GTP, for ^{15}N-Rab6aΔ27)

4 RESULTS AND DISCUSSION

4.1 Design of the Protein Expression Vectors

Defining a construct for expression of recombinant protein in *E.coli* poses a preliminary trial to combine the biophysical and biochemical properties of the resulting protein with the requirements of the experimental set-up. For structural experiments a high level of over-expression is desirable, the protein must be expressed in soluble form and have a high degree of structural order (3.8.1). This may make engineering necessary. However, molecular functionality in the physiological context under investigation must be maintained.
In the case of small GTPases, a number of family members has been characterized biochemicaly and their high resolution structures determined by X-ray or NMR (for review see [200]). Based on the similarity of the structure fold and common biochemical characteristics of this protein family, these examples can be used to guide the design of an expression construct for Rab6. Earlier structural studies on Ras and Rab7 showed that the low degree of structural order of the hypervariable C-terminus was unfavourable for crystallisation and yielded poorly diffracting crystals [201]. In most cases C-terminal truncation of Ras-like proteins does not have an impact on their interaction with nucleotides or effector molecules [12,202], this part of the molecule becomes a first target for engineering in the effort to obtain crystallisable protein.

4.1.1 Rab6a

A gene of human full-length Rab6a (1-208) in a pCR II-TOPO (Invitrogen) plasmid was kindly provided by Francis Barr and Ben Short (Max-Planck-Institut, Martinsried). To allow for later affinity purification, the full-length template was sub-cloned (3.3) into a derivative of the *E.coli* expression vector pET19b (Novagen). This plasmid contains an N-terminal hexahistidine tag followed by a TEV cleavage site that can be removed from the protein by treatment with TEV protease. This produces an N-terminal dipeptide overhang (Gly-His-) that remains as an appendage to the amino acid sequence of the recombinant protein and accounts for an additional 241.7Da. Subsequently, truncated versions of the original Rab6a constructs were generated, based on sequence comparisons with the already crystallised *Plasmodium falciparum* homolog [203]. Hence, Rab6a constructs with a deletion of the last 22 (1-186, Rab6aΔ22) or 27 (1-181, Rab6aΔ27) amino acids were obtained. A third construct lacking the N- and C-terminus (13-175, Rab6aNΔ12CΔ33) was generated.

For comparative analysis of the intrinsic GTPase activity, expression constructs of catalytically inactive mutant Rab6a(Q72L) were generated. Using the QuikChange Site-Directed Mutagenesis (Stratagene) the constructs Rab6a(Q72L) and Rab6aNΔ12CΔ33(Q72L) containing the point-mutations were obtained. The residue Gln72 (Gln61 in H-Ras nomenclature) is crucial for the ability of the GTPase to hydrolyse GTP, since it coordinates a conserved water molecule that carries out the nucleophilic attack on the γ-phosphate group of the nucleotide [204,69]. Substitution of this residue with any other amino acid leads to a dramatic decrease in GTP hydrolysis, rendering the protein constitutively activated [205]. Thus, the resulting proteins were intended as control samples in later binding- or GTPase-assays (see 4.4 and 4.12).

To enable binding of Rab6a to glutathione sepharose matrix for solid phase immobilization, a full-length construct of Rab6a was subcloned into a pGATEV plasmid [180]. This vector comprises the open reading frame for an N-terminal His_6-tag, followed directly by the glutathione-S-transferase (GST) domain and a TEV protease recognition-site adjacent to the 5'-end of the multiple cloning-site. All the Rab6a constructs are summarized in figure 9.

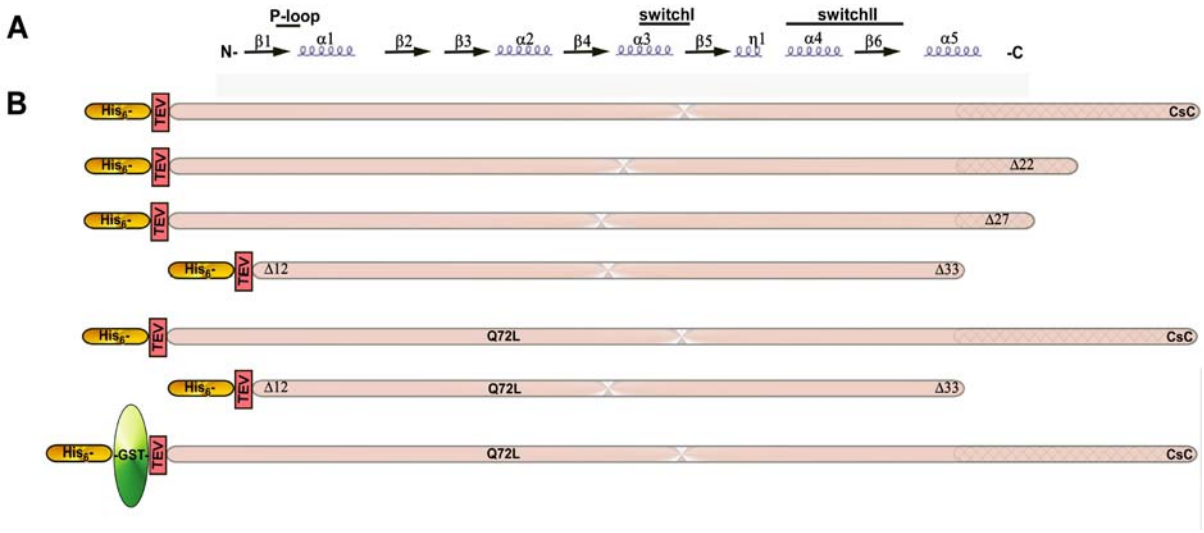

Fig.9 Schematic representation of all Rab6a expression constructs. A Schematic diagram showing structural elements (β-sheets: arrows; α-helices: spirals) and the assignment of functional motifs (P-loop, switch I and II) of Rab6a. **B** Cartoon representation of the designed Rab6a expression constructs including affinity tags (His_6-, GST-) and protease cleavage site (TEV).

4.1.2 Putative Rab6a-Effectors

Unlike the case of Rab6a, no structural information on the Rab6a-effectors was available, making rational design of expression constructs a trial and error procedure. Yeast two-hybrid screens, performed in the group of Francis Barr, gave the first indication of an interaction between the Golgi-resident protein PIST and Rab6a. These studies also confirmed earlier evidence of a direct interaction between Rab6a and the $p150_{glued}$ subunit of dynactin, as well as identifying a C-

terminal region of bicaudalD2 required for binding to Rab6a [148,120]. DNA templates for the Rab6a binding region of $p150_{glued}$ (amino acids 540-1278) and bicaudalD2 (bicD2_minimal, amino acids 706-824) as well as the full length genes were provided in pQE-31 vectors (Qiagen) by Francis Barr and Ben Short. The same group provided a full length construct for PIST.

The first expression test for all three effectors yielded no purifiable protein. Whereas for $p150_{glued}$ and PIST very low to no expression was observed, bicD2_minimal expressed to a very high level, but was found exclusively in inclusion bodies. Hence, all three effectors had to be sub-cloned, following different strategies to obtain expression of soluble and active protein.

For $p150_{glued}$ N.Kholod and M.Kulharia (Alexandrov group) generated an N- and C-terminally truncated construct comprising amino acids 540 to 1041 and cloned it into a pET19b plasmid (3.1.6). This construct (p150) yielded a sufficient level of expression and the resultant protein remained in solution after tag removal.

The full-length construct of PIST was cloned into a pIF1-plasmid [181] by M. Terbek (Alexandrov group). This pET-15b-based plasmid vector comprises the open reading frame for an N-terminal His_6-tag, followed directly by a fragment of the *E. coli* initiation factor-1(IF1) and a TEV protease recognition-site adjacent to the 5'-end of the multiple cloning-site (3.1.6). With the help of this new construct, soluble full-length PIST could be expressed in sufficient amounts and cleavage of the tag yielded soluble protein.

Expression of bicD2_minimal cloned into a pGATEV plasmid [180] resulted in a largely soluble proein where the GST-domain constitutes the larger part of the fusion construct (~29kDa), compared with the Rab6a-binding region of bicaudalD2 (13.5kDa). Removal of the GST-tag was not feasible, since bicD2_minimal precipitated upon TEV digestion. Furthermore, it proved impossible to concentrate $_{GST}$bicD2_minimal to more than ~2mg/mL (~50µM).

A summary of all Rab6a-effector constructs and their respective solubility is given in table 4 (p. 99).

4.2 Expression and Purification of Rab6a

All Rab6a constructs were expressed in *E.coli* BL21-CodonPlus-RIL cells, as described in 3.4.1. After the first purification, using step Ni-affinity chromatography (3.6.1), the recombinant protein accounted for >95% of the eluted proteins. Following TEV-protease digestion and removal of the His_6-tag the proteins were dialysed into low salt buffer and further purified using a Superdex75 size-exclusion chromatography column. In this final purification step a single peak-fraction containing homogeneous monomeric Rab6a with a purity of >99% was obtained for all constructs (see Fig. 10). The overall yield of the Rab6a expression/purification procedure was as high as $25mg_{Rab6a}/L_{culture}$ or $11mg_{Rab6a}/g_{wet\ cellpaste}$. Full-length Rab6a as well as C-terminally truncated constructs could be concentrated to more than 90mg/mL (>4mM) and stayed in solution for many days at room temperature, without showing any visible precipitation. Rab6aNΔ12CΔ33 appeared less stable. Losses during purification of this construct were greater and the protein could not be concentrated to a comparable extent without forming a precipitate.

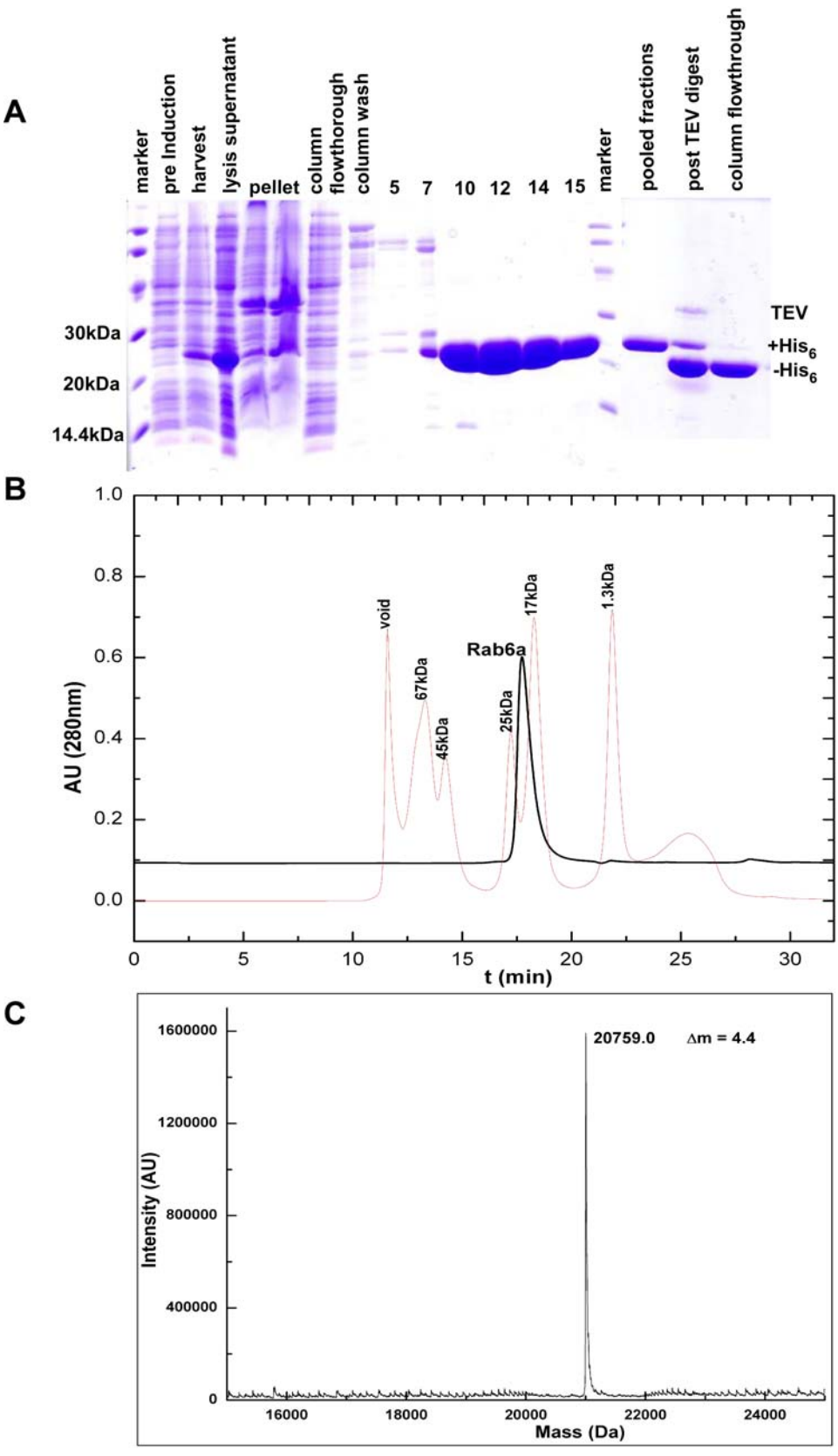

Fig.10 Summary of the results for a typical purification in this case of Rab6aΔ27. A SDS-PAGE of samples taken during Ni-affinity chromatography and to check efficiency of the tag-removal. **B** Chromatogram of the purified Rab6aΔ27 on an analytical Superdex75 size-exclusion column (black line). Red line: molecular weight standard elution profile **C** The exact molecular mass of Rab6aΔ27 (+Gly-His-) was determined using LC-ESI-MS (3.5.4). The acquired mass of 20759Da deviates from the calculated mass of 20754.6Da by only 4.4Da and confirms the results of SDS-PAGE analysis and analytical gelfiltration chromatography.

4.3 Spontaneous Nucleotide-Exchange Activity of Rab6a

Contrary to experiences with other RabGTPases, exchanging the naturally bound GTP in Rab6a with other nucleotides or with fluorescent nucleotide analogues proved to be difficult. In standard procedures for nucleotide exchange, Mg^{+2} is chelated from the nucleotide binding pocket by EDTA. This results in a loss of coordination of the β- and γ-phosphates and leads to a dramatic increase in the dissociation rate of up to three orders of magnitude [12]. In the exchange reaction the nucleotide is then replaced by incubation with a high molar excess of the new nucleotide. The new Rab nucleotide complex is stabilized by the re-addition of magnesium.

This procedure however turned out to be inefficient in the case of Rab6a, resulting in only a partial exchange of the nucleotide within the recommended incubation times. Diverse strategies were tested to overcome this limitation in an effort to obtain Rab6a bound to different nucleotides. In an attempt to achieve nucleotide exchange on matrix-bound Rab6a by incubation with excess of the new nucleotide (adapted from [206]), a GST-tagged full-length Rab6a construct was used. This method led to only minor improvements while significantly increasing the nucleotide consumption. Ultimately, Rab6a•GDP was generated by incubation of the protein sample at room temperature for two weeks, allowing sufficient time for Rab6a intrinsic GTP-hydrolysis activity to fully hydrolyse GTP. Since the protein remained stable in solution without forming a visible precipitate and the fraction of GTP-bound protein fell below the level of detection over the course of the treatment this method was employed routinely.

A variety of spectroscopic methods for the investigation of protein-protein interactions of Rabs with their effectors relies on the use of nucleotide analogues carrying a fluorescent group. Upon binding of an interaction partner to the Rab protein structural rearrangements would, in most cases, alter the environment around the nucleotide binding pocket. These alterations can often be observed by monitoring changes in the fluorescence of the fluorescent group. In order to prepare Rab6a loaded with fluorescently labelled nucleotide analogues two different strategies were successfully pursued. Rab6a loaded with mantGDP was generated adapting an EDTA-based procedure by dramatically increasing the molar ratio of the nucleotide analogue and elongating the incubation steps to yield protein samples of sufficient quality (3.6.4.1). As a fluorescent nucleotide analogue simulating the active state of Rab6a non-hydrolysable mantGppNHp was used. This was done by utilizing a procedure in which any nucleotide dissociating from the GTPase is hydrolysed by alkaline phosphatase and replaced with an equimolar amount of mantGppNHp (3.6.4.2). With these methods protein samples with a high degree of nucleotide substitution were obtained.

In order to find an explanation for why Rab6a resisted standard nucleotide exchange protocols the release of nucleotide from the protein was monitored.

Rab6a contains two tryptophan residues (W67 and W107) in close vicinity to the nucleotide binding pocket, one at the N-terminal part of the switch II region (α2) and the other in helix α3. Excitation of these residues at 295nm leads to *fluorescence resonance-energy transfer* (FRET) to the fluorescent mant-group. The resulting fluorescence signal of the protein-bound mant-nucleotide was monitored in the presence of an excess of unlabelled GDP (3.7.1). Fig.12 shows the change in the fluorescence signal over ~21 hours.

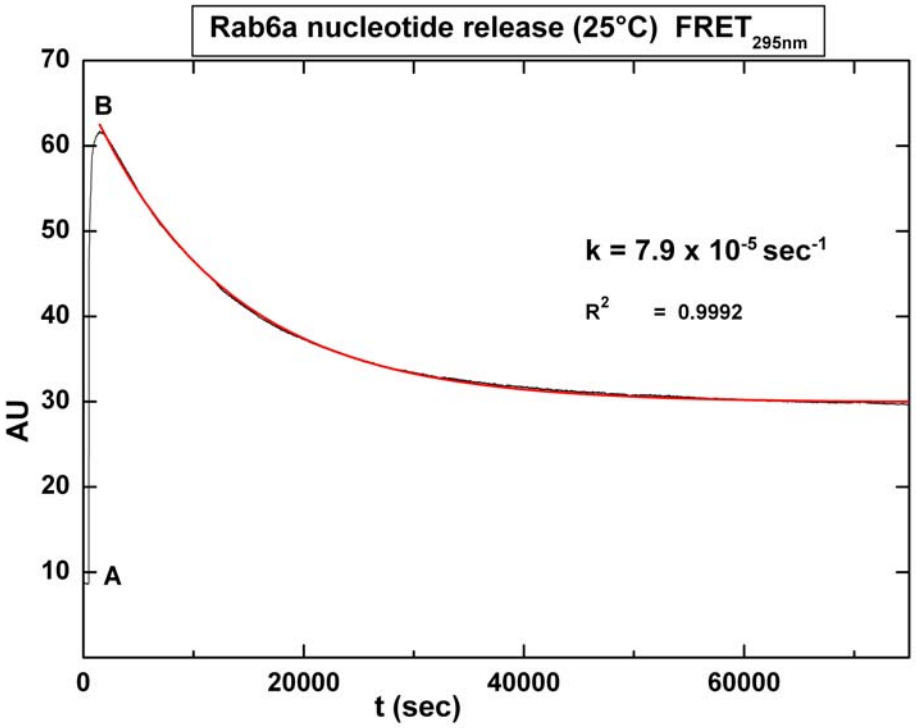

Fig.12 Spontaneous nucleotide exchange of Rab6a. Time course of the fluorescence signal of 200nM Rab6a•mantGppNHp at 25°C in buffer containing 50 mM TrisHCl pH 7.5, 150 mM LiCl, 10 mM $MgCl_2$, 5 mM DTT, 3 % glycerol and 1mM GDP. The exchange reaction was started by addition of the protein to the buffer. The sample was excited at 295nm and the fluorescence, resulting from fluorescence-resonance energy transfer between the protein's tryptophanes and the mant-group, was monitored at a detection wavelength of 448nm. The data of the signal decrease was fitted to a single exponential curve (red), giving a rate constant of 7.9 x 10^{-5} s^{-1}.

The observed signal decline results from dissociation of the mant-nucleotide from the hydrophobic environment of the binding pocket into the bulk solvent and its replacement with unlabelled GDP by the protein. For the chosen experimental conditions (4.7.1) the signal decrease can be analysed as a first order reaction following a single-exponential time course:

$$Y = Y_{\infty} + Ae^{-k_1 t}$$

where Y is the observed fluorescence, Y_∞ is the fluorescence at t = ∞, A is the signal amplitude, t is the time, and k_1 yields the rate constant, which equals k_{off} for dissociation of the used nucleotide. With a rate k_{off} = 7.9 x $10^{-5}$$sec^{-1}$ for mantGDP at 25°C, Rab6a lies well within the range of results obtained in earlier studies for Ypt1

(6 x $10^{-5}$$sec^{-1}$ [207]) or Rab8 (7 x $10^{-4}$$sec^{-1}$ [208]) under comparable conditions. Since the dissociation rate of the nucleotide does not appear to limit its release from the protein, other factors must account for the recalcitrance of Rab6a during nucleotide exchange. In the case of Rab4a single amino acid residues have been associated with the rates of nucleotide release and hydrolytic activity [209]. Detailed structural analysis of Rab6a might help to identify similar molecular determinants of its biophysical properties.

4.4 GTPase Activity of Rab6a

The function of Rab proteins as regulators of vesicular trafficking includes transmission of upstream signals to their downstream effectors. The nucleotide-state dependant formation of an effector binding interface confers the properties of a molecular switch to all Ras-like proteins. In the absence of GAPs the transition from the active GTP-bound to the inactive GDP-bound state is very slow with a rate of hydrolysis in the order of ~$10^{-5}s^{-1}$. Among the members of the Rab family investigated so far, the rates of hydrolysis differ by more than one order of magnitude (Table 1). Rab3a appears to be the most active and Rab7 the slowest RabGTPase currently known [12,210]. The same studies found that the hypervariable C-terminal region of the protein does not contribute to the hydrolysis reaction. Different intrinsic rates of GTP hydrolysis are likely to reflect pathway-specific requirements of individual Rabs. Since highest sequence and structure conservation in Rab proteins is found for regions involved in the catalytic reaction, particular interest lies in pinpointing the single amino acid residues causing the specific transition characteristics seen in the *in-vitro* assays.

Table 1 The rates for intrinsic hydrolysis of GTP at 25°C for some of the biochemically characterized Rab/Ypt-GTPases.

	k at 25°C (sec^{-1})
Rab3a	7.0×10^{-4} [211]
Rab4a	5.0×10^{-5} [209]
Rab5a	5.5×10^{-4} [12]
Rab7	4.5×10^{-5} [12]
Ypt1	3.0×10^{-5} [212]

With half times for GTP turnover between 0.25 and 4.5 hours (for Rab3a and Rab7 respectively) recombinantly expressed Rabs are typically found in the GDP bound state after purification. However, HPLC analysis of the purified recombinant Rab6A demonstrated that more than 90% of the protein was in the GTP bound form, suggesting that the intrinsic rate of hydrolysis of this GTPase is unusually low. To measure the intrinsic GTPase activity the recombinant Rab6a was incubated at 25°C over the course of 6 days while continuously analysing samples by HPLC (3.5.5). Fig.11 depicts the progressive hydrolysis of GTP by Rab6a triggered by addition of Mg^{2+} at t = 0.

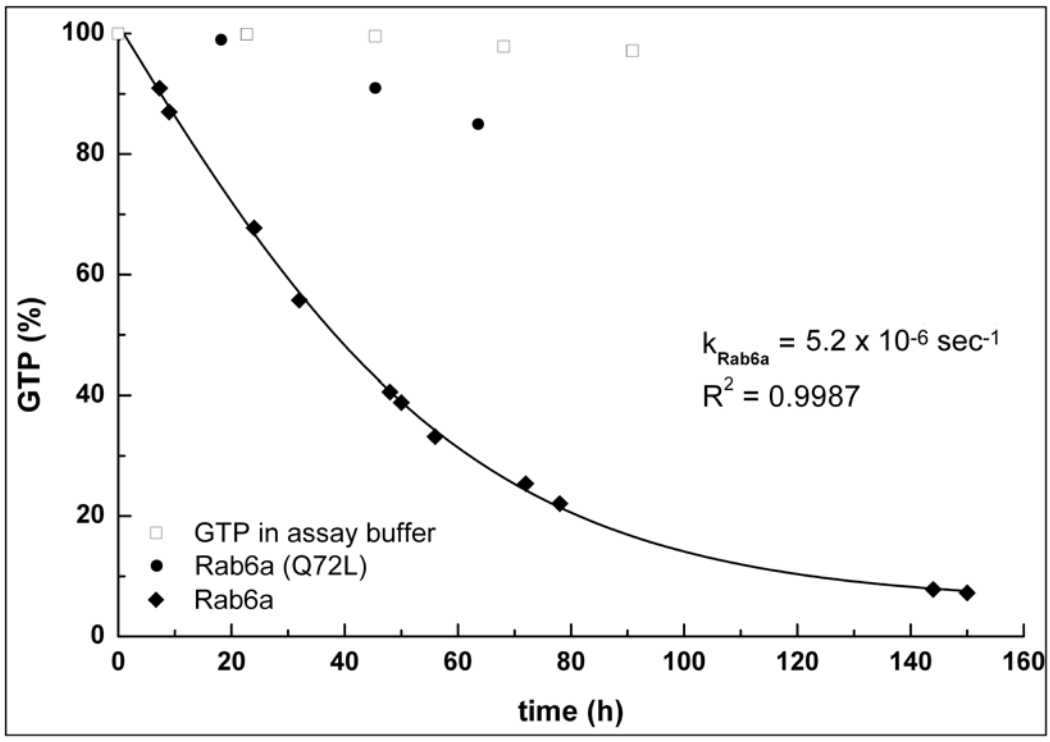

Fig.11 Hydrolysis of GTP by Rab6a and the GTPase deficient mutant Rab6a(Q72L). Time course of GTP hydrolysis for the stoichiometric complex of Rab6a (♦) or the mutant Rab6a(Q72L) (●) with GTP at 25°C in buffer containing 50mM TrisHCl pH 7.5, 100mM LiCl and 5mM dithioerythritol. As a negative control, autohydrolysis of GTP (□) was monitored under the same conditions. The hydrolysis reaction was started by addition of 10mM $MgCl_2$. Concentrations of GTP and GDP were determined by HPLC (see *4.5.5*). The single-exponential curve, to which the data of the wild type protein was fitted to a rate constant of 5 x 10^{-6} s^{-1}, is shown.

The decrease in protein bound GTP can be analysed as a first order reaction that follows a single-exponential time course with a rate constant of 5 x $10^{-6}s^{-1}$. While this is in good agreement to the GTPase rate of the yeast homologue Ypt6 (3 x $10^{-6}s^{-1}$) at 30°C [213] it is much slower than that observed for other Rab proteins under comparable conditions (Table 1). In order to confirm that the observed GTP / GDP conversion was indeed a consequence of enzymatic activity, hydrolysis by the GTPase deficient Rab6a(Q72L) was analysed. As can be seen in Figure 11, only residual activity could be detected in this mutant. In addition, autohydrolysis of the nucleotide in the reaction buffer appears to have only negligible effect on the concentration of GTP. These results confirm that, although inefficient, the observed GTP hydrolysis with the wild-type protein was indeed a consequence of Rab6A catalytic activity. Hence, Rab6a displays the lowest rate of GTP hydrolysis observed for RabGTPases so far ($t_{1/2}$ ≈ 37h).

4.5 Crystallisation of Rab6a

The extremely low hydrolysis rate of Rab6A (4.4) could enable the determination of its structure in the GTP-bound conformation, which so far has not been possible for other RabGTPases. Generally the active state of Rabs and other GTPases is simulated by complexing them with the non-hydrolysable analogues GTPγS or GppNHp. The structure of the Rab6A:GTP complex could provide an insight into the structural basis of the extreme differences in catalytic activity within the Rab family, and could also validate the use of non-hydrolysable GTP analogues for structural research on GTPases.
As a prerequisite for crystallisation experiments, freshly purified protein samples were brought to the right concentration by precipitation tests using the PEG/ION crystallisation screen (Hampton Research) before aliquoting and freezing. The concentration of the protein samples was adjusted to result in no more than 30% of all samples of any crystallisation screen to precipitate directly upon mixing with the reservoir solution at a temperature of 20°C. In initial crystallisation screens carried out with Rab6aΔ22:GTP and Rab6aΔ27:GTP small rosettes of tightly packed very small needles were observed using ammonium sulphate or polyethylene glycol (PEG). To optimise crystallisation conditions a grid screen was set up, varying the pH, the molecular weight of the PEG the concentration of PEG and of ammonium sulphate. In an attempt to overcome agglomeration and to increase the growth of single crystals the best conditions acquired were screened against different additives. However, because the quality of crystals improved only slightly (Fig.13A), a yet more truncated version of the protein was used in an effort to increase structural rigidity, which might allow for tighter packing of the molecules and hence better crystal growth. Thus, Rab6aNΔ12CΔ33:GTP was used, first to reproduce the best crystallisation results of the longer constructs and then in the further course of the crystallisation experiments, to optimise crystal growth and shape. After a successful initial trial to obtain single crystals by streak seeding, this method was optimised to give single crystals of increased size using micro seeding technique. Best results were obtained using micro seeds of crushed crystals in the hanging-drop vapour diffusion method at 293 K. Protein at 15 mg/mL in 50 mM TrisHCl pH 7.5, 50 mM LiCl, 5 mM dithioerythritol, 1 mM $MgCl_2$ and 1 mM GTP was mixed with an equal volume of reservoir solution containing 100 mM TrisHCl pH 8.0, 1 M LiCl, 32 % PEG_{1000} (w/v) and 3.3 mM Nonyl-β-D-glucoside. Crystals appeared 2 days after micro seeding as rectangular plates of low thickness that in some cases still showed a tendency to grow in multiple layers on top of each other (Fig.13B). Soaking of the crystal in cryoprotection solution prior to cooling in a 100 K nitrogen gas stream for data collection was not required, presumably due to the high PEG_{1000} content of the reservoir solution.

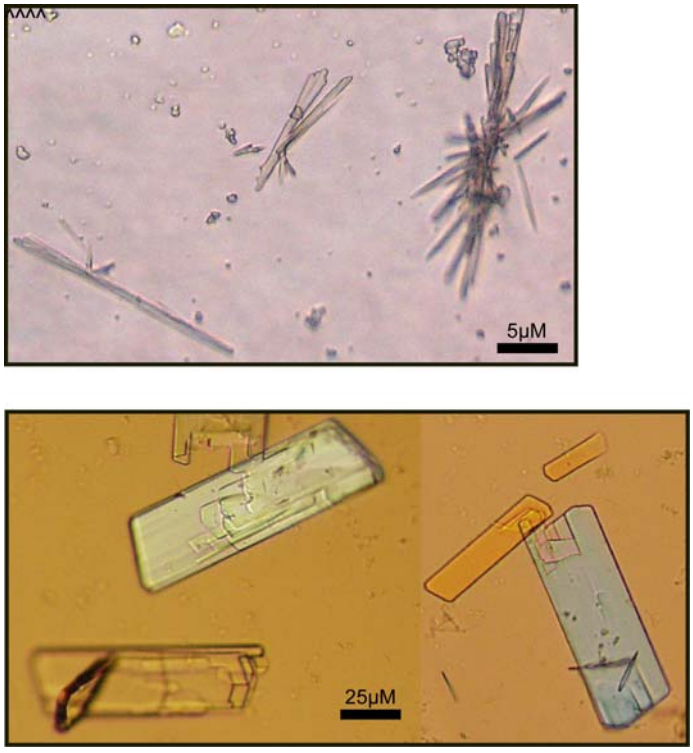

Fig.13 Crystallisation of Rab6a. ***Top*** Micrograph of Rab6aΔ27-crystals arranged in stacks and clusters of needles. ***Bottom*** Micrographs of Rab6aNΔ12CΔ33-crystals which grow as thin plates.

Diffraction tests using an in-house X-ray source yielded a diffraction pattern of clearly defined single reflexes to a resolution of 3 Å. Data with a resolution of 1.8 Å were obtained during analysis of the crystals at the ESRF beamline ID 14-3 (λ = 0.931 Å). Consistent with the observed shape, unit cell parameters were a = 39.96 Å, b = 124.75 Å, c = 66.09 Å, α = 90.0°, β = 107.5°, γ = 90.0°, classify the crystals in the monoclinic space group P21 ($a \neq b \neq c$, $\alpha = \gamma = 90° \neq \beta > 90°$) with four Rab6aNΔ12CΔ33:GTP molecules per asymmetric unit. After scaling and processing with the *XDS* suite of programs[214] the data was used for further refinement of the structure.

4.6 Structure Determination

To date structural information has been acquired for a large number of G-proteins in general and Rab/Ypt proteins in particular. Comprehensive studies have helped, not only to identify the structural elements required for specific binding of the nucleotide, but moreover have elucidated the molecular mechanisms underlying its hydrolysis and the transition from an active to an inactive conformation [215,69,216]. Single amino acids around the nucleotide binding pocket have been pinpointed as crucial factors for GTPase activity. Not surprisingly, these residues are found in the most conserved parts of the protein. However, small but significant deviations in these motifs have been found among the family of Rab proteins. These single residue changes pose the most likely explanation for the characteristic catalytic activity of a particular RabGTPase and almost certainly define effector specificity. Still, the underlying molecular mechanisms of these effects remain elusive. The very low hydrolytic activity of human Rab6a for the first time enables structural analysis of a Rab protein in its active conformation, while bound to the naturally occurring GTP. Analysing the acquired data for differences and similarities to the inactive conformation of *Plasmodium falciparum* Rab6a●GDP [134] should yield a detailed view on the transition between the 'ON' and the 'OFF' state of this Rab. Particularly, a comparison to structures of other Rabs, for which both conformations have been determined (Rab4a [209], Rab5a [217], Rab7 [218]), might help to identify determinants of Rab6a GTPase activity and to describe a possible scaffold to which effectors may bind.

4.7 The Crystal Structure of Rab6a●GTP

The crystal structure of Rab6a was solved by building a molecular replacement model using Rab6●GDP from *P. falciparum* (1D5C) as a search template. The molecular replacement solution had four molecules of Rab6aNΔ12CΔ33 per asymmetric unit. Refinement was performed using the programs CNS [(219)] and REFMAC5 [(220)]. Table 2 shows a summary of the data processing and refinement statistics.

Table 2 Statistics of diffraction data and refinement for the structure determination of Rab6a.

Beamline ID	ESRF ID 14-3
Detector	ADSC Quantum 4
Temperature [K]	100
Wavelength [Å]	1.0398
max. resolution [Å]	19.05-1.82
Space group	P21 (P 1 21 1)
Unit cell: dimensions [Å] angle [°]	a=40.01, b=124.85, c=66.16 α=90.00, β=107.57, γ=90.00
Reflections total	94779
Unique reflections	48538
Redundancy	1.9
[ab]R_{sym} (%)	3.2(14.6)
[b]Completeness (%)	87.7
<I>/σ(I)[a]	17.7 (4.3)
Refinement	
Search model	Rab6a●GDP from *Plasmodium falciparum* (PDB 1D5C)
R_{work}(%) / R_{free}(%)	20.1/26.5
number of non-hydrogen atoms	5202 + 132 hetero atoms
solvent atoms	868
B-factor [Å^2]	21.0
Occupancy-weighted average B-factor [Å^2]	25.3
Average B-factor [Å^2]:	
GTP	17.45

a $R_{sym} = \sum_{hkl}\sum_{i}\left|\left|I_i\right| + \left|\langle I\rangle\right|\right| / \sum_{hkl} n_i * \left|\langle I\rangle\right|$

b Completeness, R_{sym} and $\langle I/\sigma(I)\rangle$ are given for all data and for the highest resolution shell: 1.9-1.82Å

c $R_{work} = \sum |F_{obs}| - k|F_{calc}| \; / \sum |F_{obs}|$. 5% of randomly chosen reflections were used for the calculation of R_{free}

Figure 14A shows the GDP molecule of the *P. falciparum* Rab6a template that was used for molecular replacement with the corresponding superimposed section of the electron density map obtained for the human Rab6aNΔ12CΔ33. As can clearly be seen, a patch of surplus electron density associated with the phosphate chain of the nucleotide is found in close vicinity to and in contact with the hexa-coordinated Mg^{2+} ion. The additional electron density for the human Rab6a can only be explained by the presence of a γ-phosphate group of the nucleotide.

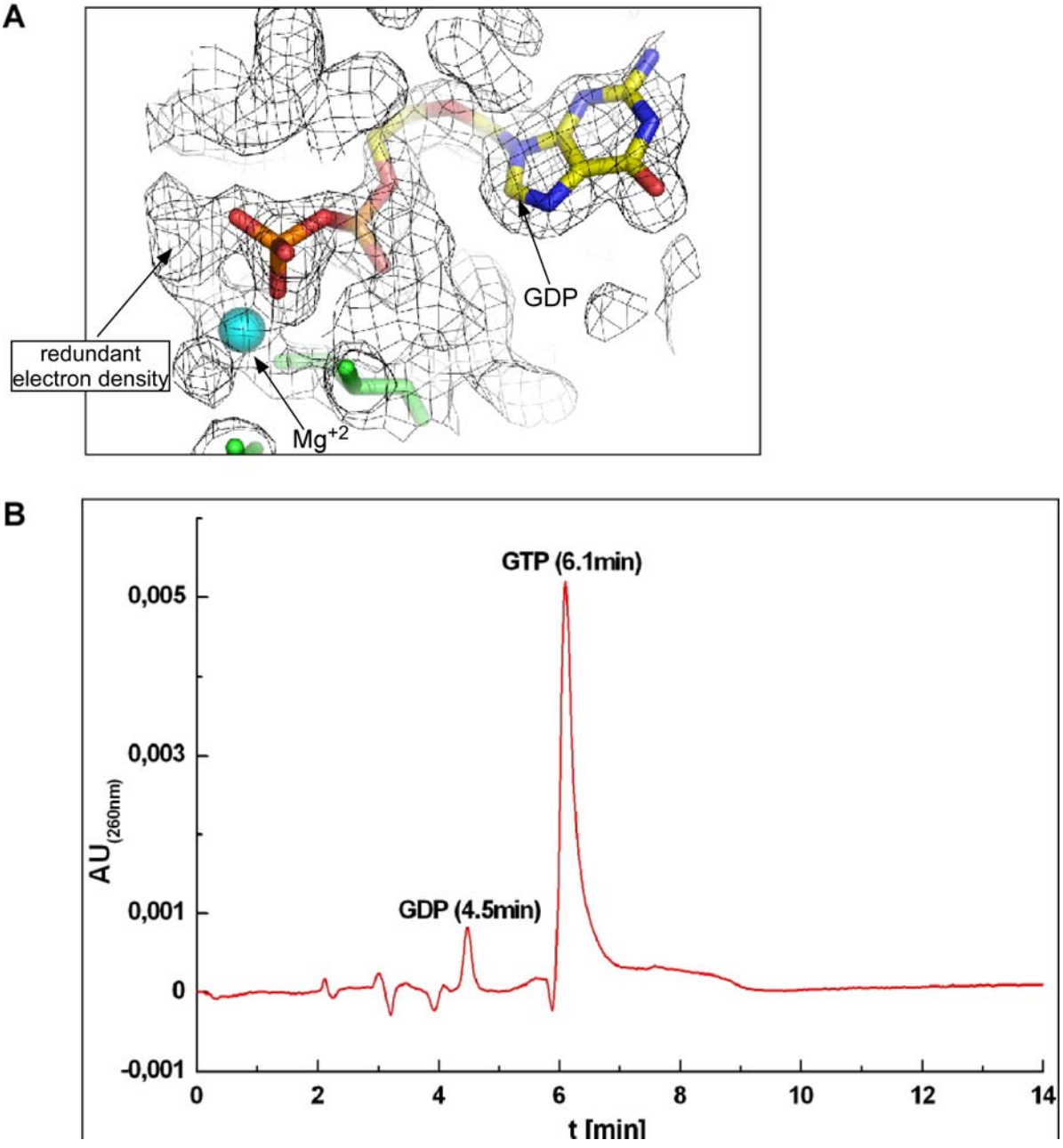

Fig.14 Identification of the nucleotide bound Rab6aNΔ12CΔ33. A GDP and adjacent amino acids of the *Plasmodium falciparum* Rab6a search model that was used for molecular replacement are displayed as sticks and the Mg^{+2} ion as a cyan sphere. Superposed is the $2F_0$-F_C electron density map that was obtained for the respective area of the human Rab6aNΔ12CΔ33 contoured at 1σ. **B** HPLC analysis of the Rab6 crystals. The crystals were separated form the mother liquid and dissolved in sample buffer. The resulting solution was separated on a C-18 HPLC column (3.5.5.). The elution positions of GTP and GDP were identified by calibration with nucleotide standards.

Furthermore, HPLC analysis of Rab6aNΔ12CΔ33 crystals, dissolved in nucleotide-free buffer, showed that more than 90% of the protein-bound nucleotide eluted at the same time as GTP standards (Fig14B). Taken together, these observations can be regarded as definitive evidence that Rab6aNΔ12CΔ33 had been crystallised in the GTP bound form.

The four molecules of the asymmetric unit cell are arranged as two dimers. These can clearly be distinguished by comparing the root mean squared deviation (rmsd) for the positions of the C_α-atoms of the different amino acid chains. While for the two dimers AC and BD rmsd values are low (0.291Å and 0.169Å respectively) any other combination of the four molecules leads to an rmsd close to 0.9Å. Differences in the rmsd values of the dimers might be explained by the finding that crystal contacts to symmetry-related molecules contribute to constraining molecules B and D of the asymmetric unit cell. These contacts are observed for the N-terminus (K13-L16) as well as for a thirteen amino acid stretch (K53-Q65) spanning β2, β3 and the connecting loop regions of the molecules (Fig. 15). In molecules A and C, the area surrounding the nucleotide binding site is free of contacts with other molecules. Hence, the structure of this region should allow an unperturbed interpretation on Rab6a in the GTP bound state.

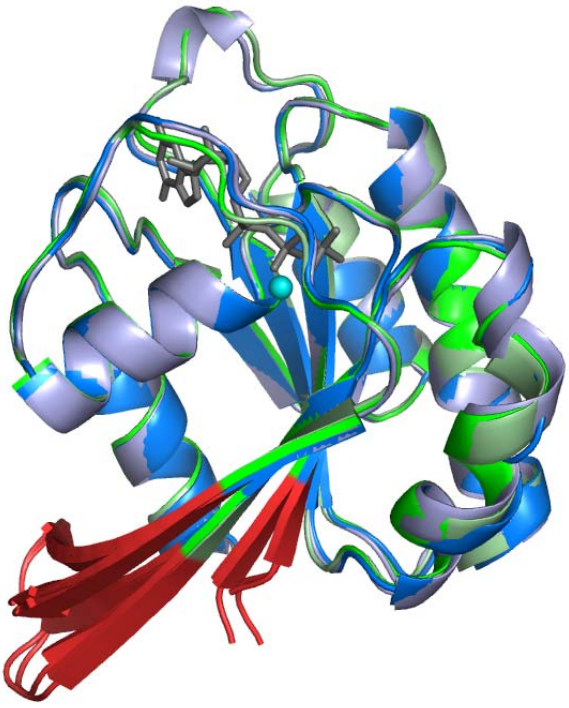

Fig.15 Superposition of the four Rab6aNΔ12CΔ33 molecules of the unit cell. Superimposed cartoon representations of molecule A (green), C (light green), B (blue) and D (light blue) that were observed in the crystallographic unit cell. Regions of the molecules in which the two dimers (A/C, B/D) deviate are coloured red, GTP is shown as a grey stick model and Mg^{+2} as a cyan sphere.

4.8 Structural Elements of the G-domain

The overall structure of Rab6a displays a typical Ras-like GTPase fold [221]. Fig.16 shows a cartoon representation of the residues (13 - 174) that were visible in the electron density map. The structure comprises five α-helices surrounding five

parallel and one antiparallel β-strands, a fold common to most small GTPases. The position of GTP and of the Mg^{+2} ion overlap with those found in GppNHp complexes of Ras, Rab3a, Rab5a and Rab6a confirming that non-hydrolysable analogues represent a good approximation of the native GTP ligand.

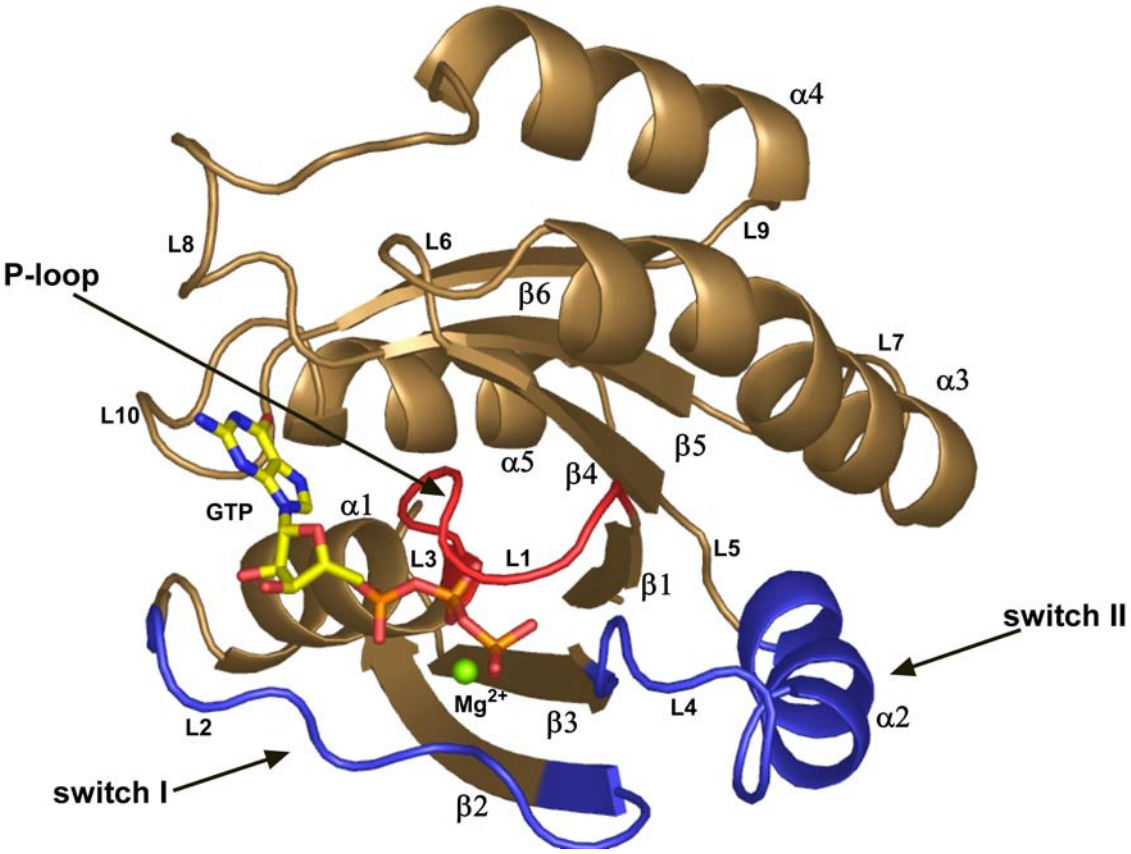

Fig.16 Structure of the Rab6a•GTP complex. The GTP molecule is shown as a stick model and the magnesium ion as a green sphere. The conformational switch regions, switch I and switch II, are highlighted in blue and the P-loop in red. The labelling of the secondary structure elements of Rab6a (as determined with the program *DSSP*) corresponds to that of the respective elements in human H-Ras.

The amino acid residues responsible for binding and hydrolysis of the nucleotide are located in the loop regions of the fold, which constitute the most conserved sequence and structure elements among Ras-like GTPases. All of these residues are found in the five loops L1, L2, L4, L8 and L10 that build the catalytic G-domain. In analogy to figure 4, loops L1, L2 and L4 coordinate the Mg^{2+} ion and contact the γ-phosphate group of the nucleotide, whereas L2, L8 and L10 bind the guanine base. Table 3 gives an overview of structural elements for the different RabGTPases that were chosen for comparative analysis of the active state structure of Rab6a.

Table 3 Functional elements and amino acid assignment for H-Ras and Rab GTPases that were used for comparative structural analysis

structure element	H-Ras	Rab4a	Rab5a	Rab6a *P. falciparum.*	Rab6a *human*	Rab7
phosphate binding						
L1 (PM1)	^{10}GAGGVGKS	^{15}GNAGTGKS	^{28}GESAVGKS	^{18}GEQAVGKT	^{20}GEQ**S**VGKT	^{15}GDSGVGKT
L4	^{60}GQEE	^{65}AGQ	^{79}GQ			
Mg^{2+}-coordination						
L1 (PM2)	S17	S22	S35	T25	T27	T22
L2	T35	T40	T53	T43	T45	T40
guaninebase binding						
G1	F28	F33	F46	F36	F38	F33
G2	^{116}N-^{119}D	^{121}N-^{124}D	^{134}N-^{137}D	^{124}N-^{127}D	^{126}N-^{129}D	^{125}N-^{128}D
G3	^{145}S-^{147}K	^{151}S-^{153}L	^{164}S-^{166}K	^{154}S-^{156}K	^{156}S-^{158}K	^{155}S-^{157}K
switch I						
L2 / β2	^{30}D-^{40}Y	^{31}K-^{45}G	^{42}V-^{59}I	^{34}D-^{48}F	^{39}D-^{50}F	^{31}L-^{44}D
switch II						
β3 / L4	^{57}DTAGQEEY	^{63}DTAGQERF	^{76}DTAGQERY	^{66}DTAGQERF	^{68}DTAGQERF	^{63}DTAGQERF
α2	^{65}S-^{74}T	^{71}R-^{75}	^{79}Q-^{91}R	^{70}Q-^{75}S	^{76}R-^{85}A	^{73}L-^{81}A

Hydrophobic interactions with the aromatic side chain of F38 (G1) on top and the aliphatic side chain of K127 below orient the guanine base within the binding pocket, where it is stabilized via polar interactions with the G2 (N126, K127, D128) and the G3 (S156, A156, K157) motifs. Specificity for the guanine nucleotides is mediated by hydrogen bonds with the main chain NH-group of A157 and the side chain carboxylic acid of D129 [**222**]. As the ribose part of the nucleotide is present in a 2'-endo conformation its 2'-OH group can form a hydrogen bond to the main chain oxygen of D39.

The L2 or P-loop [**223**] shields the β- and γ-phosphates from the solvent and, in concert with Mg^{2+} ion and residues of the L1 and L4 loop, mediates binding of these groups. The main chain NH-groups of S23, G25 and T27 as well as the ε-amino group of K26 form polar interactions with the β- and γ-phosphate, while S28 interacts with the α-phosphate group. Two crucial interactions between the γ-phosphate and two highly conserved residues induce rigidity in loops L2 and L4, thus defining the active state of the GTPase. The Mg^{2+} in the structure of Rab6a●GTP is hexa-coordinated and has interactions with T27, T45, β- and γ-phosphate and two conserved water molecules. Upon hydrolysis of the nucleotide the γ-phosphate group leaves the G-domain and coordination of Mg^{2+} with T45 is lost. Loss of polar contacts with T45 of L2 and G71 of L4 leads to distinct conformational changes in these regions that hinder binding of downstream effectors.

Current models for hydrolysis of the nucleotide describe a central role for a conserved water molecule that acts as the nucleophile in the in-line (S_N2-) attack on the γ-phosphate. The water molecule is activated and coordinated for the attack by T45 and Q72. In particular the function of Q72 in stabilizing the transition state of

the hydrolysis reaction [224] appears to be crucial for the proper function of RabGTPases. Mutational studies have shown that substitution of this residue with any other amino acid but glutamate lowers intrinsic and GAP-stimulated hydrolytic activity dramatically [204,225].

This first description and analysis of the overall fold and structure elements classifies Rab6a as a Ras-like protein of the Rab family of GTPases. However, characteristic biochemical properties, especially the very low intrinsic GTPase activity, that seem to be necessary for the function of this particular Rab can only be explained by differences in the otherwise conserved sequence motifs. The two regions of the structure of Rab6a most likely to harbour the responsible deviations are the two switch regions L2 and L4/α, as they form the catalytic core of the G-domain. Switch I, also known as the effector loopis a good candidate to modulate the duration of the interaction with downstream effectors, since it is the site of the protein scaffold to which interaction partners bind.

4.9 Analysis of the Structure of Rab6a

4.9.1 Determinants of Rab6a GTPase activity

4.9.1.1 Switch I

The switch regions of small GTPases are defined as the two regions of the protein fold that undergo the greatest conformational change during transition from the active to the inactive state and vice versa. X-ray experiments with H-Ras p21 [73] allocated switch I and II from around L2/β2 and β3/L4 to α2 respectively. Upon nucleotide hydrolysis, switch I in particular becomes more unordered, due to the loss of the interaction between the γ-phosphate and the conserved threonine. Hence, for most Rab●GDP complexes the high flexibility of switch I leads to insufficient electron density, inhibiting exact structure determination of this region of the protein. Interestingly, in the case of *P. falciparum* Rab6a●GDP sufficient electron density for switch I could be obtained to allow convenient localisation of the switch regions through comparison with Rab6a●GTP in the active conformation.
An overlay of the switch I regions of Rab4a (yellow), Rab5a (red), Rab6a (green) and Rab7 (blue) shows (Fig.17) that the L2 loops of the different Rabs in the active conformation differ only slightly in the position of the C_α-atoms. Main deviations of the C_α chain are found in the C-terminal part of the loop, towards the β2-sheet. A comparison of Rab6a●GTP with the structure of the Rab5a●GppNHp, as one of the hydrolytically most active Rabs, points to potentially important differences. The main difference to the structure of Rab5a is the presence of Y42 in the switch I region of Rab6a that covers the phosphate groups of GTP like a lid, forming a hydrogen bond with the oxygen of the γ-phosphate with its OH group.

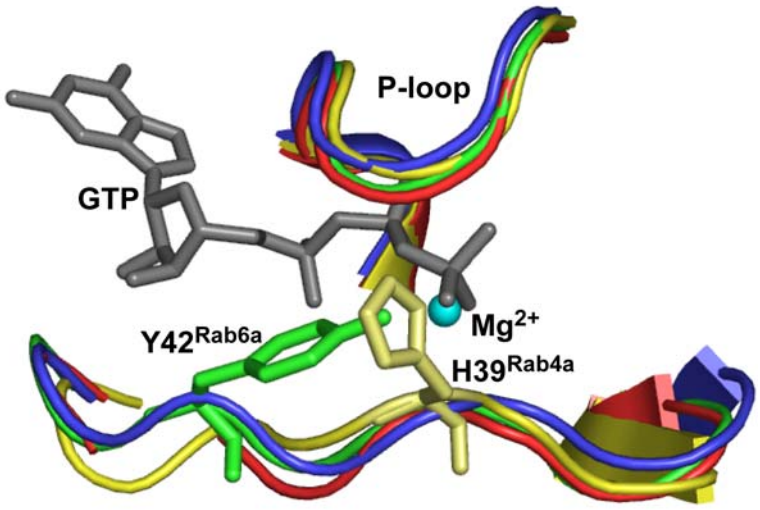

Fig.17 Comparison of structural characteristics of switch I. Superposed cartoon representation of switch I and P-loop regions of Rab4a (yellow), Rab5a (red), Rab6a (green) and Rab7 (blue). GTP, tyrosine 42 of Rab6a and histidine 39 of Rab4a are displayed as stick models. Mg^{+2} is shown as a cyan sphere.

Comparison of Rab6a solvent-exposed surfaces with that of Rab5a shows that the presence of Y42 reduces the exposed surface of the nucleotide by nearly two thirds (Figure 18). Similarities with the structure of Rab7●GppHNp, which is the second catalytically slowest RabGTPase may suggest that the occluded positioning of the phosphates might correlate with the observed rates of spontaneous hydrolyses. Interestingly, Rab7 also possesses a bulky (lid-forming) tyrosine (Y37), which also forms a hydrogen bond with the oxygen of the γ-phosphate, thus reducing the solvent exposed surface of the nucleotide. In contrast, another rapidly hydrolysing GTPase Rab3a has a phenylalanine residue at this position (F51) that cannot form a hydrogen bond with the nucleotide and does not shield the phosphates. Although it is not currently clear what the consequences of the tyrosine in switch I and its hydrogen bonding with the γ-phosphate of GTP are, this feature is not restricted to Rab6a and Rab7. Tyrosine occurs at an analogous position in a number of RabGTPases, including another catalytically inefficient RabGTPase Rab24. [226,227]. Moreover, in the structure of the more distantly related GTPase RHEB, a Y35 in switch I forms a hydrogen bond to the γ-phosphate of GTP, leading to closure of the nucleotide-binding site. As in the case of Rab6a, the GTPase activity of RHEB was low enough to enable its crystallisation in complex with GTP [228]. The position of H39 in the switch I of Rab4a has been shown to occlude the γ-phosphate of the nucleotide in a way resembling that of the tyrosine residue in Rab6a, or Rab7. Although this residue can not form polar interactions with the phosphate group, comparison with Rab9, which possesses an analogous histidine residue, suggests that it might still affect the rate of GTP hydrolysis and exchange [209].

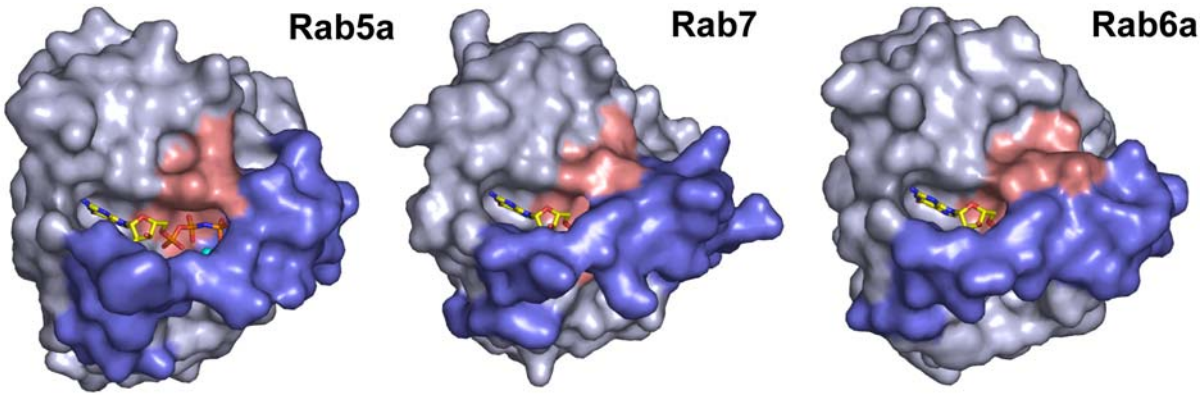

Fig.18 Surface representations of Rab5a, Rab6a and Rab7. The functional elements of the switch regions are coloured blue and the P-loop is shown in red. A stick model of the bound nucleotide is displayed in the binding pocket.

It is possible that shielding of the nucleotide binding site does not itself influence the catalytic activity but that it is an accompanying feature of slowly hydrolysing RabGTPases that increases the fidelity of Rab:GAP interactions. RabGAPs appear to be promiscuous and shielding of phosphates by a tyrosine residue may provide an additional obstacle for unspecific Rab:GAP interaction by prohibiting insertion of GAP's catalytic group(s) into the active site [229]. This model would imply that the specific Rab6a GAP would have a mechanism for flipping out the phosphate protecting tyrosine residue.

4.9.1.2 Switch II

Superposition of switch II of Rab4a (yellow), Rab5a (red), Rab6a (green) and Rab7 (blue) shows a high degree of structural order and congruency of this region for the chosen Rabs, with the exception of Rab7 (Fig.19).

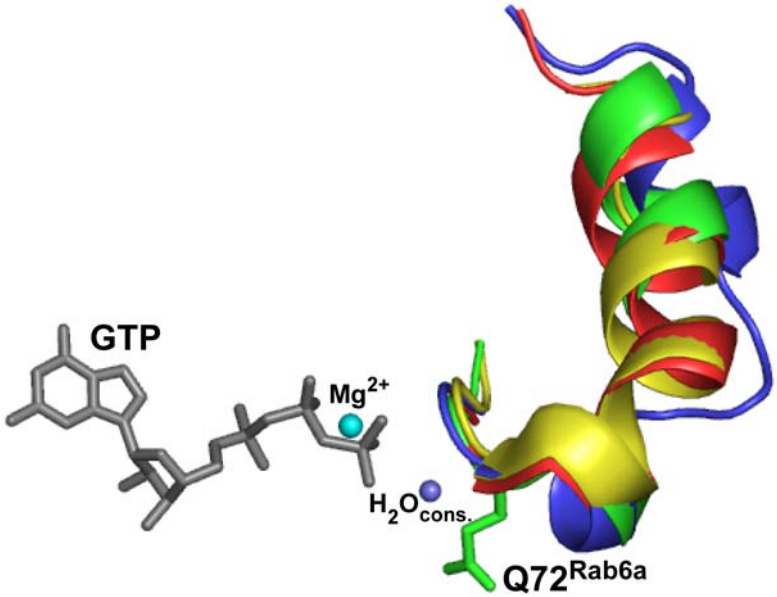

Fig.19 Comparison of structural characteristics of switch II. Superposed cartoon representation of the switch II region of Rab4a (yellow), Rab5a (red), Rab6a (green) and Rab7 (blue). GTP and glutamine 72 of Rab6a are displayed as stick models. The conserved catalytic water molecule of Rab6a and the Mg^{+2} are shown as a blue and a cyan sphere respectively.

A second possible clue to the molecular basis of the low catalytic activity of Rab6a comes from the analysis of crystallographic B-factors that reflect the flexibility of the molecule. As can be seen in figure 20, the switch II region of Rab6 appears to be the most flexible region in the active conformation of the molecule. One of the important features of the switch II region is the presence of Q72 (equivalent to Q61 of H-Ras) that is required for efficient catalysis. The function of this glutamine is firstly: to coordinate a conserved water molecule (Fig.19) for the attack on the γ-phosphate and second: to stabilise the transition state of the reaction (see 1.4). Reorientation of the catalytic glutamine is required for the correct positioning of the nucleophilic water molecule and this step seems to be rate-limiting for the hydrolysis reaction. In the structure of Rab6 the hydrogen bond between $N^{\varepsilon 2}$ and the nucleophilic water is weak [$d_{N\text{-}O}$ = 3.30Å, $\xi_{(C\text{-}N\cdots O)}$ = 96.78°] even compared to other Rab proteins (e.g. [$d_{N\text{-}O}$ = 3.26Å, $\xi_{(C\text{-}N\cdots O)}$ = 95.81°] for Rab5a [230]). Consquently, an energetic barrier preventing spontaneous alignment of the nucleophilic water could potentially cause a particularly slow hydrolytic turnover of Rab6a. Hence, it is not surprising that recent biochemical and structural studies on the small GTPase RHEB showed that displacement of the analogous residue accounts for the extremely low intrinsic catalytic activity of this protein [228]. In a comparison of B-factors of the structure of

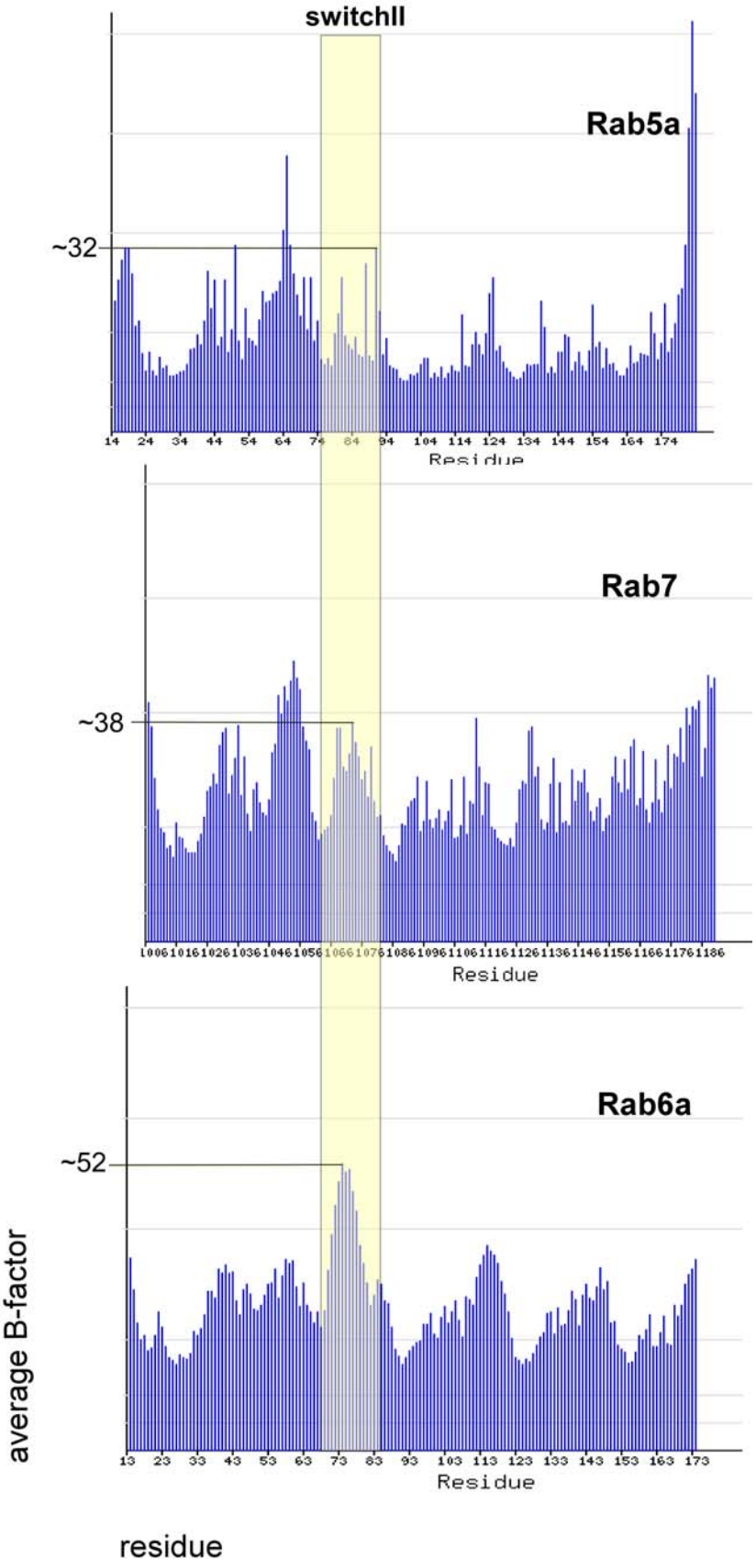

Fig.20 Comparison of B-factors for the functional switch II region of Rab5a, Rab6a and Rab7. The histograms display average B-factors for amino acid residues of Rab5a, Rab6a and Rab7. Segments of the sequences corresponding to the respective switch II regions are highlighted with a yellow bar and the maximal average B-factors observed for switch II are indicated at the ordinate.

Rab6a●GTP with the structures of Rab7●GppNHp and Rab5●GppNHp switch II appears to be most constrained in Rab5a (Fig.20).
Rab7 represents an intermediate situation with highest B-factors for the residues causing the gap in the α2 helix (Q71-V75). Therefore, it appears likely that flexibility of switch II and as a consequence of Q72 plays an important role in determining the intrinsic catalytic activity in Rabs and possibly in other GTPases.
It is conceivable that constraining the switch II region might be a mechanism by which an upstream regulator of Rab6a could enhance the hydrolytic activity of the protein.

4.9.2 Putative effector-binding motifs

Activation of Rab proteins caused by GTP binding is characterized by structural rearrangements leading to the formation of an interface for effector-binding. In the active state the surface of Rab6a displays an arrangement that is more compact compared with the GDP bound form (Fig.21B), which is a consequence of increased structural order of the two switch regions (Fig.21A). Contacts of the conserved T27 with the Mg^{2+} and between the '*lid-tyrosine*' Y42 and γ-phosphate group are absent in *P. falciparum* Rab6a●GDP. The presence of these interactions in the active of state Rab6a●GTP leads to an N-terminal translation and clockwise φ/ψ rotation of the C_α chain for all residues of switch I from D39 onwards. In the case of Y42 an N-terminal shift of 3.6Å and clockwise rotation of the aromatic side chain by ~55° in relation to the C_α-main chain of Rab6a●GTP brings the hydroxyl group of this residue from below the nucleotide binding pocket towards the vicinity of the γ-phosphate.
Furthermore, the N-terminal translation of switch I in concert with structural rearrangements of switch II to allow reorientation of the catalytic residue Q72, causes these two regions to draw more closely together. This is particularly pronounced for the two residues G47 (L2) and F75 (α2), whose distance in the active conformation is decreased by ~5.1Å as compared to the GDP-bound state. In this conformation switch I and II form a new hydrophobic interface that has been shown to be crucial for binding of downstream effectors (see 1.4).

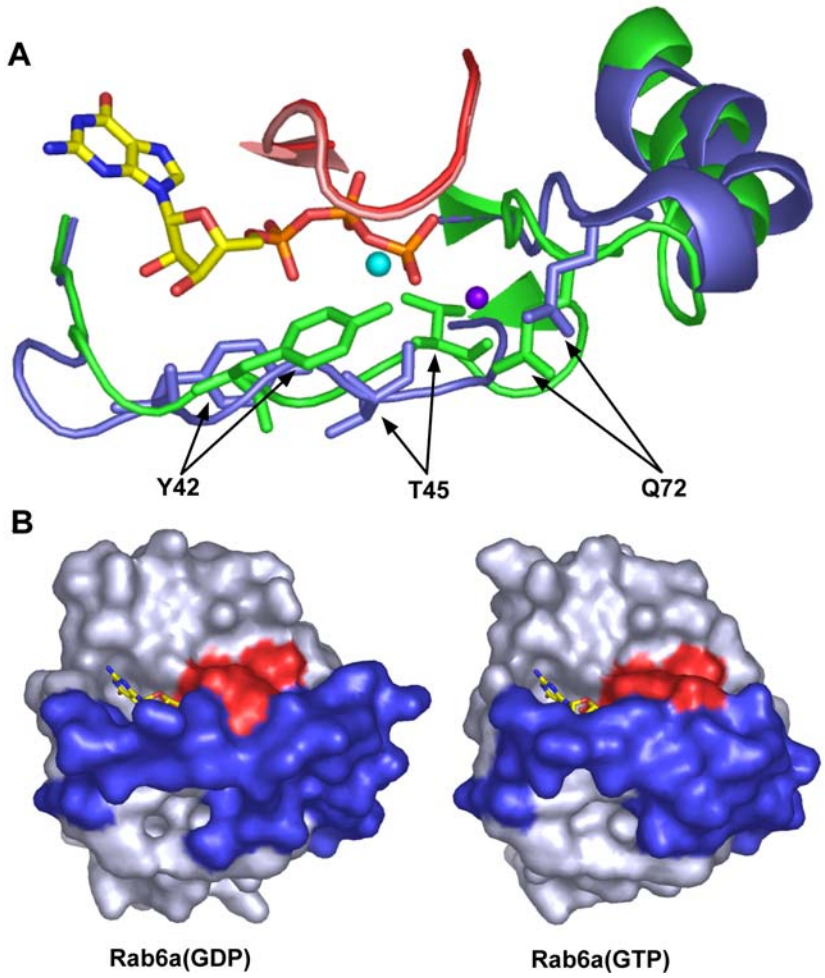

Fig.21 Illustration of the structural differences between the GTP- and GDP-bound conformations of Rab6a. A Superposed cartoon representation of the switch I region of human Rab6a•GTP (green) and *P. falciparum* Rab6a•GDP (blue). GTP, tyrosine 42, threonine 45 and glutamine 72 are displayed as stick models. The conserved catalytic water molecule of Rab6a and the Mg^{+2} are shown as a blue and a cyan sphere respectively. The P-loops (human: red, *P. falciparum*: light red) are also depicted for ease of orientation. **B** Surface representations of human Rab6a•GTP and *P. falciparum* Rab6a•GDP. The functional elements of the switch regions are coloured in blue and the P-loop in red. A stick model of the bound nucleotide is displayed in the binding pocket.

Analysis of the Rab3a:Rabphilin-3a complex led to the identification of three invariant hydrophobic residues located within the two RabF (Rab family) surfaces. F50 (RabF1), W67 (RabF2) and Y82 (RabF4 in Rab6a) appear to mediate specificity of the binding-platforms through structural plasticity that this triad displays between different Rabs [78]. Analysis of the specific conformation of the invariant hydrophobic triade of Rab6a is not trivial. Due to crystal contacts between the molecules of a dimer in the crystal unit cell residues in these regions are constraint complicating structural interpretation. Comparison of the molecules A and B of one dimer shows that the positions of the aromatic side chain of Tyr82 in the different molecules is almost congruent and does not seem to be influenced by crystal contacts. However, despite congruent conformation of the β-sheets involved in the interaction (β2, β3) the orientation of the two other residues Phe50 and Trp67 differs greatly between molecules A an B (see Fig.22).

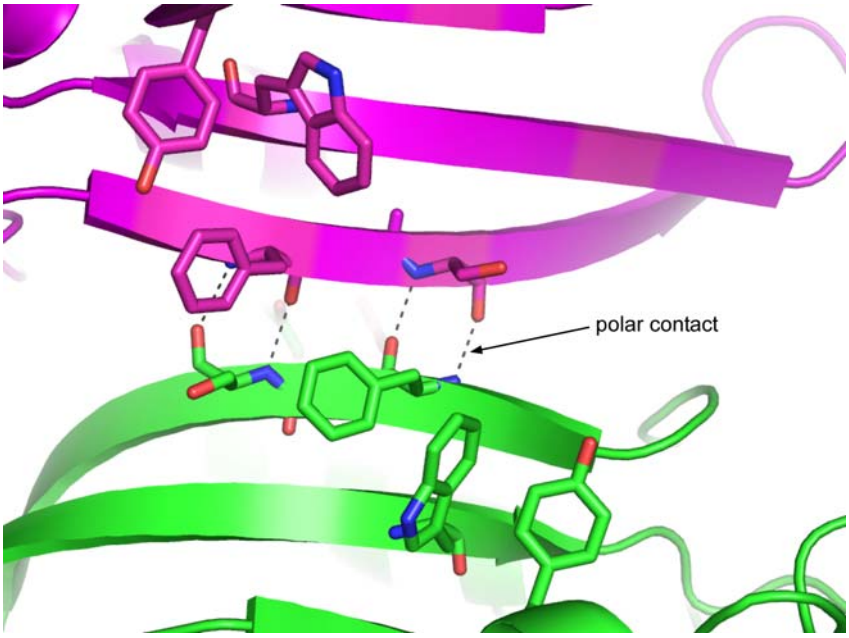

Fig.22 Conformational differences of the hydrophobic triad between molecules of the two dimers in the unit cell. Cartoon representation of the interface formed between molecules A (green) and B (magenta) in the crystal unit. Residues F50, Ser 52, W67 and Y82 are displayed as stick models. Polar contacts are shown as dashed lines.

In molecule A the tryptophan is wedged between the aromatic side chain of Phe50 on one side and Tyr82 on the other, pointing almost straight to β2, while Phe50 itself points toward the β-sheet connecting loop L3. In both molecules the main chain amino nitrogen and hydroxyl oxygen of Phe50 form polar contacts with a side chain hydroxyl oxygen and a main chain nitrogen of Ser52 from the neighbouring molecule respectively. However, its orientation seems to be determined primarily by the orientation of the aromatic Trp67 side chain. This side chain is not fixed by the adjoining two residues of the triad in molecule B, but instead is turned by about 40° toward the N-terminus of β3. In response to this the aromatic side chain of Phe40, that would otherwise clash with Trp67, is bent by ~120° at the C_β in the opposite direction and toward the N-terminus of β2. It appears that in this conformation Trp67 is in a state of higher rotational freedom as compared to molecule A. Hence, the organisation of the invariant hydrophobic triad of Rab6a from the direction of switch I (L2) toward L3 is either Tyr, Trp, Phe (Mol A) or Tyr, Phe, Trp (Mol B), which would influence the topology of the interface greatly (Fig.23A). It remains unclear whether one of the two molecules represents the physiologically apt conformation. Interestingly the conformation of the triad in the recently published structure of Rab6a' or (Rab6C) bound to GppNHp [231] is not in exact agreement with either of the two found for Rab6a●GTP (see Fig.24).

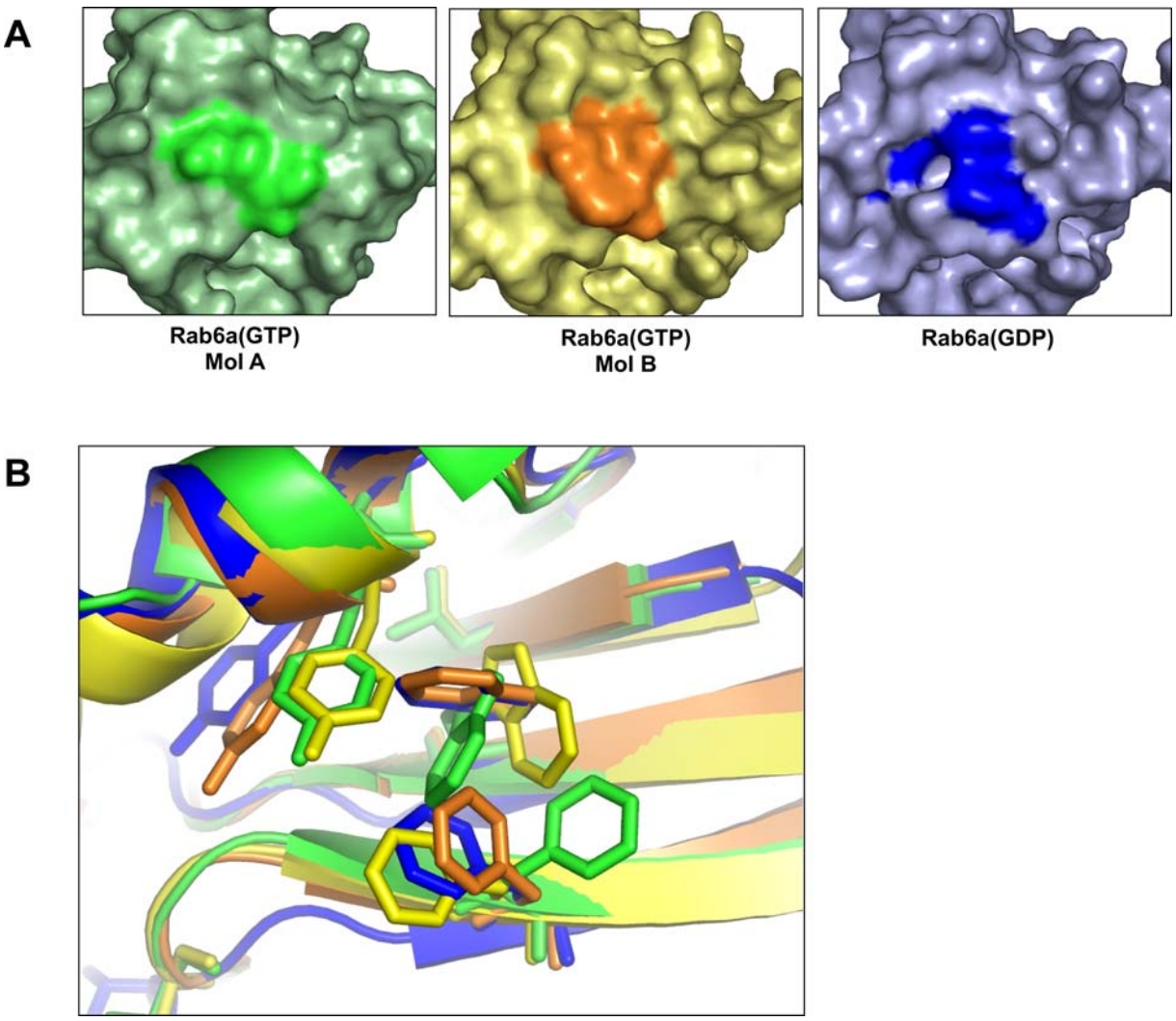

Fig.23 Conformational changes of the hydrophobic triad in Rab6a depending on the bound nucleotide. A Surface representations of Rab6a•GTP (molecule A: light green, molecule B: pale yellow) and Rab6a•GDP (light blue) with the surface area of the hydrophobic triad highlighted in green, orange and blue respectively. **B** Superposition of cartoon representations of Rab6a•GTP (molecule A: green, molecule B: yellow), Rab6a'•GppNHp (orange) and Rab6a•GDP (blue). Residues of the invariant hydrophobic triad are displayed as stick models.

It is noteworthy that one of the non-conserved residues identified by Merithew and co-workers as determinants of the specific conformation of the hydrophobic triad [232], Thr87, is substituted for Ala in Rab6a'. The observed structural differences between the two isoforms are not in agreement with interpretation of Merithew and co-workers, who suggested that the conformation of the hydrophobic triad in the active conformation was an indicator for the affiliation with a particular Rab sub-family. Rather, the residues of the hydrophobic triad in Rab6a'●GppNHp adopt a conformation very close to that of the inactive conformation found for *Plasmodium falciparum* Rab6a●GDP, which also comprises an Ala in the position equivalent to Thr87 in the human Rab6a. Comparisons of Rab4a (orange), Rab5a (red) and Rab6a (MolA green, MolB yellow) in the active conformation (Fig.24) seem to suggest that, in order to form a binding platform distinctly discernable from the other two Rabs, the triad of Rab6a would more likely have to adopt the conformation

found in molecule B. An arrangement of the triad as found in molecule A however would put Rab6a close to Rab4a and Rab5a, which differ only slightly in the orientation of the tryptophane and the alternative orientation of the tyrosine side chain in Rab5a.

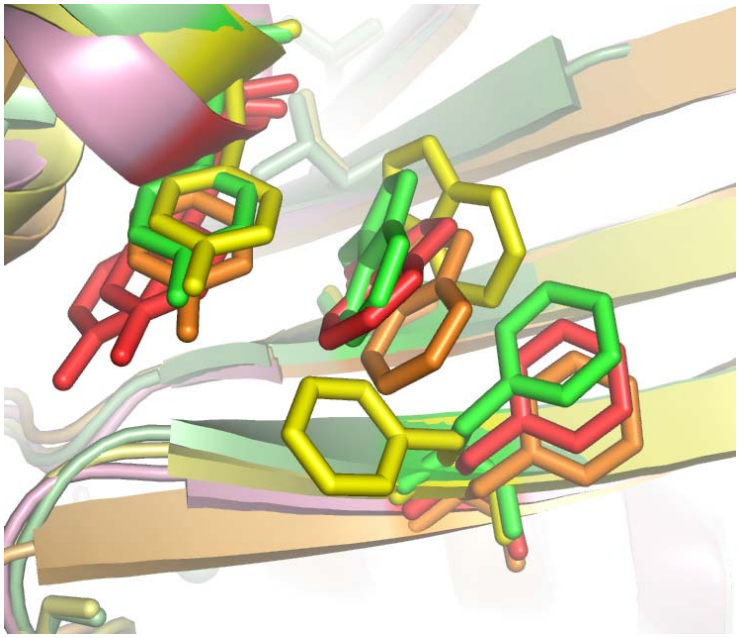

Fig.24 Conformational characteristics of the hydrophobic triad of Rab 4, 5 and 6. Superimposed cartoon representation of Rab6a•GTP (molecule A: green, molecule B: yellow), Rab4a•GppNHp (orange) and Rab5a•GppNHp (red). Residues of the invariant hydrophobic triad are displayed as stick models.

4.10 Interpretation of Rab6a Structural and Biochemical Characteristics

From the cell-biological perspective it can be assumed that, whereas GAPs would be involved in accelerating the low intrinsic rates of Rab proteins in their cellular environment, the differences in the GTPase activities assayed *in vitro* reflect pathway-specific requirements of individual Rabs. It has been noted before [12] that the half-life for GTP hydrolysis at 37°C of Rab5 corresponds to the time required for Rab5 controlled transport events from the plasma membrane to early endosomes and in endosome fusion (2-10min). [233]. Similar correlations were found for Rab7 GTP hydrolysis and the transport from early to late endosomes (30-60min), as well as for Rab9 and associated transport from the late endosomes to the trans-Golgi network (~3h). [234]

The role of Rab6a in vesicular trafficking has been implicated in many aspects of microtubule-dependent retrograde traffic, ascribing control functions to the GTPase spanning the entire stretch of the cell, from the periphery, through the Golgi and to the ER. In the light of these findings the very low observed hydrolysis rate for GTP of Rab6 ($t_{1/2}$ = 37h), which essentially renders the protein constitutively active and receptive for effector-interaction, becomes interpretable. To ensure control function over transport processes, that in some cases would take several hours, Rab6a must not loose its active conformation and must maintain binding platforms for the time required. Only at the target membrane compartment, and clearly under the effect of as yet unidentified GAPs, would Rab6a return to the inactive state.

4.11 Expression and Purification of the Effector Proteins

All effector constructs were over-expressed in *E.coli* BL21-CodonPlus-RIL cells, as described in 4.4.2. As the first purification step Ni-affinity chromatography (4.6.1.2) was used. In contrast to the instructions of the manufacturer, a washing step with low concentration of detergent (CHAPS) was included for all effector proteins. This procedure prevented the formation of non-proteinaceous (most likely lipidic) precipitation during later purification steps. After Ni-affinity purification the recombinant protein accounted for >85 % of the eluted proteins. While $_{GST}$bicD2_mini was further purified as a GST-tagged protein, the tags were removed from all other proteins using TEV-protease digest. As a final purification step size-exclusion chromatography using a Superdex200 column (3.6.1) was employed and fractions containing homogeneous monomeric protein with a purity of >90 % were obtained for all constructs (see Fig. 25). Full-length PIST as well as the truncated p150 construct could be concentrated to more than 10 mg/mL (~200 and ~190 µM respectively) and remained in solution for many days at room temperature without showing any visible precipitation.

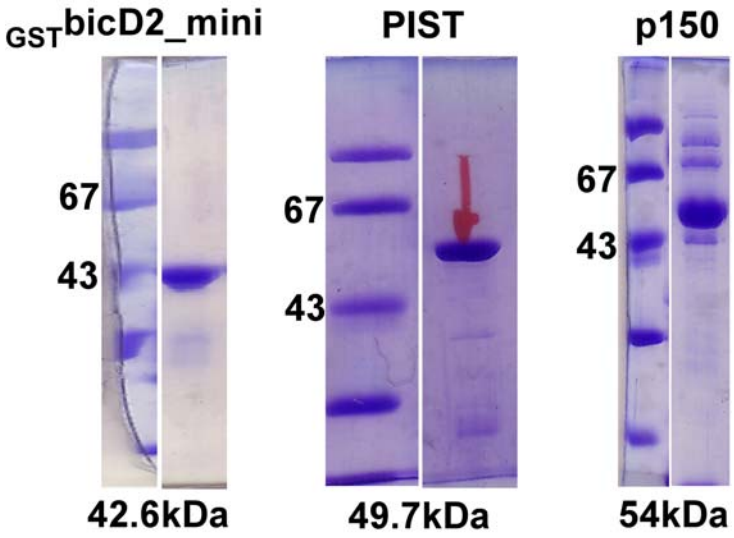

Fig.25 Purity of the preparations of $_{GST}$bicD2_mini, PIST and p150 SDS-PAGE analysis of protein samples of $_{GST}$bicD2_mini, PIST and p150 to demonstrate the purity achieved after the final purification step using size-exclusion chromatography on a Superdex200 column. The gel samples are shown with their respective molecular weight marker. The calculated masses are displayed at the bottom of the corresponding gel scan.

$_{GST}$bicD2_mini appeared less stable. Losses during purification of this construct were greater and the protein could not be concentrated to more than 2 mg/mL (~50 µM) without forming a precipitate.

Samples of the effector proteins were analysed by MALDI-MS (3.5.3). The observed masses for $_{GST}$bicD2_mini (42793.6Da, Δm = +201.6Da), PIST (49946.9Da, Δm = 31.6Da) and p150 (54239.0Da, Δm = -17.3Da) confirm the results of the SDS-PAGE analysis and, with the exception of $_{GST}$bicD2_mini, were

found to be in accordance with the calculated masses of the proteins (+ Gly, His appendage). Reasons for the different observed and calculated masses in the case of $_{GST}$bicD2_mini remain unclear. However, since the amino acid composition of the protein had been validated by sequencing the expression construct, the integrity of the effector was assumed.

4.12 Binding Assay with Affinity Matrix

Truncation of a protein can lead to the loss of structural features that are essential for interaction with other protein binding partners. Furthermore, addition of affinity tags can potentially lead to steric hindrance of such interactions. In particular, use of the larger molecular weight GST-tag [235] might affect the binding properties of the smaller minimal Rab6a-binding domain of bicaudalD2. To evaluate whether interaction of Rab6a with the effector domain $_{GST}$bicD2_minimal was still possible, a binding assay was carried out. For this $_{GST}$bicD2_minimal was immobilised on GSH-sepharose[188] affinity matrix and incubated with either GDP- or GTP-bound untagged Rab6a. Since this method enables easy removal of unbound protein through a series of washing steps, eluting the tag-bound protein from the matrix should co-elute only proteins displaying specific interaction (Fig.26).

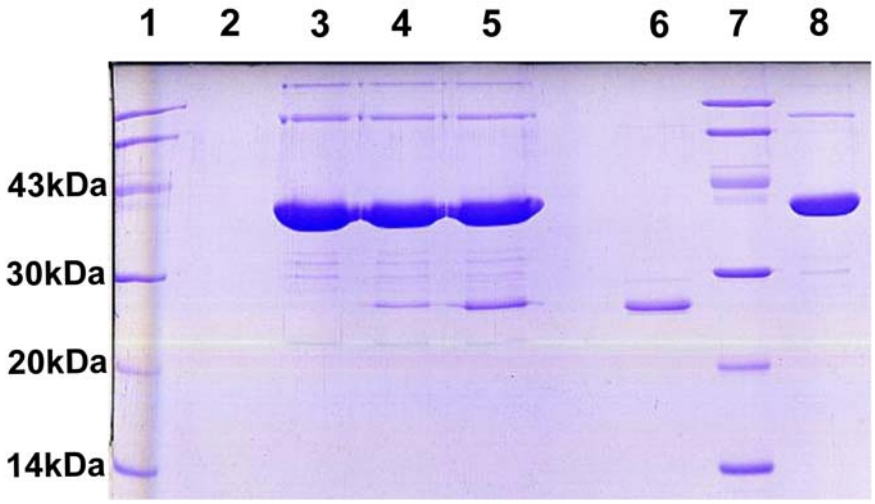

Fig.26 Pull-down assay with matrix-bound $_{GST}$bicD2_mini. SDS-PAGE showing: **1** molecular weight marker; **2** negative control: elution sample of GSH-beads incubated with Rab6a alone, after washing; **3** elution sample of GSH-beads incubated with $_{GST}$bicD2_mini alone, after washing; **4** as in **3** + incubation with Rab6a●GDP; **5** as in **3** + incubation with Rab6a●GTP; **6** protein sample of Rab6a; **7** molecular weight marker; **8** protein sample of $_{GST}$bicD2_mini. For the exact procedure and buffer conditions see (3.6.2).

Rab6a alone does not bind unspecifically to the GSH-sepharose matrix, as no protein could be detected by Comassie staining of the gel in figure 26 (2). However, Rab6a could be observed to co-elute where it had been incubated with $_{GST}$bicD2_minimal. Moreover, from this assay it appeared as if binding of Rab6a and $_{GST}$bicD2_minimal was preferential for, but not restricted to, the GTP-bound state of the GTPase. Though a number of Rab effectors have already been shown to bind their particular GTPase when it is bound to GDP (for review see [236]), this finding was surprising, because the minimal Rab6a-binding domain of bicaudalD2 had been identified to bind specifically Rab6a●GTP [237].
Taking into account the procedure employed for the preparation of Rab6a●GDP (allowing GTP to be hydrolysed to GDP by intrinsic GTPase activity; see 4.6.3) it

appears more reasonable to assume that the Rab6a-band in lane 4 (Fig.26) can be accounted for residual Rab6a●GTP from a protein sample in which the nucleotide had not been completely hydrolysed. An alternative explanation would be that $_{GST}$bicD2_minimal shows a much reduced affinity to Rab6a●GDP, which nevertheless was enough to retain a part of the GTPase bound.
The result of this pull-down assay provided evidence that the protein domain construct $_{GST}$bicD2_minimal is sufficient for binding to Rab6a and the presence of the GST-tag is not a steric obstacle for this interaction. Furthermore, $_{GST}$bicD2_minimal shows preference for the GTP-bound form of Rab6a.

4.13 Preparation of Rab6a-Effector Complexes

As a first attempt to form complexes of Rab6a and its effectors, bacterial expression strains were co-transformed with two expression plasmids. One bearing open reading frames of either of the three effectors with a C-terminal affinity tag, the other with the hydrolysis deficient mutant Rab6aNΔ12CΔ33(Q72L) without an affinity tag. Recombinant co-expression of Rab GTPases and their respective effectors has previously been shown to yield nearly stoichiometric complexes of the two proteins, formed directly after expression. In small scale expression tests, with all combinations of Rab6a and the three effectors under investigation, recombinant expression of GTPase and effectors was observed in a 1:1 ratio in soluble form. However, attempts to scale up the expression cultures failed As the relative expression level of Rab6aNΔ12CΔ33(Q72L) decreased, this prevented stoichiometric binding with the effector and ultimately obliterated preparation of the complex in amounts sufficient for purification. Loss of the expression plasmid or competition for components of the transcription machinery to the disadvantage of Rab6a might have caused these effects, however the exact reasons for these observations remain unclear.

As the attempts to form complexes *in vivo* was not successful, Rab6a-effector complexes had to be prepared from purified proteins (3.6.3). To purify Rab6a in complex with the minimal Rab6a-binding domain of bicaudalD2, a slurry of $_{GST}$bicD2_minimal immobilized on GSH-sepharose was incubated with Rab6aCΔ27. The Rab6aCΔ27:bicD2_minimal complex was cleaved off the matrix, by incubation with TEV protease (Fig.27).

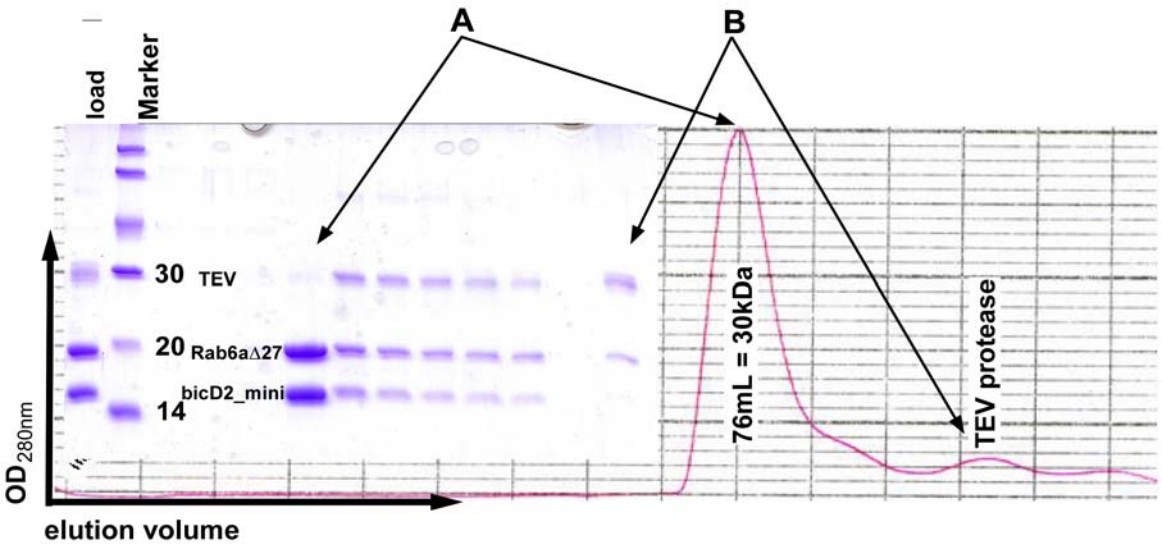

Fig.27 Purification of the Rab6aCΔ27:bicD2_minimal complex. The elution chromatogram of a Superdex75 16/60 gelfiltration chromatography column and the corresponding SDS-PAGE analysis (inset) for the purification of Rab6aCΔ27:bicD2_minimal. **A** absorption peak of the protein complex and corresponding gel sample. **B** absorption peak and gel sample of TEV protease and excess Rab6aΔ27.

A molar excess of the GTPase ensured complex formation and prevented precipitation of free bicD2_minimal. While the GST-tag remained on the matrix, TEV protease (~29 kDa) was separated from the new formed complex (~34kDa) using size-exclusion chromatography.
Rab6aCΔ27:bicD2_minimal eluted from the gelfiltration column as a single peak at an elution volume corresponding to a molecular weight of ~30 kDa, indicating that the protein sample consisted of the homogenously monomeric complex. SDS-PAGE analysis revealed (**A**) two protein bands of a 1:1 stoichiometry at ~15 kDa and ~20 kDa. A second, much smaller absorption peak (**B**) corresponds to eluted TEV protease and an excess of Rab6aΔ27. Comparison of the GSH-sepharose supernatant, which had been injected onto the gelfiltration column, and sample (**A**) shows that TEV protease and any unbound protein were efficiently separated from the complex.
While the elution volume of the Rab6aCΔ27:bicD2_minimal complex is in agreement with its calculated mass, the apparent molecular size of bicD2_mini alone, as observed in the SDS-PAGE analysis, does not correspond to its calculated mass. This might be due to a different migratory behaviour of this protein in the polyacrylamide gel matrix and could potentially be indicative of structural characteristics that differ from that of globular proteins, which were used for calibration of the chromatography system (see 4.17.1).
A sample of the Rab6aCΔ27:bicD2_minimal complex was analysed for stability by incubation at room temperature over three days. During this period, the sample did not show any visible precipitation (Fig.28).

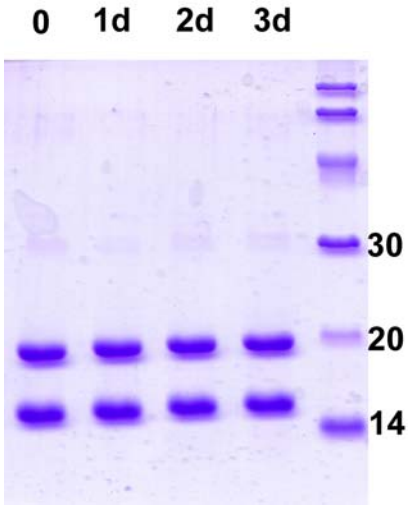

Fig.28 Stability of Rab6aCΔ27:bicD2_minimal at room temperature. SDS-PAGE analysis of Rab6aCΔ27:bicD2_minimal in a buffer consisting of 30 mM TrisHCl pH 7.5, 50 mM LiCl, 5 mM DTT and 100 µM GTP at room temperature. Samples were taken after one (1d), two (2d) and three (3d) days, mixed with an equal volume of SDS-loading buffer and stored at -20°C for later analysis.

The complex of Rab6aCΔ27:bicD2_minimal could be concentrated up to 8 mg/mL and was subsequently used for crystallographic and biochemical experiments.
Preparing complexes of Rab6a with p150 or PIST turned out to be less tedious, since the purified effectors could be obtained and remained soluble even after tag cleavage. Hence, simple incubation of a mixture of Rab6a (in molar excess) with each of the two proteins in the presence of GTP on ice, followed by gelfiltration chromatography, was sufficient to obtain samples of high purity and homogeneity.

Figure 29 shows the SDS-PAGE analysis of samples taken during a typical size-exclusion chromatographic purification of Rab6a:p150.

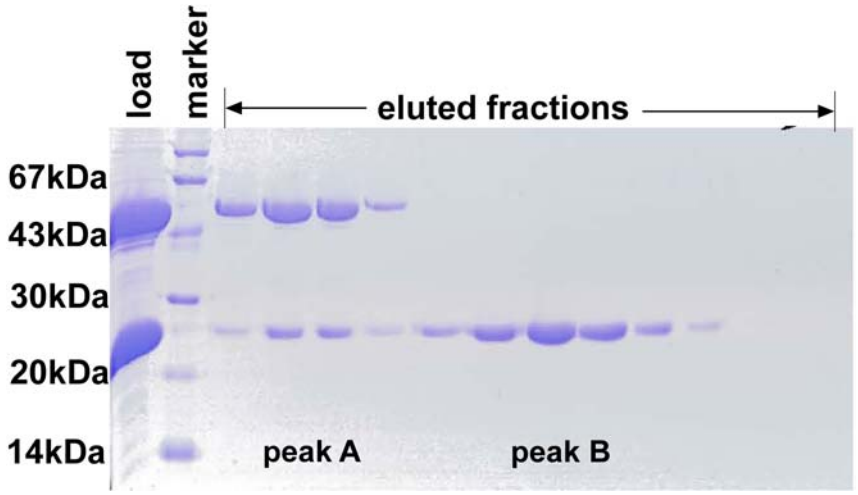

Fig.29 Preparation of the Rab6a:p150 complex. SDS-PAGE analysis of the gelfiltration chromatography of Rab6a:p150 using buffer consisting of 20 mM TrisHCl pH 7.5, 30 mM LiCl, 5 mM DTT and 100 µM GTP. Two distinct absorption peaks were observed for the complex (peak A) and excess Rab6a (peak B) using a Superdex200 26/60 chromatograpy column.

The injected protein sample eluted as two distinct absorption peaks, corresponding to the complex (peak A) and excess Rab6a (peak B), from a Superdex200 26/60 gelfiltration chromatography column. The observed purity and homogeneity of the samples obtained in the case of Rab6a in complex with PIST were comparable with that shown for Rab6a:p150. Both complexes were analysed for their stability at room temperature and could be concentrated to more than 10 mg/mL without showing any visible precipitation.
Initial precipitation experiments with p150 or PIST in complex with full length Rab6a yielded precipitated protein samples only. This may have been caused be either insufficient structural rigidity or stability of these complexes. Hence, Rab6a:p150 and Rab6a:PIST were not taken into consideration for crystallographic screening, but they were used for further biochemical characterization.

4.14 Construction of Expression-Vectors for Truncated Effector Proteins

A high degree of structural rigidity of a protein is a primary prerequisity for its successful crystalisation. Unstructured regions or loops can impede tight packing of the protein molecules for crystal formation. Hence engineering, especially of larger proteins, is almost always necessary. In order to identify domains of high structural order within a protein, the higher susceptibility of unstructured regions to protease cleavage can be exploited. In an attempt to improve the chances of crystallisation, truncated expression constructs of the three Rab6a effectors were designed based on a limited proteolysis assay in combination with bioinformatic structure analysis. For limited proteolysis, unlike complete digestion, a protein sample is incubated with varying concentrations of a protease for a limited time. After defined time intervals, aliquots are taken for analysis by SDS-PAGE and MALDI-MS. By this method identification of structured protein domains, which are less susceptible to cleavage than unstructured regions, is feasible. Analysing the amino acid sequence of the protein for potential protease cleavage sites allows the correlation of the observed fragments to a predicted fragmentation pattern. Stable fragments can be assigned to protein domains that are predicted to be structurally orderd, based on primary structure analysis. For bicaudalD2 and PIST primary structure analysis using the programs *PAIRCOIL* and *MULTICOIL* [177,176] predicts a number of stretches with a high propensity for formation of dimeric coiled-coils. Furthermore, the group of Francis Barr showed that the domain required for Rab6a-interaction in both effector proteins contains a coiled-coil motif. Due to their specific structure fold (see 1.12) coiled-coils are largely resistant to protease digestion or chemical denaturation [238], which should allow detection of these domains as stable fragments in a limited proteolysis assay.

The interaction of two proteins can lead to structural rearrangements and shielding of surface exposed parts of the single proteins. This can lead to protection of otherwise susceptible protease sites and, as a consequence, to a different cleavage pattern. Therefore, limited proteolysis of the single proteins as well as of the corresponding complex was carried out whenever possible. In this way Rab6aNΔ12CΔ27 and PIST were analysed as a basis for analysis of the complex Rab6aNΔ12CΔ27(Q72L):PIST. Since bicD2_mini was soluble only in its GST-tagged form, this protein was analysed only in complex with Rab6aNΔ12CΔ27(Q72L).

Figure 30 displays the results of an optimisation for the limited proteolysis of Rab6aNΔ12CΔ27 using the proteases trypsin and elastase.

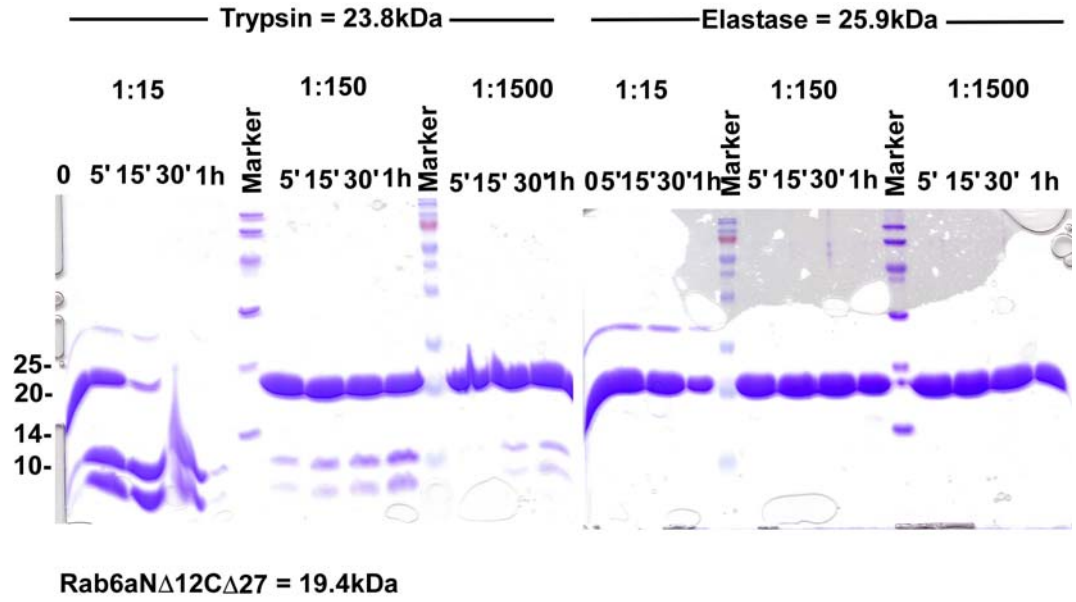

Fig.30 Limited proteolysis of Rab6aNΔ12CΔ27 by trypsin and elastase. SDS-PAGE analysis of samples taken after five, 15, 30 minutes and one hour from proteolytic digest reactions of Rab6aNΔ12CΔ27 that had been incubated at room temperature either trypsin or elastase at molar ratios of 1:15, 1:150 or 1:1500. See 3.6.5 for the exact procedure and buffer compositions.

Judging by SDS-PAGE analysis trypsin appears to rapidly cleave Rab6aNΔ12CΔ27 into two main fragments of ~8 kDa and ~11 kDa, whereas elastase does not show significant protease activity on the GTPase. As can be seen for trypsin at final molar ratios of 1:15 and 1:150, the two cleavage products that appear instantly after starting the reaction are stable for up to thirty minutes under the conditions of the digest. After this time the protein bands in the gel fade, which should account for further digest into smaller fragments that already migrated off the gel. For the elastase digest very faint protein bands of 9 kDa become detectible only after one hour incubation at the highest enzyme concentration. Samples of the trypsin digest (1:150, 15min) and the elastase digest (1:15, 1h) were analysed by MALDI-MS, after stopping the digest by addition of the protease inhibitor PMSF (2 mM final). Thus, two main fragments were identified in the trypsin digest (11116 and 7886 kDa) and one using elastase (9463 kDa). The molecular weight corresponds to the migratory pattern of the protein bands in the respective SDS-PAGE. Interestingly, a species of ~18.9 kDa was observed in both MALDI-MS samples. This molecular weight is very close to that of Rab6aNΔ12CΔ33 (18.6 kDa), which was used for structure determination. Thus, the limited proteolysis method can be viewed as confirmation of the approach to further truncate the expression construct to promote crystallisation (3.1.1.).

The observed protein fragments identified by SDS-PAGE and MALDI-MS were attributed to Rab6aNΔ12CΔ27 in the analysis of the effector complexes and not taken into consideration as possible effector fragments.

Figure 31 summarizes the results of the limited proteolysis assay with Rab6aNΔ12CΔ27(Q72L):bicD2_mini. In complex with its effector Rab6a appears less susceptible to protease digestion by trypsin or elastase, as a decrease in the

intensity of the corresponding protein band is not perceptible (Fig.31 B). The protein fragment, which appeared most prominent in the SDS-PAGE analysis, could be attributed to distinct species of correlating molecular weight that were detected during MALDI-MS analysis (Fig.31 C). The obtained results were compared with the protease cleavage pattern of bicD2_mini as calculated by the program *PAWS*. Combining these methods an attempt was made to assign observed cleavage products to the predicted coiled-coil domain of the protein (Fig.31A). Based on this, two constructs for the expression of truncated versions of bicD2_minimal were designed. While bicD2_miniΔ10 contained amino acids 706 to 814 of the full length bicaudalD2, bicD2_miniCORE was designed as a 70 amino acid protein domain, comprising only the residues with highest potential to form a coiled-coil structure (Table 4).

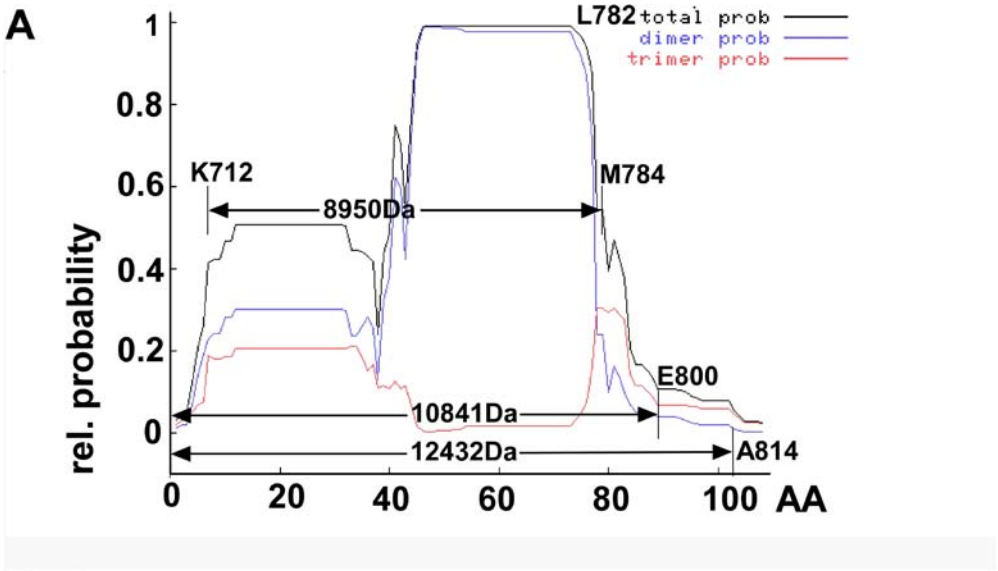

C

	protease	SDS-PAGE [kDa]	MALDI-MS [Da]	fragment amino acids *(PAWS)*	fragment mass [Da] *(PAWS)*
Rab6aNΔ12CΔ27 : bicD2_mini	trypsin	12	12608	1 - 106	12290
				9 - 118	12627
			6303	9 - 60	6153
				29 - 83	6294
	elastase	12	11878	15 - 118	11893
		8	8722	1 - 76	8705
			8273	1 - 72	8277

Fig.31 Limited proteolysis and primary structure analysis of Rab6aNΔ12CΔ27(Q72L):bicD2_mini.
A Graphic representation of a primary structure analysis of bicD2_mini using the program *Multicoil* [176]. The per-residue probability of forming a two- (blue) or three-stranded (red) coiled-coil structure; total probability (black) is shown. Calculated molecular weights of predicted cleavage fragments are displayed, delimiting amino acid residues are indicated. **B** SDS-PAGE analysis of samples taken from the limited proteolysis of Rab6aNΔ12CΔ27:bicD2_mini, using trypsin (1:150 molar ratio) or elastase (1:15 molar ratio) after 0, 1, 3, 5 and 10 minutes at room temperature. See 3.6.5 for the exact procedure and buffer compositions. **C** Summary of the molecular weight of protein cleavage products as observed using SDS-PAGE, MALDI-MS and the proteolytic fragments of the relevant weight range, as predicted by the program *PAWS*.

Limited proteolysis was also employed for further engineering of truncated PIST expression constructs. Figure 32 summarizes the results for PIST and the complex Rab6aNΔ12CΔ27(Q72L):PIST that were included in this assay. A peculiarity of this experiment was the striking discrepancy in the molecular weights of cleavage products of PIST as observed by SDS-PAGE and MALDI-MS (Fig.32 C). Although the same samples were used for both methods, mass spectroscopy of the protein digest did not detect fragments of a molecular weight greater than ~5 kDa. Two problems may have caused these observations. One is that insufficient ionization ihibited detection of the cleavage products during mass spectroscopy. Alternatively, the higher than expected positions of the protein bands in the SDS-PAGE may be indicative of unusual migration behaviour of the fragments. For further analysis of these observations, the most prominent protein band of the trypsin digest of PIST alone (at ~15 kDa, Fig.32 B) was excised from the SDS-gel and, following a whole protein extraction step as adapted from Cohen and Chait [239], analysed by MALDI-MS. Two distinct species of 11.2 kDa and 11.3 kDa were detected (indicated with * in Fig.32 C). Apparently, cleavage fragments of PIST do indeed migrate through the polyacrylamide gel with a higher apparent molecular weight, however, unknown problems prevented proper mass determination of the fragments in the digest reaction mixture during MALDI-MS analysis.

Compared to PIST, Rab6 appears more resistant against protease digest in the Rab6aNΔ12CΔ27(Q72L):PIST complex, which had also been observed for the interaction with bicD2_mini. Again, the obtained results of SDS-PAGE and MALDI-MS were compared with the predicted protease cleavage pattern of PIST. Most prominent observed cleavage products were assigned to the region around the two putative coiled-coil domains of the protein (see 1.11).

Based on this data, three constructs for expression of truncated versions of PIST were designed. PISTcc1 contains amino acids 29 - 133, which equals an aminoterminal deletion of 29 residues and inclusion of the aminoterminal putative coiled-coil domain required for Rab6a-interaction. PIST2cc comprises both putative coiled-coil domains, between residues 89 and 193. PISTcc1-CORE was designed as a 44 amino acid protein domain, comprising only the residues with highest potential to form the N-terminal coiled-coil structure (89 - 133, Fig.32 A).

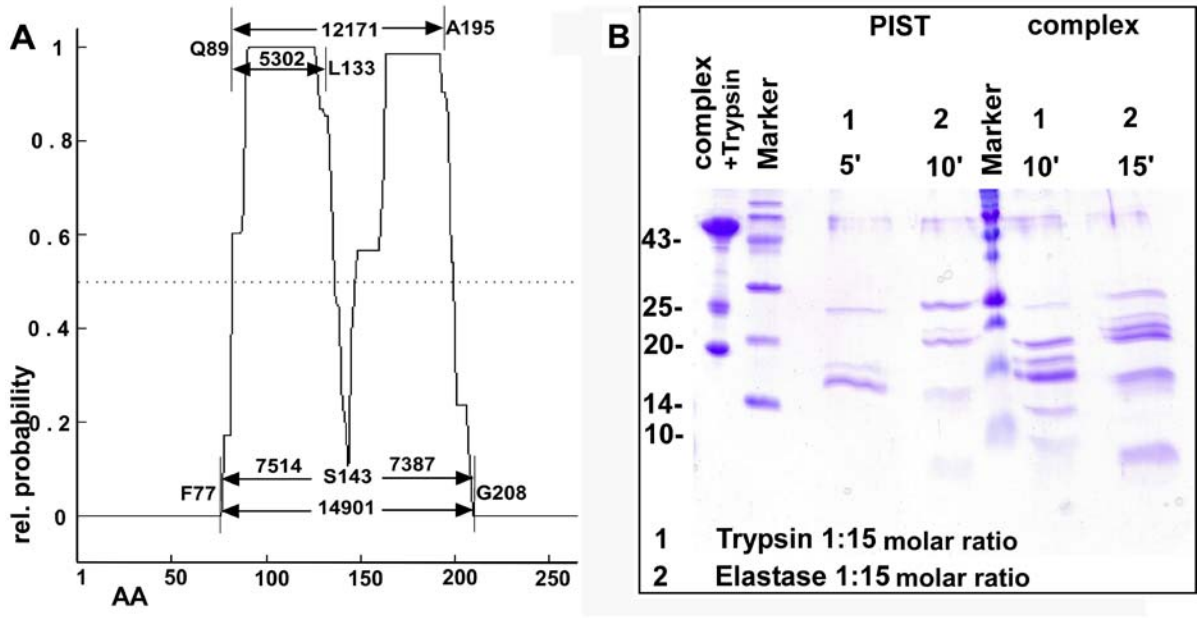

C

	protease	SDS-PAGE [kDa]	MALDI-MS [Da]	fragment amino acids (*PAWS*)		fragment mass [Da] (*PAWS*)
PIST	trypsin	24			single protein	
		17				
		15				
			* 11337	84 - 183		11391
			* 11196			
	elastase	25				
		19				
		18				
		15				
		8				
			5708			
			4448			
Rab6aNΔ12CΔ27:PIST	trypsin	17				
		15				
		14	14797	70 - 200		14720
		11	11967			
		8	7573	77 - 143		7514
	elastase	18				
		17				
		14				
		6	5704			
			5497			

Fig.32 Limited proteolysis and primary structure analysis of PIST alone and in complex with Rab6aNΔ12CΔ27(Q72L).

A Graphic representation of a primary structure analysis of PIST using the program *Paircoil* [176]. The per-residue probability of forming a parallel two-stranded coiled-coil structure is shown. Calculated molecular weights of predicted clevage fragments are displayed, delimiting amino acid residues are indicated. **B** SDS-PAGE analysis of samples taken from the limited proteolysis of PIST and Rab6aNΔ12CΔ27(Q72L):PIST, using trypsin (1:15 molar ratio) or elastase (1:15 molar ratio) after 5 and 10 (PIST) or 10 and 15 minutes (complex) respectively at room temperature. See 3.6.5for the exact procedure and buffer compositions. **C** Summary of the molecular weight of protein cleavage products as observed using SDS-PAGE, MALDI-MS and the proteolytic fragments (amino acid numbering and calculated molecular weight) of the relevant weight range, as predicted by the program *PAWS*.

A construct for the expression of a truncated version of p150 was designed without the experimental set-up of a limited proteolysis, but by analogy to the results obtained for bicD2_mini and PIST. Primary structure analysis using the program *Multicoil* [176] identifies one putative coiled-coil domain between residues 957 and 1024 in the successfully expressed p150. Hence, according to the predicted localization a 67 amino acid containing domain, p150cc, was defined. Table 4 summerizes all constructs used for expression of Rab6a effectors and truncated versions thereof. The resulting proteins were used for structural and biochemical analysis

Table 4 Summary of all recombinantly expressed Rab6a effector constructs.

protein origin	fragment name	amino acids	mol. Mass [kDa]	tag	expression / solubility
BicaudalD2		824			
	bicD2_minimal	706-824	13.5 (42.6)	His_6-GST-	high / medium
	bicD2_minimalΔ10	706-814	12.4 (41.6)	His_6-GST-	high / high
	bicD2_miniCORE	712-782	8.2 (37.6)	His_6-GST-	high / high
PIST / GOPc		454			
	PIST	1-454	49.7 (51.8)	His_6-IF-	high / medium
	PISTcc1	29-133	12.1 (14.3)	His_6-	high / high
	PIST-2cc	89-193	12.0 (41.2)	His_6-GST-	medium / medium
	PISTcc1-CORE	89-133	5.2 (34.4)	His_6-GST-	high / high
$p150_{glued}$		1278			
	p150	540-1041	54.2 (56.1)	His_6-	high / high
	p150cc	957-1024	7.8 (37.0)	His_6-GST-	high / high

4.15 Crystalisation of Rab6a : Effector Complexes

Samples of all effector proteins and complexes with Rab6a that could be formed were subjected to crystallisation assays. Freshly purified protein samples were brought to the right concentration via precipitation tests using the PEG/ION crystallisation screen (Hampton Research) before aliquoting and freezing. The protein concentration of the samples was adjusted such that in no more than 30% of all samples in any crystallisation screen precipitated directly upon mixing with the reservoir solution at a temperature of 20°C.
In crystalisation trials carried out with Rab6aΔ27:bicD2_mini small rosettes of tightly packed small needles were observed using 100mM Hepes pH 7.5 and 18% (w/v) PEG 600 after two days at 293K. Optimisation of crystalisation conditions turned out to be demanding, as simple reconstitution of the buffer components corresponding to the screen Stura II [240] condition number A2 did not result in crystal growth. Crystallisation was observed only when solution from the original screen or very old samples of PEG 600 were used. One possible explanation for this is that crystallisation of the complex occurs only with an oxidized form of PEG 600, which can be found in older solutions due to their contact with air. Consequently, crystallisation conditions of the original screen could be reproduced only in some cases where the PEG 600 solution had been aerated for several hours prior to use. Crystallisation trials using the same composition of mother liquor for varying concentrations of Rab6aΔ27 and Rab6aNΔ12CΔ27 did not yield crystal growth, indicating that the observed crystals consisted of the complex of Rab6aΔ27:bicD2_mini. To optimise crystalisation conditions a grid screen was set up, varying the pH, the molecular weight and concentration of PEG. In an attempt to overcome agglomeration the best conditions acquired were screened against different additives and detergents. However, quality of the crystals improved only slightly. Best results were obtained using the hanging-drop vapour diffusion method at 293 K with protein at a concentration of 4 mg/mL in 30 mM TrisHCl pH 7.5, 50 mM LiCl, 5 mM DTT and 1 mM GTP (Fig.33). 2 µL protein solution were mixed with an equal volume of reservoir solution containing 100 mM Hepes pH 8.0 and 18 % (w/v) PEG monomethyl ether 550 (MMPEG 550) and 5 mM D-Trehalose. Crystals appeared two days after setting up the drops but disintegrated after three weeks. Disintegration of the crystals may be explained as a consequence of GTPase activity of Rab6a and the subsequent breaking up of the protein complex. However, in the absence of complex crystals containing the GTPase-deficient Rab6aNΔ12CΔ27(Q7L), definitive proof for this hypothesis is still missing.

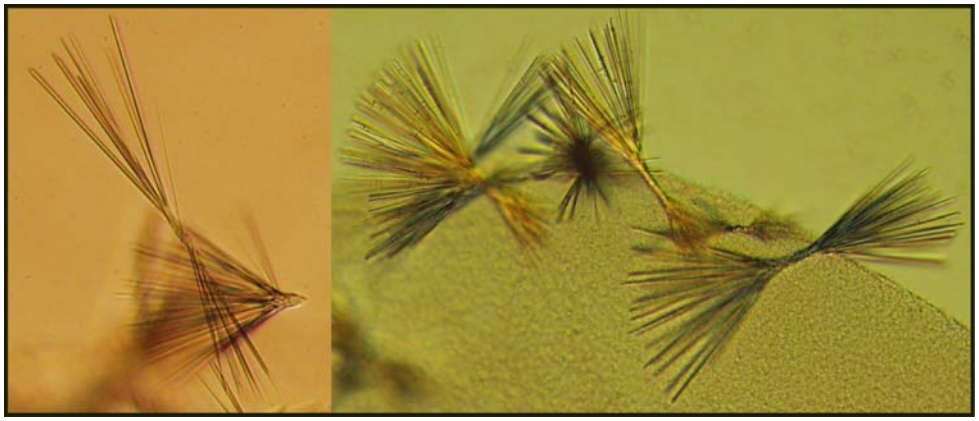

Fig.33 Crystals of Rab6aΔ27:bicD2_mini. Micrograph of Rab6aΔ27:bicD2_mini crystals arranged in stacks and clusters of needles as observed in crystallisation conditions using 100mM Hepes pH 8.0, 18% (w/v) polyethylene glycol monomethyl ether 550 (MMPEG 550) and 5mM D-Trehalose at 293K.

Although various attempts to further optimise crystallisation conditions were made, crystal quality of Rab6aΔ27:bicD2_mini could not be improved beyond the state that is displayed in figure 33.
Furthermore, Rab6aΔ27:bicD2_mini represents the only Rab6a-effector complex for which crystal growth could be observed, despite extensive screening.

4.16 NMR

Attempting to define the effector-binding interface of Rab6a and to obtain structural information of the effector proteins, Rab6aΔ27, PISTcc1, PISTcc1-CORE and p150cc were used in heteronuclear NMR-spectroscopy. In a first experiment Rab6aΔ27 was uniformly labelled with stable ^{15}N-isotopes (3.4.3) and a ^{1}H/^{15}N-HSQC spectrum was recorded from a sample at a concentration of 200 µM (3.8.2). Figure 34 shows that the acquired ^{1}H/^{15}N-signals are dispersed over a large part of the ^{1}H-frequency (6.1 - 11.1 ppm). The spectrum displays little signal overlap, which can be attributed to a high degree of structural order of the protein. ^{1}H-resonances around 6.9 to 8.0 ppm indicate that the corresponding residues are involved in an α-helical fold, whereas signals at 8.1 to 9.8 ppm are associated to β-sheet secondary structure elements.

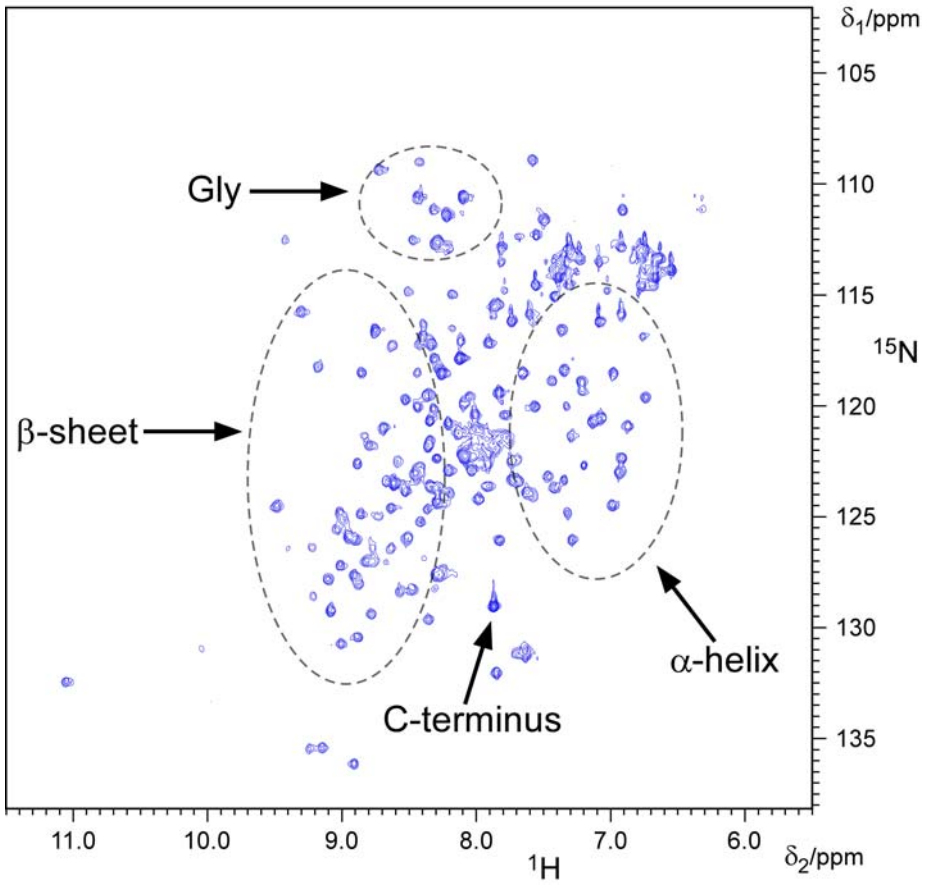

Fig.34 ^{1}H/^{15}N-HSQC spectrum of Rab6aΔ27. ^{1}H/^{15}N-resonances of Rab6aΔ27 of an HSQC-spectrum recorded over four hours at pH 6.2 and 27°C. Resonances corresponding to distinct secondary structure elements or individual residues are indicated. See 3.4.3 and 3.8.2 for the exact setup and buffer composition.

Despite the absence of an NMR-assignment for Rab6a, some features of the spectrum can be associated with primary structure elements of the GTPase. Thus, ^{1}H/^{15}N-HSQC resonances stemming from the carboxy terminus of Rab6a and the well resolved resonances of the glycines are indicated in figure 34. Overall, the well resolved spectra confirm the high homogeneity and the α/β-structural content of the Rab6a protein preparation.

In the following experiments unlabeled PISTcc1 was used for stepwise titration against ^{15}N-labelled Rab6aΔ27, in molar ratios of 0.25, 0.5, 1 and 1.25, aiming at complete saturation of the GTPase. However, upon titration the majority of the ^{1}H/^{15}N-resonances vanished after the second addition of PISTcc1 (Fig.35). The resulting spectrum mainly displays overlapping signals, some single resonances and signals from the C-terminus. The complete disappearance of signals originating from α-helical and β-sheet structures can be explained by binding of PISTcc1.

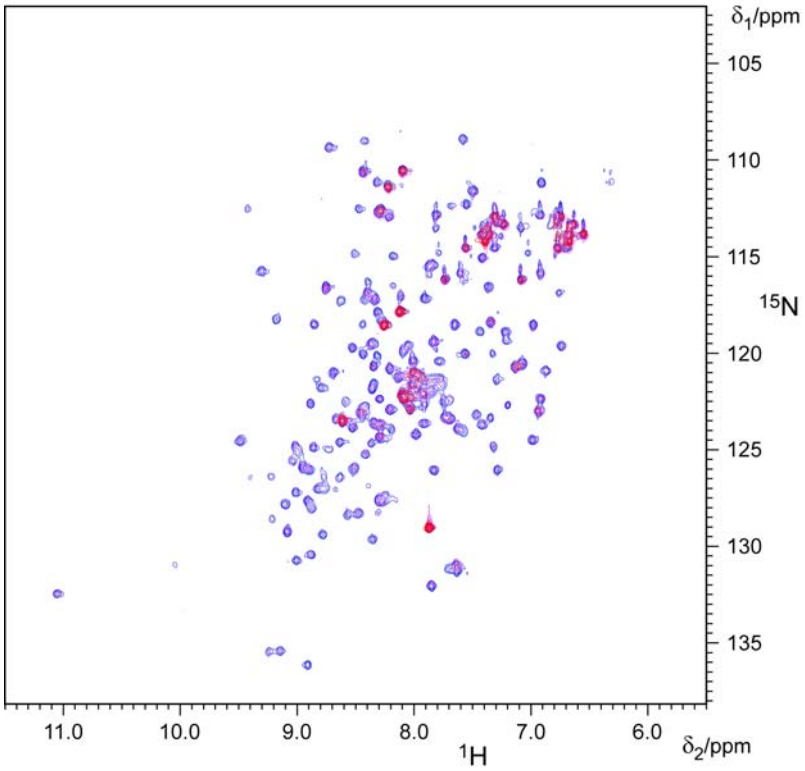

Fig.35 Titration of PISTcc1 against (^{15}N)Rab6aΔ27. Overlay of the ^{15}N/^{1}H-resonances of (^{15}N)Rab6aΔ27 alone (blue) and with added PISTcc1 at molar ratios of 1:0.25 (purple) and 1:0.5 (red). HSQC-spectra were recorded over four hours at pH 6.2 and 27°C. See 3.4.3 and 3.8.2 for the exact setup and buffer composition

Direct interaction with the effector domain would change diffusion and rotational properties only of the parts of the GTPase involved in effector binding. Since the ~33 kDa (^{15}N)Rab6aΔ27:PISTcc1 complex should have rotational properties that would still allow detection of resonances, the rapid vanishing of signals may have been caused by PISTcc1-induced agglomeration. As a control experiment an ^{1}H/^{15}N-HSQC spectrum of uniformly labelled (^{15}N)PISTcc1 was recorded (Fig.36). Labelling the smaller of the two interacting proteins could potentially enable more detailed analysis of the binding interface by giving a spectrum with fewer resonances.

Although the sample showed no visible sign of precipitation at the concentration used (~400 µM), only a few, mostly overlapping signals around 7.5 to 8.2 ppm and 6.6 to 7.5 ppm in the highfield of the proton-resonance frequency were detected by NMR.

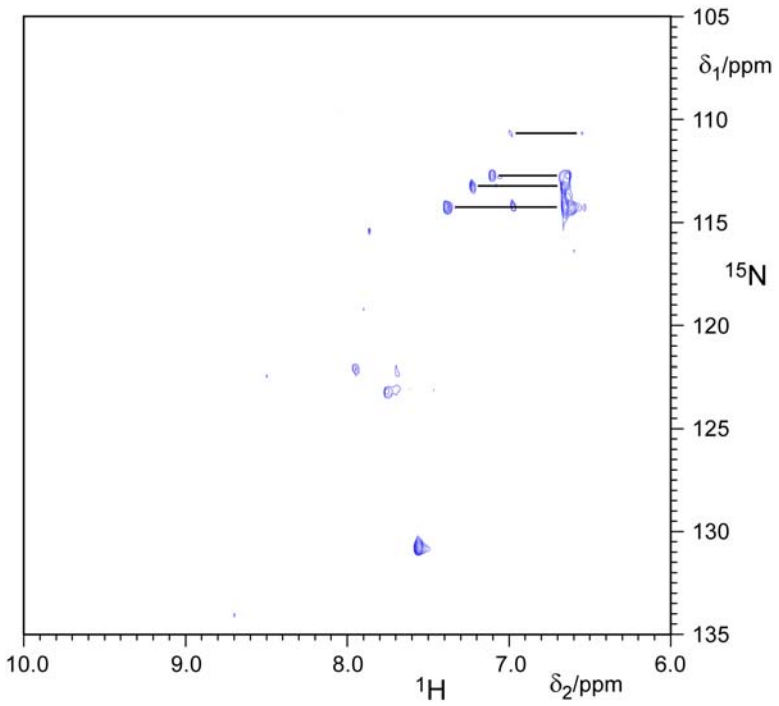

Fig.36 HSQC-spectrum of (^{15}N)PISTcc1. ^{1}H/^{15}N-resonances of the 12 kDa (^{15}N)PISTcc1 of an HSQC-spectrum recorded over twelve hours at pH 6.4 and 27°C. Black lines indicate resonances of spin-spin-coupled $-NH_2$ groups of Gln and Asn. See 3.4.3 and 3.8.2 for the exact setup and buffer composition.

This observation adds further support for the assumption that PISTcc1 forms aggregates of higher molecular mass in solution, which in turn would explain why crystallyzation trials with PISTcc1 alone and in complex with Rab6a were unsuccessful. Nevertheless, the oligomeric state of the protein and its binding behaviour to Rab6a need to be further addressed by different means, such as size-exclusion chromatography (3.17.1).

In another series of experiments unlabelled PISTcc1-CORE was titrated against(^{15}N)Rab6aΔ27 in a procedure equivalent to that used for PISTcc1 (Fig.37).

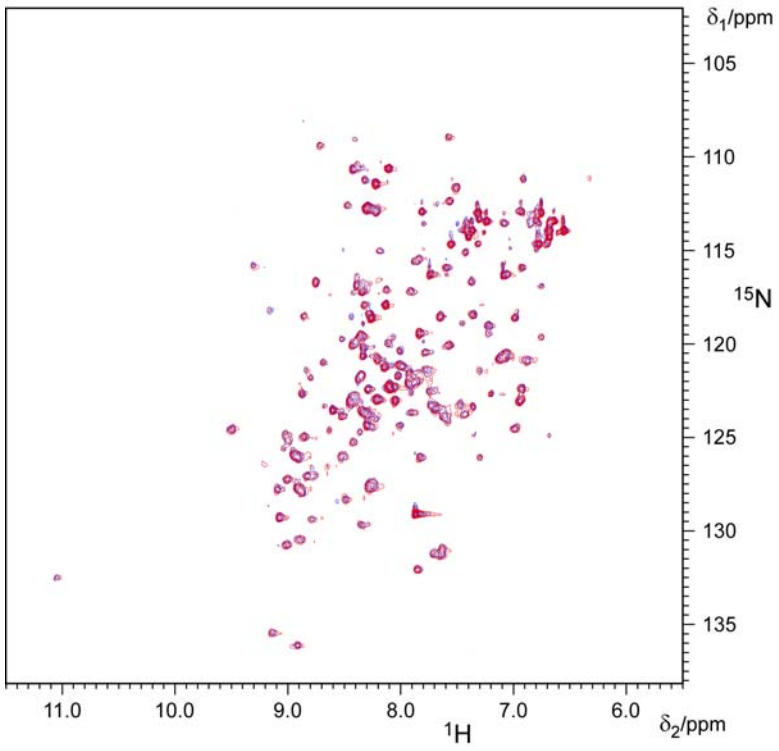

Fig.37 Titration of PISTcc1-CORE against (^{15}N)Rab6a.
Overlay of the ^{1}H/^{15}N-resonances of (^{15}N)Rab6aΔ27 alone (blue) and with added PISTcc1 at molar ratios of 1:0.5 (purple) and 1:0.75 (red). HSQC-spectra were recorded over two hours at pH 6.4 and 27°C.

Despite increasing the amount of PISTcc1-CORE to a twofold molar ratio, a shift or a disappearance of $^{1}H/^{15}N$-resonances was not detected. This observation suggests that binding of Rab6a and PISTcc1-CORE did not occur under the chosen conditions. To verify this assumption in a reverse approach, an attempt was made to detect the chemical shift of $^{1}H/^{15}N$-HSQC resonances caused by binding of Rab6aΔ27 to (^{15}N)PISTcc1-CORE (Fig.38).

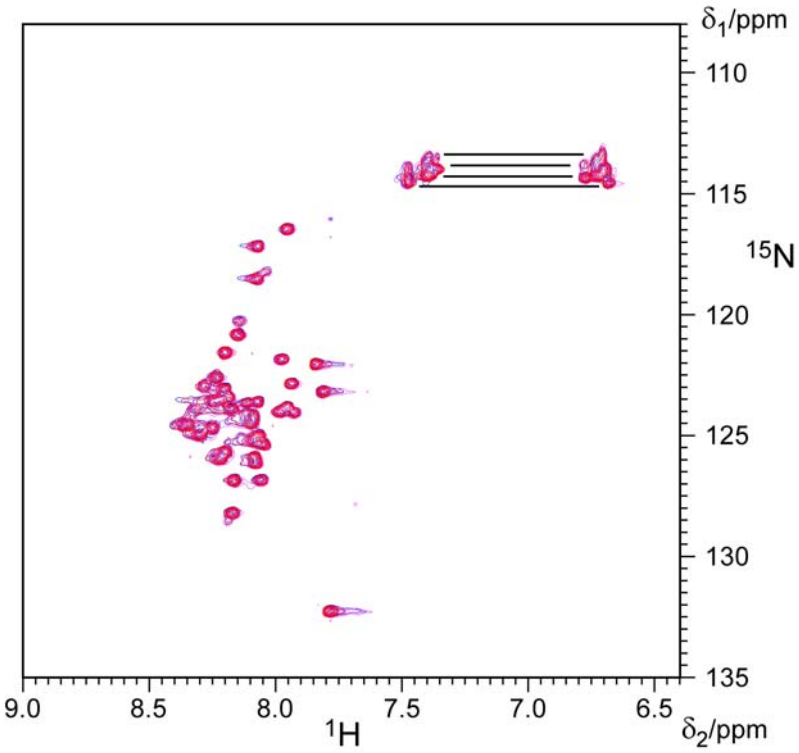

Fig.38 Titration of Rab6aΔ27 against (^{15}N)PISTcc1-CORE. Overlay of the $^{1}H/^{15}N$-resonances of (^{15}N)PISTcc1-CORE alone (blue) and with added Rab6aΔ27 at molar ratios of 1:0.5 (purple) and 1:0.75 (red). HSQC-spectra were recorded over two hours at pH 6.4 and 27°C.

The acquired NMR-spectrum of PISTcc1-CORE alone shows that the protein fragment is intrinsically unstructured. 40 of 47 resonances were detected. They display low dispersion and are found at positions typically occurring in random coil fragments. A main cluster of signals between 7.8 and 8.4 ppm of the ^{1}H-resonances is separated from some high field resonances between 6.7 and 7.5 ppm that can be attributed to Asn and Gln $–NH_2$ groups. However, the latter are seen to be two to four overlapping resonances, while the $–NH_2$ groups of the Asn Gln residues in (^{15}N)PISTcc1-CORE would be expected to produce eight distinct signals displaying clear separation in a well folded domain.

Considering the limited length of the protein fragment, of 47 amino acids, the only arrangement conceivable to form a coiled-coil domain structure would be a left-handed parallel homodimer. Necessary for the stable association of a parallel dimeric coiled-coil would be the formation of attractive ionic interactions between the heptad repeat positions g of one strand and e' of the opposite strand (denoted as i → i'+5). However, primary structure analysis based on a Lupas algorythm [241] indicates deviations from the criteria of the Peptide Velcro (PV-) hypothesis that would need to be met in order to form a coiled-coil structure (see 1.12 and [242,243]). The presence of hydrophilic residues in an otherwise hydrophobic core and repulsive charges at the surface of PISTcc1-CORE (Fig.39) appear to hinder folding

in such a structure. This would imply that PISTcc1-CORE is unstructured (random coil) and as such cannot interact with Rab6a.

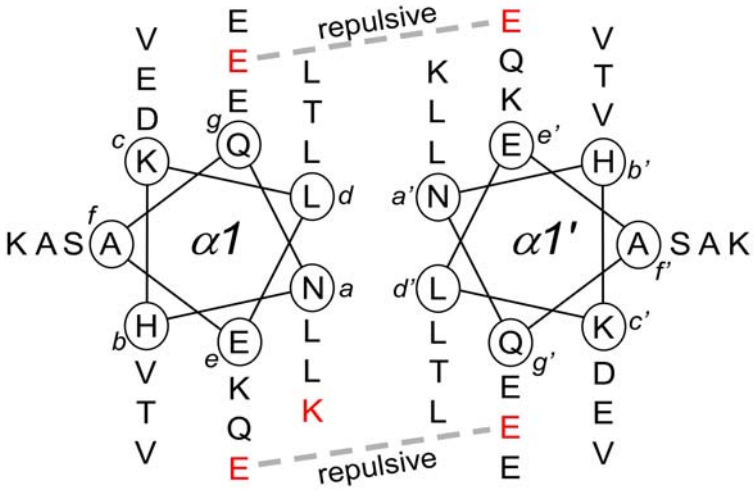

Fig.39 Helical wheel representation of PISTcc1-CORE. Helical wheel diagram constructed for the residues of PISTcc1-CORE calculated to have highest potential to form a parallel lefthanded coiled-coil, based on a *Lupas algorithm* [241]. Repulsive charge-charge interaction and hydrophilic residues in the coiled-coil interface are displayed in red.

Primary structure analysis of p150cc suggests a similar situation, as criteria of the PV-hypothesis are not met in this truncation construct (Fig.40). Although the protein was soluble at concentrations >1 mM, chemical shifts of the C_αH- and NH-resonances from ^{1}H-NMR experiments with p150cc confirmed that the 69 amino acid fragment of p150 is unstructured (Fig.41).

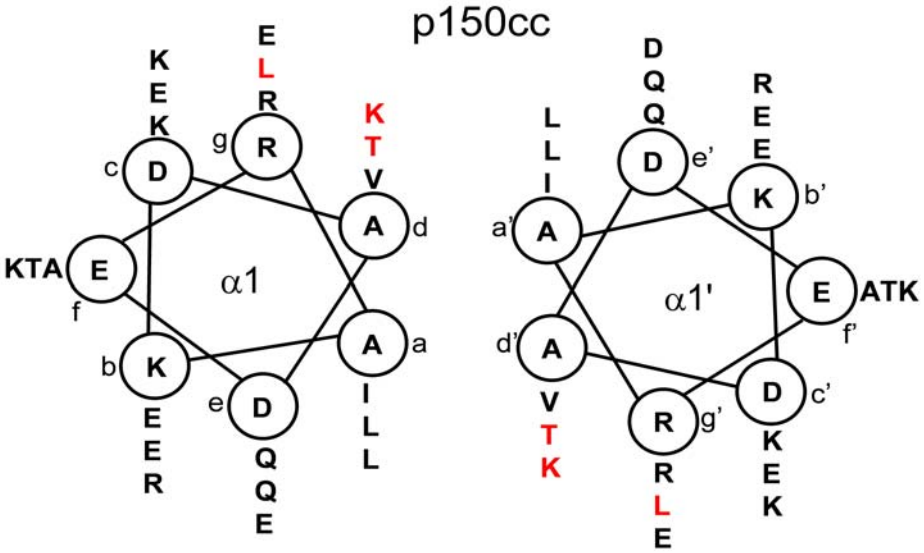

Fig.40. p150cc helical wheel diagram. Construction of the diagram as described for figure 39. Residues not in accordance with the *Peptide Velcro* hypothesis are displayed in red.

Furthermore, binding of p150cc was not detected during titration against (^{15}N)Rab6aΔ27 in ^{1}H/^{15}N-HSQC experiments.

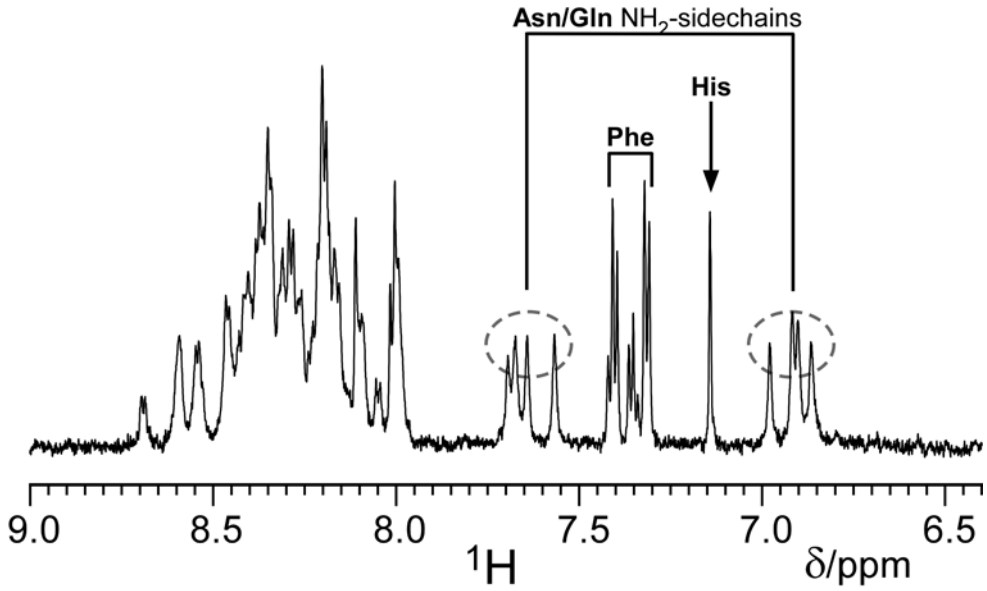

Fig.41 ^{1}H-spectrum of p150cc. The low dispersion in the NH-backbone region from 7.95 - 8.70 ppm suggests that the protein is not well folded. Proton resonances of His, Phe and the NH_2-groups of Asn and Gln are indicated.

Attempts to obtain a ^{1}H/^{15}N-HSQC spectrum of the preformed (^{15}N)Rab6a∆27:bicD2_mini complex, for comparison with the spectrum of (^{15}N)Rab6a∆27 alone, failed due to the instability of the complex under the pH- and temperature conditions of the experiment. For the more stable (^{15}N)Rab6a∆27:$_{GST}$bicD2_mini complex no resonances could be detected. A possible explanation for this finding is that the rotational properties of the GST-tagged complex are insufficient for NMR-spectroscopy, due to the size constraint of the method.

Taken together, the observations made for PISTcc1-CORE and p150cc suggest that the unstructured effector constructs interaction with Rab6a is lost. The interactions appear to require a structural integrity which potentially involves formation of a coiled-coil fold that is still present in PISTcc1 and the larger effector constructs bicD2_mini, PIST and p150. Further investigations are necessary to verify these conclusions obtained on the basis of NMR measurements. Results of an analytical size-exclusion chromatography may indicate an oligomeric solution state and a degree of structuring of effector constructs and Rab6a-effector complexes. Equilibrium measurements and transient kinetic methods can be employed to characterize the interaction of Rab6a with its effectors in more detail.

4.17 Characterization of the Interactions of Rab6a with its Effectors

4.17.1 Analytical Size-Exclusion Chromatography

The stoichiometry of Rab6-effector complexes, as well as the affinity of the interactions, is as yet unknown. Furthermore, no data is available to draw conclusions about possible oligomerization of the effector proteins. In an attempt to address these issues size-exclusion chromatography was used to analyse samples of the full-length effector constructs and preformed complexes with Rab6a on a Superdex200 gelfiltration column. Truncated effector constructs were analyzed using a Superdex75 gelfiltration column as described in 3.5.6. For analysis of complexes, the proteins were pre-incubated for one hour at 4°C using a molar excess of the effector protein in the presence of 1mM GTP, before injecting the sample on the chromatography column. Elution of PIST, p150 and their complexes with Rab6a could be followed monitoring the absorption at 280 nm. However, in the absence of any aromatic side-chain residues in the smallest truncation constructs of the effector proteins, elution of bicD2_miniCORE, PISTcc1-CORE and p150cc had to be monitored at an absorption wavelength of 220 nm. The molecular mass of a protein was calculated, correlating its retention time to a calibration curve, which was based on proteins of known masses between 1.35 and 158 kDa (3.5.6). Table 4 summarizes molecular masses of the effector proteins and Rab6a-effector complexes observed in the size-exclusion chromatography experiments. The observed masses of PIST and p150 correspond, within error, to that calculated for the monomeric proteins. Rab6a appears to form a dimer with a 1:1 molecular ratio with bicD2_mini and p150. The value of 91 kDa obtained for the Rab6a:PIST complex deviates significantly from that expected of a 1:1 complex (73kDa) and is closer to the mass of a 2:1 complex, with two molecules of Rab6a bound to one molecule of PIST (97 kDa). However, calculated elution volumes for all possible combinations up to a 2:2 complex differ by less than one mL under the given experimental conditions. Thus, resolution of the used size-exclusion chromatography system is insufficient for a definitive determination of the Rab6a:PIST complex stoichiometry.
Unusual migratory behaviour in gel-filtration chromatography has been reported for a number of Rab-effectors [244], and is usually associated with the shape of the coiled-coil domains these proteins contain. The rod-like shape of the coiled-coil domains (see 1.10) could potentially cause the higher than expected retention times of the effector constructs and their complexes with Rab6a. Figure 42 depicts chromatograms of Rab6aNΔ12CΔ27(Q72L), PISTcc1 and PISTcc1-CORE as single proteins, as well as after incubation to form the respective complexes with Rab6a.

Table 4 Summary of all protein constructs analyzed by size-exclusion chromatography, indicating molecular masses calculated based on amino acid sequence and on elution volume and apparent oligomeric state.
n/d: not determined

protein	molecular mass [kDa]		apparent stoichiometry
	CALCULATED	OBSERVED	
Rab6a	23.7	24	monomer
Rab6aNΔ12CΔ27(Q72L)	19.3	20.2	monomer
bicD2_minimal	13.4	n/d	n/d
PIST	49.7	50	monomer
p150	54.2	62	monomer
Rab6aNΔ12CΔ27(Q72L) : bicD2_minimal	32.7	29	1:1
Rab6a: PIST	73.5	91	2:1
Rab6a : p150	78	77	1:1
PISTcc1	12.1	32	trimer
Rab6aNΔ12CΔ27(Q72L) : PISTcc1	31.4	38.2	1:1
bicD2_miniCORE	8.2	35.3	pentamer
PISTcc1-CORE	5.2	12.4	dimer
p150cc	7.8	18.8	dimer

As the comparison with Rab6aNΔ12CΔ27(Q72L) shows, the two truncated constructs of PIST elute from the column much earlier than would be expected based on their molecular masses. The most probable explanation for this is that the calibration curve for the chromatography column was based on globular proteins. Coiled-coil protein domains or unstructured peptide chains are described as a rod-like shape or more accurately a freely rotating chain. Because of this, their hydrodynamic radius is much larger than that of a globular sphere with the same molecular mass. Hence, the molecular masses of the coiled-coil domain containing Rab6a-effectors can not be directly correlated to their elution volume in all cases. In the case of PISTcc1, NMR-spectroscopy already indicated a tendency for agglomeration in the protein (4.16), which is an alternative explanation for the faster than expected elution.
An inherent problem with analysing Rab6a complexes with truncated effector constructs via size-exclusion chromatography is apparent in figure 42.

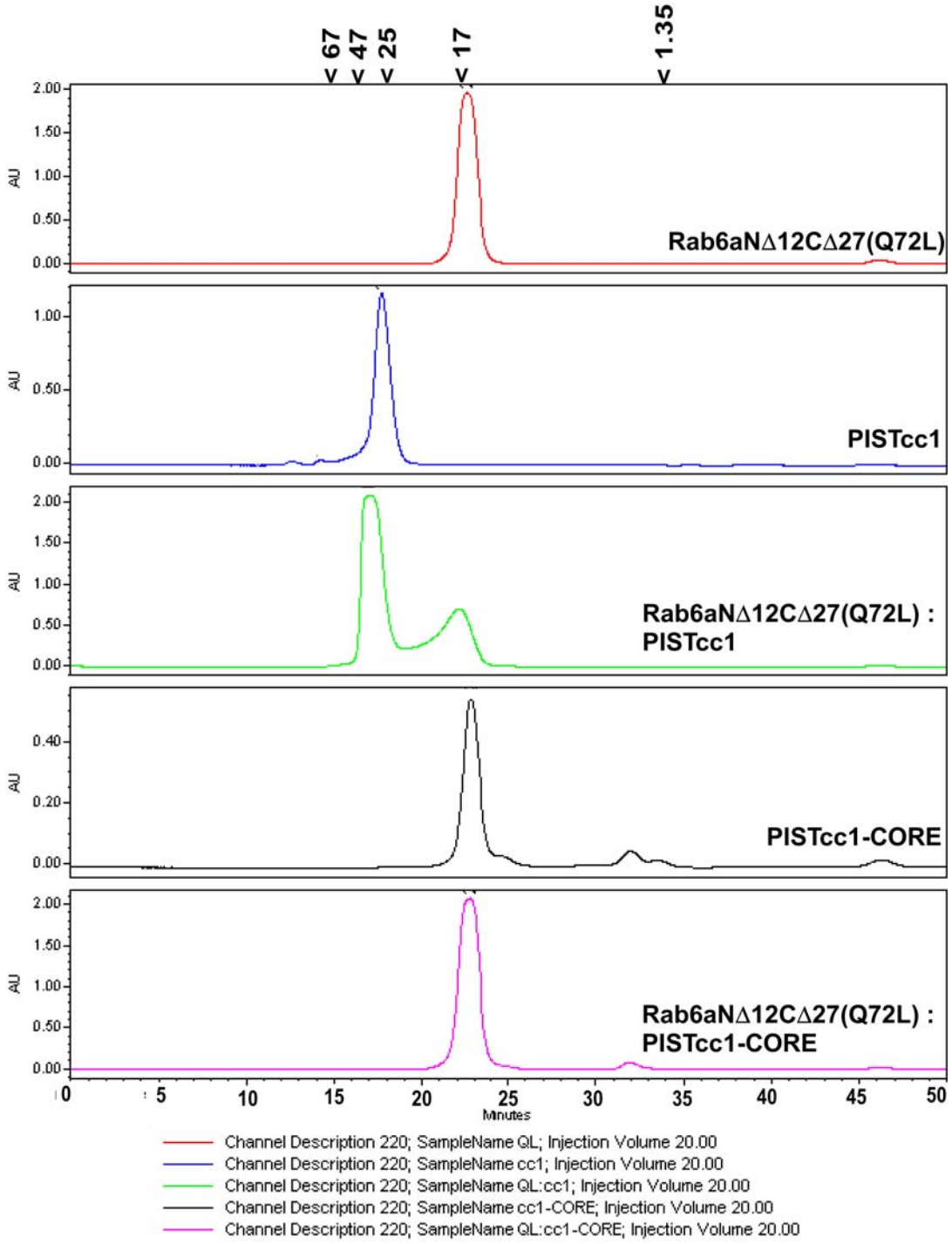

Figure 42 Size-exclusion chromatography of Rab6a alone and in complex with effector domains of PIST. Chromatograms of Rab6aNΔ12CΔ27(Q72L), PISTcc1 and PISTcc1-CORE as well as their respective complexes are shown. Samples were analysed on a Superdex(75) 10/30 gelfiltration column with a flowrate of 0.5 mL/min using buffer containing 50 mM TrisHCl pH 7.5, 100 mM NaCl, 10 mM $MgCl_2$, 5 mM DTT and 2% (v/v) glycerol at 293 K. The absorption was monitored at 220 nm.

In both cases samples of the effector domains together with Rab6a show an increased absorption as compared to the single proteins, which is caused by the co-elution of the two proteins. However, a shift of the elution peak, corresponding to the larger molecular mass of the complex, is observed only for the sample of PISTcc1 that had been incubated with Rab6aNΔ12CΔ27(Q72L). For PISTcc1-CORE as well as for bicD2_miniCORE and p150cc (Fig. 43) incubation with

Rab6aNΔ12CΔ27(Q72L) does not cause the elution peak to shift to shorter retention times, even though the intensity did change.

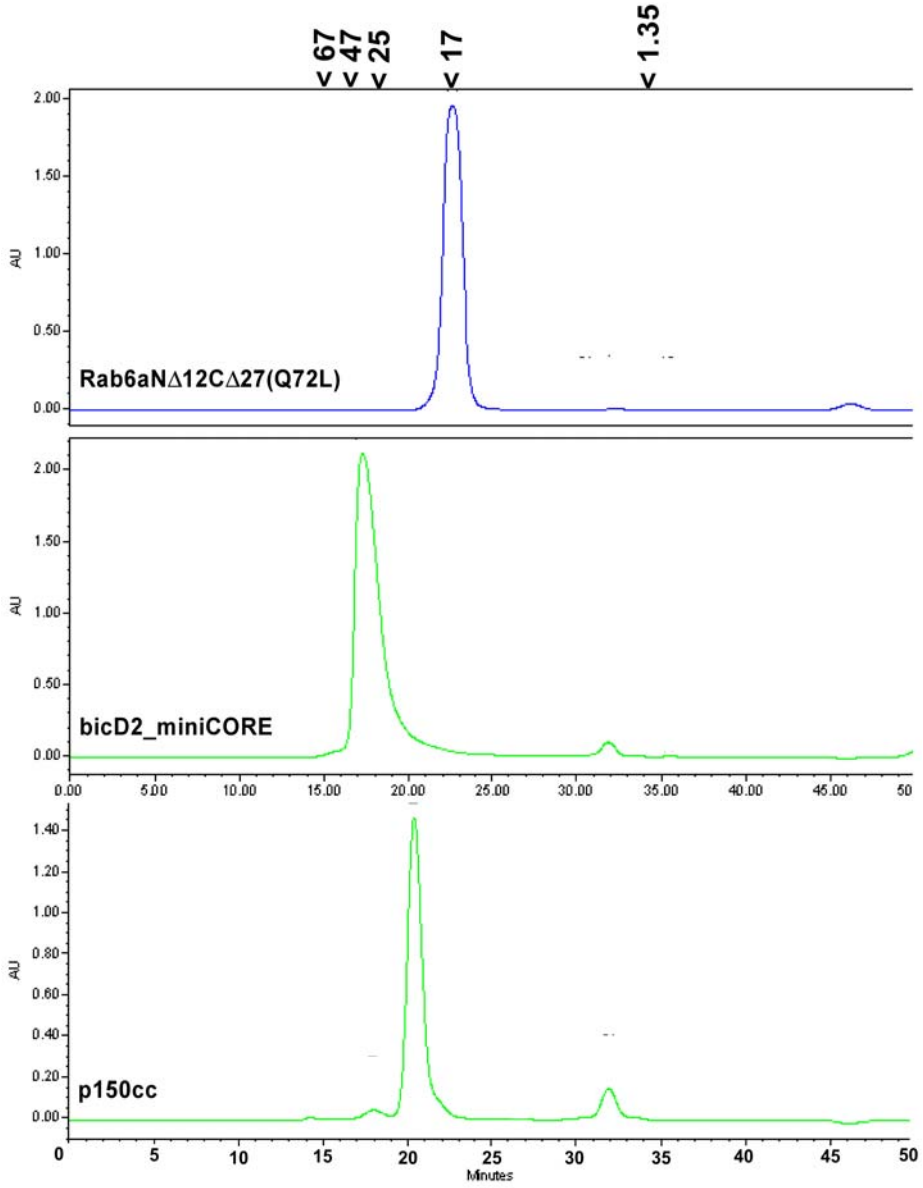

Fig. 43 Size-exclusion chromatography of Rab6a, bicD2_miniCORE and p150cc. Chromatograms of Rab6a, bicD2_miniCORE and p150cc are shown. Samples were analysed as described for Fig.42.

Since the truncated effector constructs alone elute after approximately the same or shorter retention times than Rab6a, results of the gelfiltration chromatography are not sufficient to rule out formation of the complexes, as suggested by NMR experiments. Furthermore, although primary sequence analysis suggests a potential dimer formation for all three effector constructs (see 4.14), size-exclusion chromatography alone can not discriminate between oligomerization and unusual migratory behaviour caused by coiled-coil or random coil domains. Hence, more sensitive experimental methods have to be employed for detection and further characterization of the interactions of Rab6a with its effectors. These are described in the following chapters.

4.17.2 Thermodynamics of the Rab6a – Effector Interactions

Protein-protein interactions are mediated by formation of salt bridges, burial of solvent-exposed surfaces and van der Waals interactions. In an attempt to characterize the thermodynamics of the interactions of Rab6a with its effectors, *isothermal titration calorimetry* (ITC) was used [245,246]. ITC is a quantitative approach to determine thermodynamic properties of protein interactions, which are characterized by free energy (ΔG), enthalpy (ΔH), entropy (ΔS), association constant (K_a) and stoichiometry. The time-dependent input of power that is required to maintain equal temperatures between a sample cell in which two binding partners associate and a reference cell is monitored. Since the heat that is absorbed or generated during a titration is proportional to the fraction of bound interaction partner, the equilibrium of the interaction can be measured directly.
Samples of PIST, p150 (100 µM) and $_{GST}$bicD2_mini (50 µM) were titrated with a tenfold molar excess of Rab6a bound to either GDP or GTP at 298 K after extensive degasing and dialysis to bring all proteins into the same buffer condition. Because bicD2_miniCORE, PISTcc1-CORE and p150cc stayed in solution at higher concentrations, reverse experiments titrating a tenfold molar excess of the effector domains to Rab6a●GTP was also carried out for the truncated constructs.
Assuming one binding site for the interaction, the heat generated by addition of the binding partner can be calculated using the equation:

$$Q = \frac{V_0 \Delta H_b [M]_t K_a [L]}{(1 + K_a [L])}$$

where V_0 is the volume of the cell, ΔH_b is the enthalpy of binding per mole of titrated binding partner, $[M]_t$ is the total concentration of protein provided in the cell including free and bound fractions, K_a is the binding constant and [L] is the concentration of the free binding partner in the syringe. The acquired data needs to be corrected for the increase in volume and for the heat generated through dilution of the titrated binding partner, which were determined in separate control experiments. The free energy of binding was calculated according to:

$$\Delta G = -RT \ln K_a$$

and from this: $-T\Delta S = \Delta G - \Delta H$.

Figure 44 shows typical ITC results for the interaction of Rab6a with p150, including titration of Rab6a●GTP to p150 (■), Rab6a●GDP to p150 (□) and Rab6a●GDP to p150cc (▼). The obtained values for the corresponding thermodynamic parameters are summaryzed in table 5.

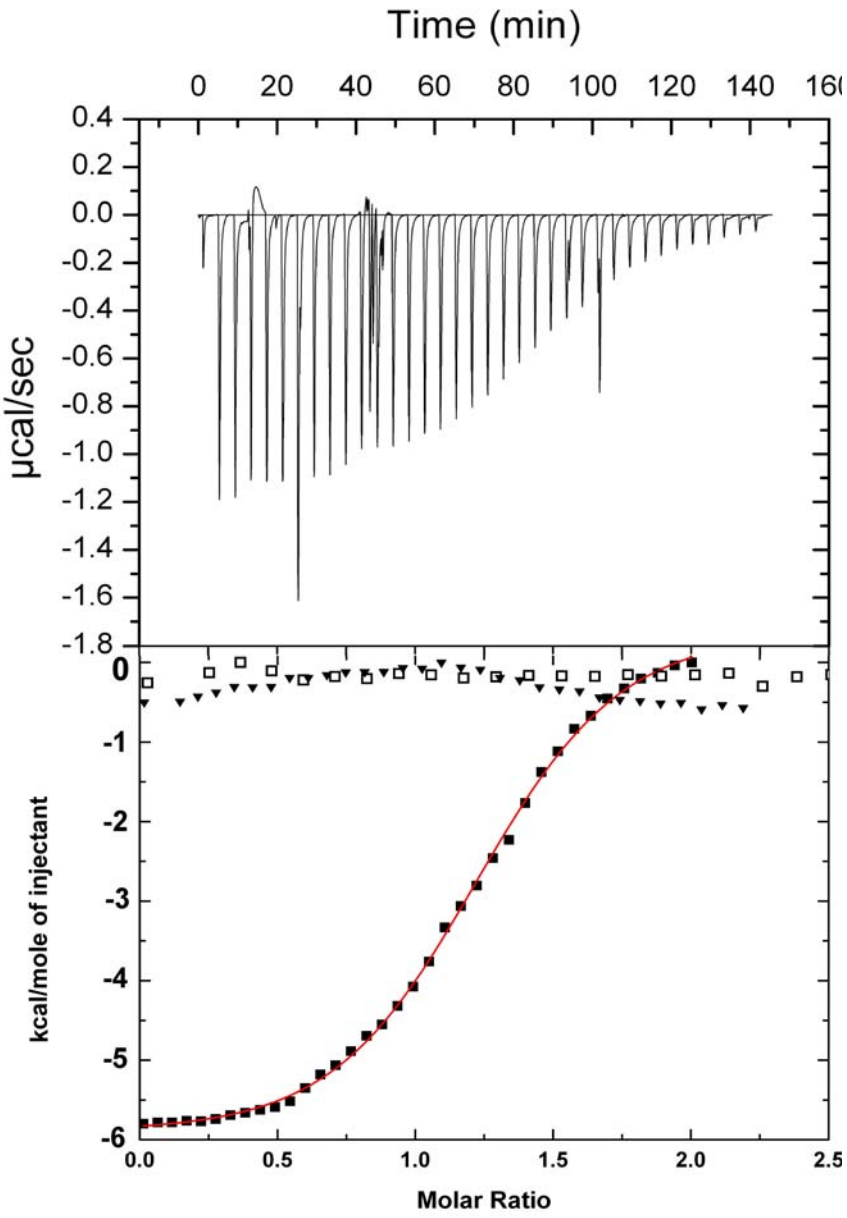

Fig. 44 Thermodynamics of the Rab6a – p150 interaction as determined by ITC. Titrations of Rab6a●GTP against p150 (■), Rab6a●GDP against p150 (□) and Rab6a●GTP against p150cc (▼) at pH 7.5 and 298K are shown. ***Top*** Differences between sample and reference cell containing water and 0.01 % sodium azide during titration of Rab6a●GTP to p150. ***Bottom*** Enthalpy per mole of Rab6a●GTP injected versus molar ratio of PIST and Rab6a. The heat of dilution of Rab6a in buffer was subtracted and the volume corrected for the increase during titration. Data analysis and figure preparation was carried out with the program *Origin* (Microcal). See 3.7.4 for a detailed description of the procedure used.

Table 5 Thermodynamic parameters of the interaction between Rab6a and p150 as determined by ITC at 298 K.

interaction	**ΔG^0** (kcal mol^{-1})	**ΔH^0** (kcal mol^{-1})	**ΔS^0** (cal mol^{-1} K^{-1})	**$T\Delta S$** (kcal mol^{-1})	**K_d *** (µM)	**N**
Rab6a●GTP → p150	-7.71	-5.86	-6.19	-1.85	2.2	1.19
Rab6a●GDP → p150	not determined				>100	

* with $K_d = 1/K_a$

Binding of p150 to Rab6a is an exothermic process, which, confirming earlier studies [131,120], appears to be specific for the GTP-bound GTPase. Variations in the heat generated at injection numbers 4, 7, 12 and 27 were most probably caused by bubbles that had got trapped in the sample cell. Since these fluctiations could cause erroneous overall results, the corresponding values were subtracted before data analysis. The affinity of the two proteins, expressed by the dissociation constant, is determined to be 2.2 x 10^{-6} M and the interaction is apparently entropically favoured. The stoichiometry of the Rab6a:p150 complex is 1.19, which would imply that more than one Rab6a molecule was bound to one molecule of p150. Exact determination of protein concentrations is a crucial prerequisite for ITC experiments. However, since purification of the effectors yielded samples containing ≤10% contaminating proteins (see Fig. 25), deviations in the effective concentrations might have caused incorrect calculation of the stoichiometry. Thus, the obtained result appears, within error, to confirm the 1:1 stoichiometry of the Rab6a:p150 complex that was observed in the size-exclusion chromatography experiment (see 4.17.1).

Binding of p150 to GDP-bound Rab6a was not observed in the ITC experiments. This could mean that either the effector cannot interact with Rab6a in the off-conformation or that the K_d of the interaction is higher than the final concentration of the proteins used for the measurements (~100 µM). Nevertheless, with a difference of at least two orders of magnitude in the K_d, p150 clearly discriminates between the GTP- and the GDP-bound form of the GTPase.

An interaction between p150cc and Rab6a was not observed, independent of order in which sample and titrant were mixed. Since p150cc was used at concentrations of up to 1 mM, the most likely explanation for this finding is that truncation of the effector led to a loss of the binding-interface for Rab6a.

Similar results were obtained for ITC experiments to analyse the binding behaviour of PIST and $_{GST}$bicD2_mini, as well as their truncated constructs to Rab6a in both the GTP- and the GDP-bound form (Fig. 45, 46)

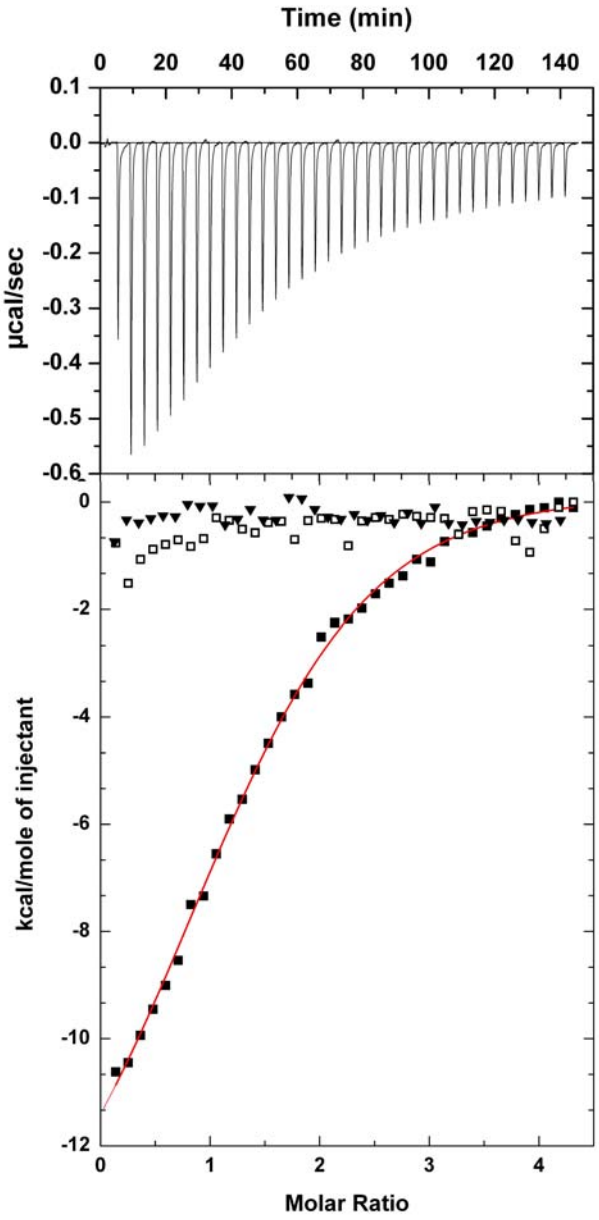

Fig. 45 Thermodynamics of the Rab6a – PIST interaction as determined by ITC. Results are displayed as in Fig.44, with Rab6a●GTP titrated against PIST (■), Rab6a●GDP titrated against PIST (□) and Rab6a●GTP titrated against PISTcc1-CORE (▼) at pH 7.5 and 298 K.

Table 6 Thermodynamic parameters of the interaction between Rab6a and PIST as determined by ITC at 298 K.

interaction	**ΔG^0** (kcal mol^{-1})	**ΔH^0** (kcal mol^{-1})	**ΔS^0** (cal mol^{-1} K^{-1})	**TΔS** (kcal mol^{-1})	**K_d** (µM)	**N**
Rab6a●GTP → PIST	-7.56	-9.58	-6.74	-2.02	2.84	0.97
Rab6a●GDP → PIST	not determined				>100	

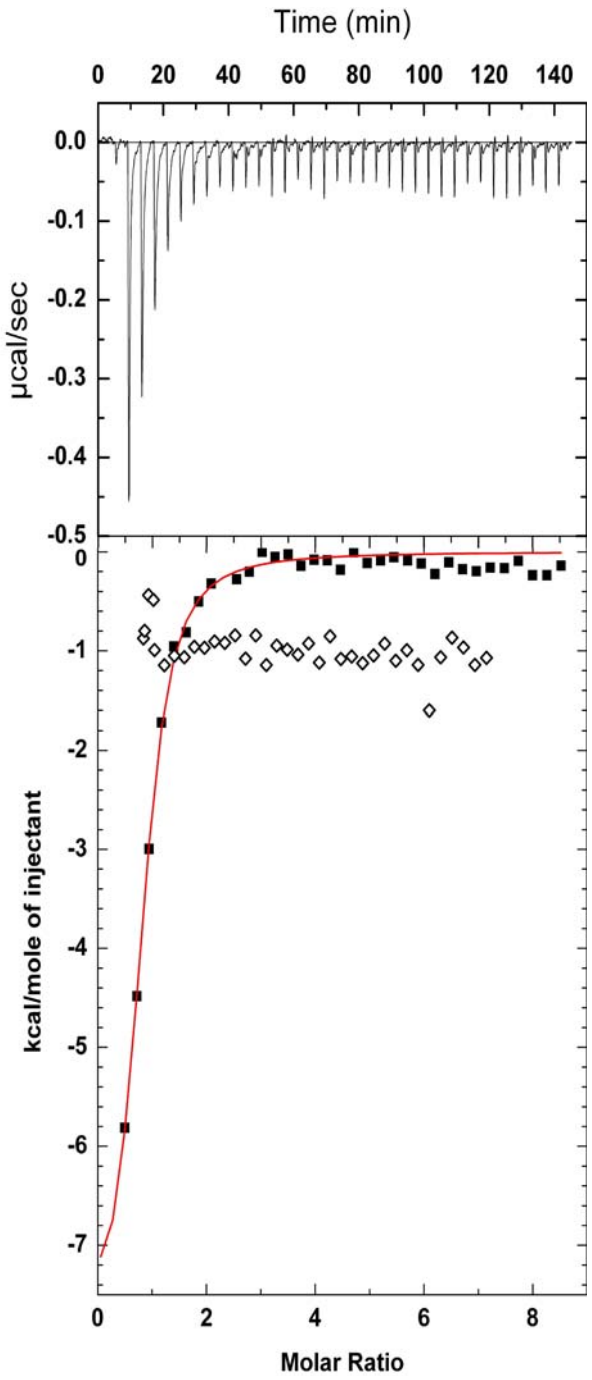

Fig. 46 Thermodynamics of the Rab6a – $_{GST}$bicD2_mini interaction as determined by ITC. Results are displayed as in Fig.44, with Rab6a●GTP titrated against $_{GST}$bicD2_mini (■), Rab6a●GDP titrated against $_{GST}$bicD2_mini (◊) at pH 7.5 and 298 K.

Table 7 Thermodynamic parameters of the interaction between Rab6a and $_{GST}$bicD2_mini as determined by ITC at 298 K.

interaction	**ΔG^0** (kcal mol^{-1})	**ΔH^0** (kcal mol^{-1})	**ΔS^0** (cal mol^{-1} K^{-1})	**TΔS** (kcal mol^{-1})	**K_d** (µM)	**N**
Rab6a●GTP → $_{GST}$bicD2_mini	-8.15	-8.14	0.0605	-0.01	1.05	0.78
Rab6a●GDP → $_{GST}$bicD2_mini	not determined				>50	

In the case of both PIST and $_{GST}$bicD2_mini, binding of the effector protein to Rab6a●GTP is an exothermic process. While binding of PIST appears to be thermodynamically more comparable to that of p150, interaction of $_{GST}$bicD2_mini with Rab6a is mainly enthalpy driven, with a negligible entropic contribution. The dissociation constants for the binding of PIST or $_{GST}$bicD2_mini to Rab6a were determined to be 2.84 x 10^{-6} M or 1.05 x 10^{-6} M respectively. Interactions of the three Rab6a effectors with the GTPase evidently fall in the low micromolar range of affinity. It cannot be ruled out that using the minimal Rab6a-binding domain of bicaudalD2 instead of the full length protein caused the slightly lower K_d observed for $_{GST}$bicD2_mini. However, addition of the 30 kDa GST-tag does not appear to have negative effects on Rab6a binding to $_{GST}$bicD2_mini.

Interaction with GDP-bound Rab6a was not observed for either of both PIST and $_{GST}$bicD2_mini. Due to low solubility of $_{GST}$bicD2_mini, it could not be used at concentrations higher than 50 µM, Hence, interaction of the effector with Rab6a●GDP at higher concentrations can not be completely excluded. Nevertheless, since $_{GST}$bicD2_mini was used at its maximal obtainable concentration, ITC results support the hypothesis that earlier observation of Rab6a●GDP interacting with matrix-bound $_{GST}$bicD2_mini (3.12) was caused by contamination with GTP-bound GTPase.

As in the case of p150, a stoichiometry deviating from the anticipated 1:1 ratio was determined for the complex of Rab6a and $_{GST}$bicD2_mini. Whether the presence of the GST-tag actually causes more than one $_{GST}$bicD2_mini molecule to bind to one Rab6a molecule remains elusive. Another explanation for this finding is the fast saturation of the binding reaction observed during ITC, this might have lead to an inaccurate fit and to misinterpretation of the data. The latter appears to be the more probable scenario, considering the results obtained in analytical and preparative size-exclusion chromatography (see 4.17.1 and Fig. 27). The ITC results argue for a 1:1 stoichiometry for the Rab6a:PIST complex, implying that the larger than expected mass determined by analytical size-exclusion chromatography was caused by unusual migratory behaviour of the effector bound to the GTPase (see 3.17.1).

Binding of either of the effector domains PISTcc1-CORE or bicD2_miniCORE to Rab6a was not observed in the ITC experiments. This would suggest that, due to truncation of the effector proteins, interaction with Rab6a was either lost completely or occurs with a K_d above 400 µM.

Prior to a detailed discussion of the results obtained in the ITC experiments, Rab6a effector binding needs to be characterised. Highly sensitive spectroscopic methods can be used to elucidate the kinetics of protein-protein interactions. Rapid-mixing fluorescence spectroscopy was used as an independent method to support the results obtained so far by an independent method.

4.17.3 Kinetics of Rab6a – Effector Interactions

For a more detailed analysis of the kinetics of the interaction between Rab6a and its effectors bicaudalD2, PIST and p150, stopped-flow (3.7.2) measurements were carried out. This rapid mixing technique allows time resolved observation of the fluorescence signal coming from a fluorescent nucleotide analogue bound to Rab6a, during association with an effector protein. The method is explained based on an attempt to determine the concentration dependence of the observed rate constant (k_{obs}) for the association of $_{GST}$bicD2_mini with Rab6a•mantGppNHp. A constant amount of Rab6a (0.4 µM final) bound to a fluorescently labelled nucleotide is rapidly mixed with increasing concentrations of the effector. Figure 47 displays the fluorescence signal observed upon mixing of the two proteins. To improve the signal to noise ratio, data from eight to twelve single measurements were averaged and used for further analysis. As a signal fluorescence of the mant-group caused by FRET resulting from the excitation of the tryptophans in the two proteins, was monitored. For the chosen experimental conditions with [Rab6a] << [$_{GST}$bicD2_mini] association can be considered to be a pseudo-first order reaction and the fluorescence signal analysed by fitting to a single exponential equation.

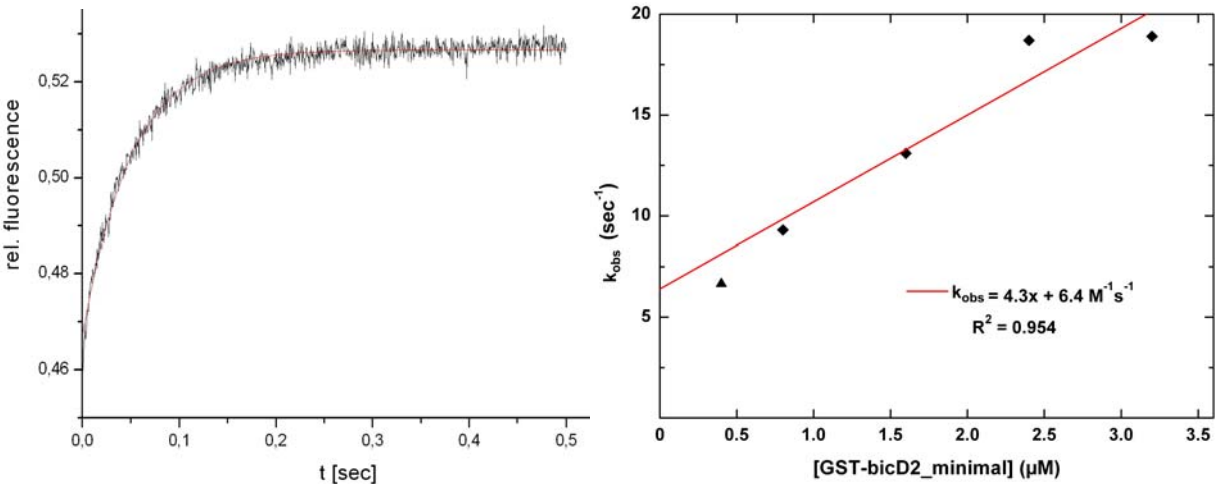

Fig.47 Concentration dependence of the association kinetics for interaction of Rab6a with $_{GST}$bicD2_mini. ***left*** Typical time course of the fluorescence signal upon rapid mixing of 0.4 µM Rab6a•mantGppNHp with 0.8 µM $_{GST}$bicD2_mini at 25°C in a buffer containing 50 mM TrisHCl pH 7.5, 100 mM LiCl, 10 mM $MgCl_2$ and 5 mM DTT. The sample was excited at 295 nm and the fluorescence, resulting from fluorescence-resonance energy transfer between the proteins' tryptophans and the mant-group, was monitored at a detection wavelength of 448 nm.The single-exponential curve, to which the data fitted to a rate constant of 9 s^{-1}, is shown.
right Dependence of k_{obs} on the $_{GST}$bicD2_mini concentration.

Plotting the observed rate constants against the corresponding concentrations of $_{GST}$bicD2_mini yields a linear relation (Fig. 47). The rate of association (k_{on} or k_1) can be derived from the slope of the straight line (4.3 x 10^{-6} M^{-1} s^{-1}), while the dissociation rate (k_{off} or k_{-1}) results from the intercept with the ordinate (6.4 s^{-1}). Based on k_{on} and k_{off}, the dissociation constant (K_d) for binding of $_{GST}$bicD2_mini to

Rab6a is determined as 1.5 µM. However, the calculated K_d strongly depends on the dissociation rate, a factor that cannot be determined with great accuracy employing this indirect approach. Even slight deviations in the experimentally observed pseudo-first order rates lead to dramatic shifts of the intercept with the y-axis, and thus, to changes in k_{off}. In an attempt to directly determine the dissociation rate a displacement experiment was carried out. For this, a preformed complex of Rab6a(mantGppNHp):$_{GST}$bicD2_mini is rapidly mixed with a large molar excess of unlabelled Rab6a. Displacement of the fluorescently labelled Rab6a from the complex can be observed in a time resolved fashion by monitoring the change in the fluorescence signal (Fig.48).

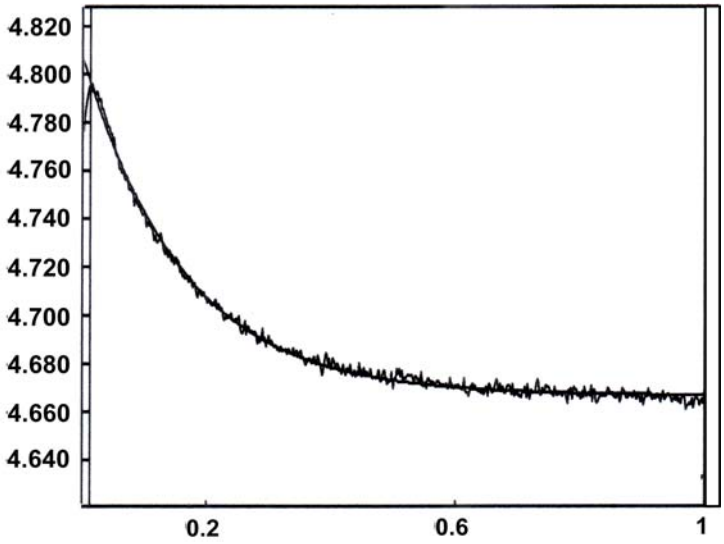

Fig.48 Dissociation kinetics of Rab6a from a complex with $_{GST}$bicD2_mini. The Fluorescence signal change upon rapid mixing of a preformed Rab6a•mantGppNHp:$_{GST}$bicD2_mini with a 10-fold excess of Rab6a•GTP at 25°C, in buffer containing 50 mM TrisHCl pH 7.5, 100 mM LiCl, 10 mM $MgCl_2$ and 5 mM DTT. The sample was excited at 295 nm and the fluorescence, resulting from fluorescence-resonance energy transfer between the proteins' tryptophanes and the mant-group, was monitored at a detection wavelength of 448 nm.The single-exponential curve, to which the data was fitted to a dissociation rate (k_{off}) of 6.2 s^{-1}, is shown.

Control measurements mixing Rab6a(mantGppNHp):$_{GST}$bicD2_mini with buffer excluded the possibility that the observed signal decrease accounted for dilution of the labelled protein. The observed change in the fluorescent signal (Fig.48) was fitted to a single exponential equation, which yields the dissociation rate of 6.2 s^{-1}. Thus, this approach to measure k_{off} directly confirms the results obtained for the indirect determination of the dissociation rate.

The method described for $_{GST}$bicD2_mini was also employed to examine the kinetics for the interaction of Rab6a with PIST and p150. Figure 49 displays typical fluorescence signals obtained after mixing 0.4 µM Rab6a(mantGppNHp) with a 16-fold molar excess of either PIST or p150, as well as the corresponding plots to determine the concentration dependence of the observed rate constants.

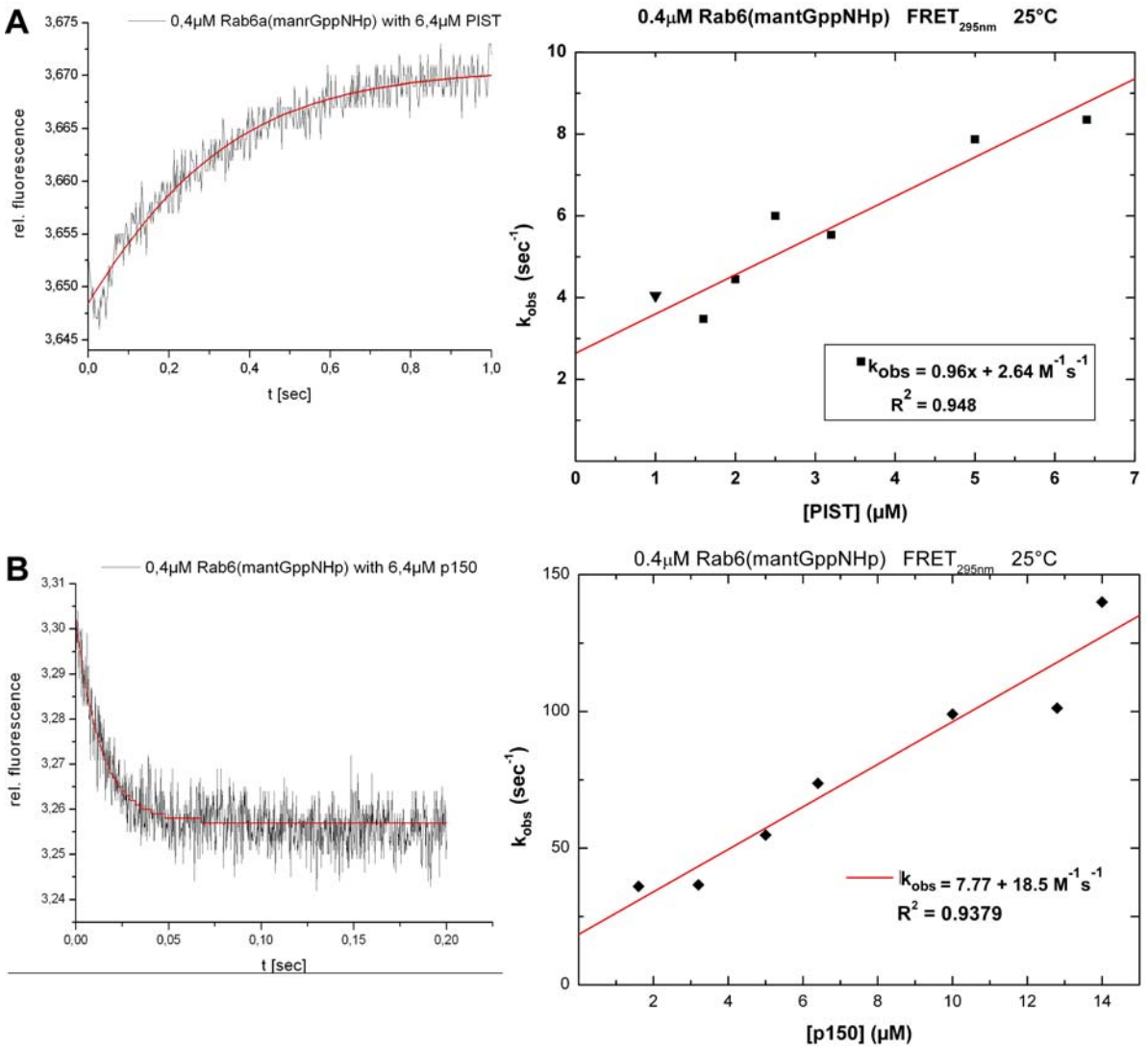

Fig. 49 Concentration dependence of the association kinetics for interaction of Rab6a with PIST and p150. A *left* Time course of the fluorescence signal upon rapid mixing of 0.4 µM Rab6a•mantGppNHp with 6.4 µM PIST at 25°C. The data was fitted to a single exponential curve, giving a rate constant of 8.4 s^{-1}. *right* Dependence of k_{obs} on the PIST concentration. **B** *left* As in **A** using 6.4 µM p150. The data was fitted to a single exponential curve, giving a rate constant of 70 s^{-1}. *right* Dependence of k_{obs} on the p150 concentration.All measurements were carried out in a buffer containing 50 mM TrisHCl pH 7.5, 100 mM LiCl, 10 mM $MgCl_2$ and 5 mM dithioerythritol. The samples were excited at 295 nm and fluorescence, resulting from fluorescence-resonance energy transfer between the proteins' tryptophans and the mant-group was monitored at a detection wavelength of 448 nm.

Confirming observations made in the ITC experiments (4.17.2), K_d values of 2.75 µM for PIST and 2.38 µM for p150 were obtained. Thus, affinity of Rab6a for all of the three effectors appears to be in the same low micromolar range. ITC and stopped-flow experiments were used under comparable conditions on Rab11●GppNHp interaction with the Rab-binding domain (RBD) of Rip11 to determine a K_d of ~60 nM [247]. However, the same study reports a dissociation constant of around 0.3 µM for Rab11 binding to FIP3-RBD constructs. Furthermore, fluorescence equilibrium titration of Rab4a●GppNHp at 25°C yielded K_d values between 2.8 and 3.8 µM for the interaction with constructs of rabaptin-5 [244]. Thus, while the obtained K_d values do not file Rab6a effector interactions in the high

affinity range, they are comparable to those of other Rab effector complexes and most likely reflect a physiologically relevant situation.
Stopped-flow measurements with $_{GST}$bicD2_mini and p150 at the lower temperature of 4°C led to an increase in the K_d values by a factor of four and two respectively. Although these values do not represent a likely physiological situation, this poses an observation relevant for the purification of Rab6a-effector complexes. While the affinity of the Rab6a to its effectors is significantly lowered at a 4°C, the observed K_d values still allow formation of the complexes under these conditions, as long as a the individual proteins are kept at sufficiently high concentrations (>10µM - mM).
Binding of any of the effectors to Rab6a●mantGDP was not observed in the stopped-flow measurements. Furthermore, using the smallest constructs of all three effector proteins did not yield any analysable data. Rapid mixing of either bicD2_miniCORE, PISTcc1-CORE or p150cc with Rab6a(mantGppNHp) at 25°C did not generate any fluorescence signal, indicating that interaction of these constructs to Rab6a is completely obliterated. The results of all stopped-flow experiments with Rab6a and constructs of bicD2_mini, PIST and p150 are summarized in table 8.

Table 8 Association rates (k_1), dissociation rates (k_{-1}) and dissociaction constants (K_d) obtained from stopped-flow measurements with Rab6a and constructs of bicD2_mini, PIST and p150at 25°C and 4°C (in brackets).

effector construct	k_1 [x 10^{-6} M^{-1} s^{-1}]	k_{-1} [s^{-1}]	K_d [x 10^{-6} M]
bicD2_minimal	4.3 (0.03)	6.4 (0.19)	1.5 (6.3)
bicD2_miniCORE	/	/	/
PIST	0.96	2.64	2.75
PISTcc1-CORE	/	/	/
p150	7.8 (0.99)	18.5 (5.10)	2.38 (5.15)
p150cc	/	/	/

Taken together, analytical size-exclusion chromatography, ITC and stopped-flow spectroscopy serve as independent methods to support the following conclusions:

1. The minimal Rab6a-binding domain of bicaudalD2, p150 and PIST bind to Rab6a in a GTP-dependend fashion.

2. Interaction of Rab6a●GTP with the three effectors leads to formation of protein complexes with a 1:1 stoichiometry displaying dissociation constants in the low (1 - 3) micromolar range at 25°C.

3. bicD2_miniCORE, p150cc and PISTcc1-CORE that were constructed based on primary sequence analysis and limited proteolysis assays to only contain the coiled-coil domains essential for Rab6a binding lost their ability to bind the GTPase. This could be because:

   a) The truncation constructs of the effectors are over-engineered and can not form a coiled-coil structure anymore, as indicated by results of NMR spectroscopy.

   b) Not all residues essential for formation of a Rab6a binding interface are located in the predicted coiled-coil domains of the effectors.

4.17.4 Consequences of the Interaction of Rab6a with its Effectors

Some RabGTPases display altered hydrolytic activity as a consequence of their interaction with effector proteins. Interaction of Rabphilin-3a with Rab3a was shown to have a weak stimulating effect on the intrinsic GTPase activity, while concurrently inhibiting GAP stimulated hydrolysis [248]. In a mechanism counteracting inactivation, other Rab-effector interactions reduce the intrinsic GTPase activity of the complex. This has been observed for Rab5a and Rabaptin-5 [249] as well as for Rab4a binding to Rabaptin-4 [250] and -5 [244].
In analogy to the measurements with Rab6a alone (4.4), the GTPase activity of Rab6a-effector complexes was determined by incubating samples of Rab6a:bicD2_mini, Rab6a:p150 and Rab6a:PIST at 25°C over the course of 12 days while continuously analysing samples by HPLC (3.5.5 and 3.7.3). Fig.50 depicts the progressive hydrolysis of GTP upon triggering the reaction by addition of Mg^{2+}.

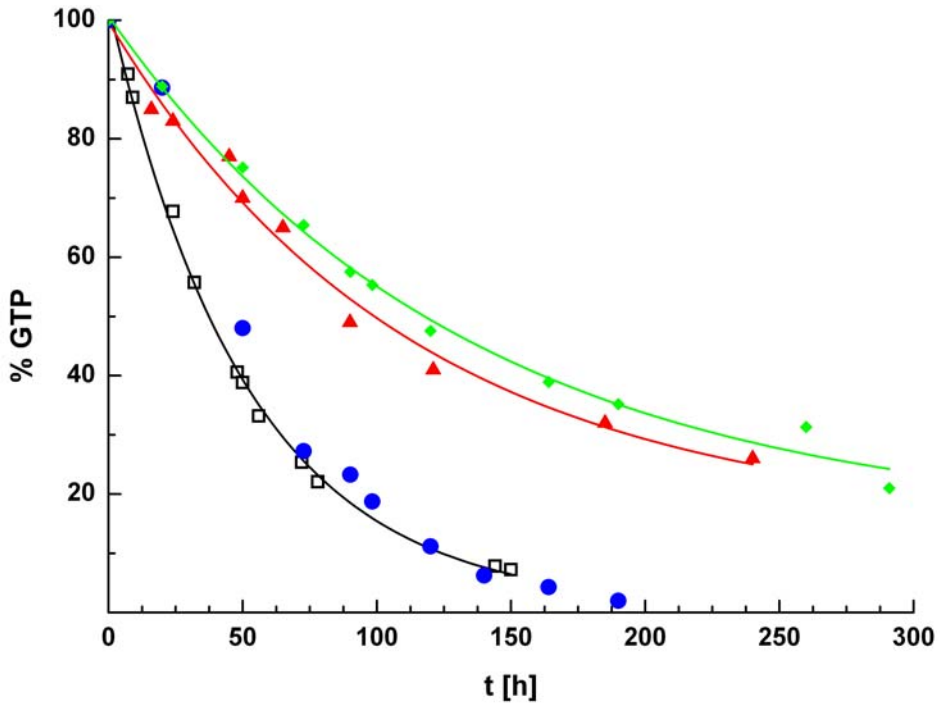

Fig.50 Hydrolysis of GTP by Rab6a-effector complexes compared to the GTPase alone. Time course of GTP hydrolysis by Rab6a alone (□) as well as in stoichiometric complexes with the effector proteins bicD2_mini (♦), p150 (▲) and PIST (●) at 25°C in buffer containing 50 mM TrisHCl pH 7.5, 100 mM LiCl and 5 mM DTT. The hydrolysis reaction was initiated by addition of 10 mM $MgCl_2$. Concentrations of GTP and GDP were determined by HPLC (3.5.5). The single-exponential curves to which the data was fitted are shown.

The decrease in protein bound GTP follows a single-exponential time course that can be analysed to yield the rate constant of the assumed first order reaction. Table 9 summaryses the rates for GTP-hydrolysis of the different Rab6a-effector complexes.

Comparison of the observed hydrolysis rates of the GTPase-complexes shows that the Rab6a-effectors under investigation fall into two classes.

Table 9 The rates for hydrolysis of GTP at 25°C for Rab6a alone and in complex with bicD2_mini, p150 and PIST

protein complex	hydrolysis rate $x10^{-6}$ [s^{-1}]
Rab6a:p150	2.1
Rab6a:bicD2_mini	2.5
Rab6a:PIST	5.4
Rab6a	5.8

While binding of PIST appears to have only a limited effect on the rate of hydrolysis, interactions with bicD2_mini or p150 lead to a decrease of the already low intrinsic hydrolysis activity of Rab6a by a factor of ~2-3. Since no protein degradation was observed for any of the involved proteins over the course of the experiment and stability of the complexes as expressed by the K_d (see 4.17.2 and 4.17.3) differs only slightly, these factors could not have caused the differences in the catalytic activity. Rather, maintaining the active conformation of Rab6a may be a way to stabilize the respective complex for proper function in its specific physiological environment. In this context it is interesting to note that *in vitro* GTP hydrolysis of Rab6a in complex with bicD2_mini and p150, two proteins that are thought to belong to the same Rab6a-controlled pathway of microtubule dependent retrograde trafficking, occurs on the same time scale.

5 SUMMARY AND OUTLOOK

5.1 Summary and Outlook (English)

Small GTPases of the Rab family of proteins play a crucial role as molecular switches in vesicular transport. Rab6a has been identified as a regulator of microtubule-dependent retrograde trafficking. Like all small GTPases, Rab6a function is based on the transition between an active, GTP-bound, and an inactive, GDP-bound conformation. As a means of temporal control, this transition is modulated via guanine nucleotide-exchange factors (GEFs) and GTPase-activating proteins (GAPs). An element of spatial specificity is added through interactions of the GTP-bound Rab with a variety of specific effector proteins. The duration of these interactions is limited either by intrinsic or by GAP mediated hydrolytic activity of the Rab protein. Within the Rab family, the rates of intrinsic hydrolysis vary, which is thought to reflect differences in the specific physiological functions of the individual Rabs. These differences in the GTPase-activity cannot be explained by amino acids that take part in the binding of the nucleotide as these are highly conserved, nevertheless, they should be seen in structural differences of the individual GTPase.

In order to generate a detailed description of the factors that determine the rate of GTP-hydrolysis, structure information of Rab6a in its active conformation had to be acquired. Furthermore, the putative Rab6a effectors BicaudalD2, $p150_{glued}$ and PIST, and their interactions with the GTPase, needed to be characterised. The central aim of this project was to elucidate the structural and biochemical characteristics of Rab6a and its three effectors and discover which factors are required in order for them to interact with each other and facilitate their specific transport step.

Truncated constructs for recombinant expression of Rab6a were generated, in an attempt to enable crystallisation and structure determination. At the beginning of the project the three effectors under investigation could not be obtained in sufficient quantities and the proteins turned out to be susceptible to precipitation. Therefor, methods for expression had to be optimised in order to obtain adequate amounts of protein. Obtaining protein samples of high quality should allow the kinetic and thermodynamic characterisation of the interactions with Rab6a. Furthermore, constructs for the expression of the truncated effectors were intended for structural characterisation and biophysical analysis of the coiled-coil domains that are thought to be responsible for interaction with Rab6a.

Analysis of the intrinsic GTPase-activity showed that, with a rate of hydrolysis of $5x10^{-6}s^{-1}$, Rab6a displays the slowest GTP-hydrolysis of GTP so far observed for any Rab GTPase. This particularly low hydrolytic activity enabled the crystallisation

of a Rab protein in its natural GTP-bound conformation for the first time. The structure of Rab6aNΔ12CΔ33 was solved with a resolution of 1.8 Å. Comparison with structures of other Rabs, in particular with the *P. falciparum* Rab6a homolog bound to GDP, showed that Rab6a adopts the typical fold of all small GTPases and allowed a description of the transition between the active and the inactive conformation. Furthermore, the structure of GTP-bound Rab6a displays a high degree of similarity to that of other Rab proteins in complex with the GTP analogue GppNHp. Rab6a specific characteristics are, firstly, a lid-tyrosine (Tyr 42) covering the nucleotide-binding pocket. This may influence nucleotide exchange and nucleotide hydrolysis, through its bulky side-chain, in a way analogous to a histidine in Rab4a and a tyrosine in the small GTPase RHEB that were found to adopt a similar position. Secondly, Rab6a displays increased flexibility of a catalytically important glutamine, which may hinder efficient hydrolysis of the nucleotide. In the absence of a GAP, Rab6a is effectively constitutively active, which, considering its physiological function, appears to be quite conceivable. The transport processes that are thought to be controlled by Rab6a range from the cell periphery, through the Golgi and to the ER. This would require maintenance of the active (i.e. effector accessible) conformation until the acceptor membrane is reached.

The effector proteins BicaudalD2, $p150_{glued}$ and PIST individually, as well as their interaction with Rab6a, were initially analysed by means of analytical size-exclusion chromatography. In the case of the complex of Rab6a with PIST the observed elution volume of was higher than calculated. The same was found for truncated constructs of the effectors. These had been generated, based on a limited proteolytic digest assay of the individual proteins and their complexes with Rab6a, with the intention to isolate only the coiled-coil domain necessary for Rab6a-binding. NMR-spectroscopy showed that these smallest fragments of the effector proteins are intrinsically unstructured or, in one case, have a tendency to aggregate, which explains their atypical migratory behaviour in the size-exclusion chromatography. For a kinetic and thermodynamic characterisation of the Rab6a effector interactions, the minimal Rab6a-binding domain of BicaudalD2, amino acids 540 to 1041 of $p150_{glued}$ and full-length PIST were used in fluorescence spectroscopic (stopped-flow) and calorimetric (ITC) experiments. The results of these independent approaches are in good agreement with each other and allow the conclusion that Rab6a forms complexes of a 1:1 stoichiometry with each of the effectors under investigation. However, the affinity of these effector proteins to Rab6a is comparatively low with K_d values of 1.5 µM for bicD2_minimal, 2.4 µM for p150 and 2.7 µM for PIST. *Single-turnover* hydrolysis experiments with the complexes showed that binding of effectors can have an influence on the intrinsic GTPase-activity of Rab6a. In the case of the minimal Rab6a-binding domain of BicaudalD2 and p150, this leads to a two-fold reduction in the rate of hydrolysis, while for interaction with PIST no such effect was observed. Although sufficient amounts of Rab6a in complex with the three full-length effectors were isolated, their stability was apparently insufficient for crystallisation.

It seems conceivable that only the affinity of the individual effector proteins to Rab6a may be low. Amino acid sequence analysis of the effectors under investigation not only predicts coiled-coil domains, but a variety of other binding domains. Furthermore, in some cases Rab effectors are thought to exert their function in cooperation with other Rab effectors, which some studies suggest also for dynamin ($p150_{glued}$) and BicaudalD2. Should these Rab effectors really act in a modular way, it may well be possible that they only exhibit a high binding affinity for the functional complex of GTPase and additional effector proteins.
Based on this hypothesis, further investigations on the Rab6a effector interaction would include combinations of different effector proteins, to further elucidate the signalling pathways required for Rab6a-controlled retrograde transport. A prerequisite for a more detailed characterisation of the effectors would be the generation of new expression constructs to enable structure determination of these proteins and their complexes with Rab6a. Based on the structural data of Rab6a, single point mutational studies may show if the exchange of tyrosine 42 with glycine or serine leads to the expected increase in the intrinsic rate of hydrolysis. This would help to explain the molecular mechanisms underlying the great variation in the intrinsic rate of hydrolysis among the family of Rab proteins.

5.2 Summary and Outlook (Deutsch)

Kleine GTPasen aus der Familie der Rab-Proteine üben als molekulare Schalter eine entscheidende Rolle im vesikulären Transport aus. Rab6a wurde als Regulator des Mikrotubuli-abhängigen, vesikulären retrograd Transports identifiziert. Wie bei allen kleinen GTPasen basiert auch die Funktion von Rab6a auf dem Wechsel zwischen einer aktiven, GTP gebundenen, und einer inaktiven, GDP gebundenen, Konformation, der durch Guaninnukleotid-Austauschfaktoren (GEF) und GTPase-aktivierenden Proteinen (GAP) moduliert wird. Diese zeitliche Steuerung der Schalterfunktion wird ergänzt durch ein Element räumlicher Spezifität, das auf der Interaktion des GTP gebundenen Rabs mit einer Vielzahl spezifischer Effektorproteine beruht. Die Dauer dieser Interaktion wird bestimmt durch intrinsische bzw. GAP vermittelte Hydrolyseaktivität des Rab Proteins. Die intrinsischen Hydrolyseraten variieren innerhalb der Rab-Familie stark, was im Allgemeinen mit Unterschieden in der spezifischen physiologischen Funktion der einzelnen Rabs assoziiert wird. Die Variationen der GTPase Aktivität lassen sich anhand der an der Nukleotidbindung beteiligten, hochkonservierten Aminosäuren nicht erklären, sollten sich jedoch in der Strukture der einzelnen GTPase manifestieren.
Im Rahmen dieser Arbeit sollte, für eine möglichst detaillierte Beschreibung der Hydrolyserate-bestimmenden Faktoren, Strukturinformation von Rab6a in seiner aktiven Konformation ermittelt werden. Des Weiteren sollten die potentiellen Rab6a

Effektorproteine BicaudalD2, $p150_{glued}$ und PIST sowie ihre Wechselwirkungen mit der kleinen GTPase weitergehend charakterisiert werden. Zentrale Fragestellung dieser Arbeit war es, welche strukturellen und biochemischen Charakteristika Rab6a und seine drei potentiellen Effektoren besitzen müssen um miteinander zu interagieren und somit die entsprechenden Transportschritte zu ermöglichen.
Zu diesem Zweck wurden von Rab6a verkürzte Expressionskonstrukte hergestellt um die Kristallisation und Strukturaufklärung des Proteins zu ermöglichen. Da die drei untersuchten Effektorproteine ursprünglich nicht in ausreichenden Mengen erhalten werden konnten und sich als vergleichsweise schwer handhabbar herausstellten, mussten zunächst Methoden für eine hinreichende Überexpression entwickelt werden. Die so erhaltenen Proteinproben von hoher Qualität sollten die kinetische und thermodynamische Charakterisierung der Wechselwirkungen mit Rab6a gewährleisten. Ferner sollten verkürzte Expressionskonstrukte der Effektoren die eventuelle strukturelle Charakterisierung und biophysikalische Analyse, der für die Wechselwirkung mit Rab6a verantwortlichen coiled-coil Domänen, ermöglichen.
Untersuchungen der intrinsischen GTPase-Aktivität zeigten, dass Rab6a, mit einer Hydrolyserate von $5x10^{-6}s^{-1}$, die langsamste bisher bei einer Rab GTPase gemessene Umsetzung von GTP aufweist. Diese besonders niedrige Hydrolyseaktivität erlaubte erstmalig die Kristallisation eines Rab Proteins in seiner natürlichen GTP-gebundenen Konformation. Die Struktur von Rab6aNΔ12CΔ33 konnte mit einer Auflösung von 1.8 Å bestimmt werden. Vergleiche mit den Strukturen anderer Rab Proteine, insbesondere mit dem *P. falciparum* Rab6a Homolog in seiner GDP Konformation, zeigen das Rab6a die typische Faltung der kleinen GTPasen einnimmt und erlauben die Beschreibung des Übergangs zwischen aktiver und inaktiver Konformation. Ferner wird große Übereinstimmung zwischen GTP-gebundenem Rab6a und Rab Proteinen in Komplex mit dem Nukleotidanalog GppNHp beobachtet. Rab6a spezifische Merkmale sind zum einen ein, die Nukleotidbingungstasche abschirmendes, Tyrosin (Tyr 42), das in anaologer Weise zu einem ähnlich positionierten Histidin in Rab4a und einem Tyrosin in der kleinen GTPase RHEB durch seine sperrige Seitenkette Einfluss auf Nukleotidaustausch und -hydrolyse haben könnte. Zum anderen zeigt Rab6a erhöhte Flexibilität eines für die Katalyse essentiellen Glutamins, was einer effiziente Hydrolyse des Nukleotids im Weg steht. In Abwesenheit entsprechender GAPs ist Rab6a quasi konstitutiv aktiv, was in Betracht auf seine physiologische Funktion durchaus erklärbar scheint. Die mit der Kontrollfunktion von Rab6a assoziierten Transportprozesse erstrecken sich von der Zellperipherie, durch den Golgi Apparat, bis zum endoplasmatischen Retikulum, wofür die Erhaltung der aktiven, für Effektorbindung zugänglichen, Konformation bis zum Erreichen der Zielmembran notwendig wäre.
Die Effektorproteine BicaudalD2, $p150_{glued}$ und PIST, sowie ihre Wechselwirkungen mit Rab6a, wurden zunächst mittels analytischer Gelpermeations-Chromatographie untersucht. Dabei wurde für den Komplex von Rab6a mit PIST ein höher als zu

erwartendes Elutionsvolumen beobachtet. Gleiches galt auch für verkürzte Effektor Konstrukte, die, mit dem Ziel nur die Rab6a bindenden coiled-coil Domänen zu isolieren, in einem limitierten Proteaseverdau der Effektor Proteine und ihrer Komplexe mit Rab6a identifiziert worden waren. Durch NMR-spektroskopische Untersuchungen konnte gezeigt werden, dass diese maximal verkürzten Effektor Fragmente intrinsisch unstrukturiert sind bzw. zu Agglomeration neigen, wofür auch ihr ungewöhnliches Laufverhalten in der Gelpermeations-Chromatographie spricht. Für eine kinetische und thermodynamische Charakterisierung der Wechselwirkungen zwischen Rab6a und den drei untersuchten Effektoren wurde die minimale Rab6a-bindende Domäne von BicaudalD2, Aminosäuren 540 bis 1041 von $p150_{glued}$ sowie PIST in voller Länge für fluoreszenz-spektroskopische (stopped-flow) und kalorimetrische (ITC) Untersuchungen verwendet. Die Ergebnisse dieser unabhängigen Methoden bestätigen sich gegenseitig und lassen den Schluss zu, dass die untersuchten Rab6a-Effektor Komplexe in einer 1:1 Stöchiometrie vorliegen, die Effektorproteine jedoch mit K_d-Werten von 1.5 µM für bicD2_minimal, 2.4 µM für p150 und 2.7 µM für PIST vergleichsweise niedrige Affinität zu Rab6a aufweisen. *Single-turnover* Hydrolyseexperimente mit den Komplexen zeigten, dass die Bindung der Effektoren an Rab6a einen Einfluss auf die intrinsische GTPase-Aktivität haben kann. Dies führt im Fall der Rab6a-bindenden Domäne von BicaudalD2 sowie bei p150 zu einer Halbierung der Hydrolyserate von Rab6a, während für die Bindung von PIST keine Veränderung der GTPase-Aktivität nachweisbar ist. Obwohl ausreichende Mengen der Rab6a-Effektor Komplexe isoliert werden konnten, scheint deren Stabilität nicht ausreichend für eine erfolgreiche Kristallisation zu sein.

Es erscheint möglich, dass die Affinität nur der einzelnen Effektoren zu Rab6a niedrig ist. Für die untersuchten Effektoren werden in Aminosäuresequenzanalysen neben coiled-coils auch weitere andere Bindungsdomänen vorhergesagt. Weiterhin besteht für verschiedene Rab Effektoren der Verdacht, dass diese ihre Funktion im Zusammenspiel mit anderen Rab Effektoren ausüben, was einige Studien auch für BicaudalD2 und dynamin($p150_{glued}$) nahe legen. Sollten Rab6a Effektoren tatsächlich modular sein, wäre es wahrscheinlich, dass ihre Affinität nur zum funktionellen Komplex aus GTPase und weiteren Effektoren hoch ist.

Auf dieser Hypothese aufbauend, könnten sich Experimente zur Rab6a Effektor Wechselwirkung mit verschiedenen Kombinationen von Effektor Proteinen anschließen, was die für den Rab6a-kontrollierten retrograd Transport notwendigen Signalwege weiter beleuchten würde. Voraussetzung für eine weitergehende detaillierte Charakterisierung der Effektoren wäre die Generierung neuer Konstrukte, welche die Strukturaufklärung dieser Proteine und ihrer Komplexe mit Rab6a ermöglichen. Auf den Strukturdaten von Rab6a basierend könnten Mutationsstudien zeigen, ob ein Austausch des Tyrosin 42 gegen Glycin oder Serin die erwartete Erhöhung der Hydrolyserate bewirkt. Dies würde helfen die molekulare Basis für die großen Unterschiede der intrinsischen Hydrolyseraten innerhalb der Familie der Rab Proteine zu erklären.

6 BIBLIOGRAPHY

Reference List

1. Colicelli, J. Human RAS superfamily proteins and related GTPases. Sci.STKE. 2004(250), RE13. 14-9-2004.

2. Perucho, M., Goldfarb, M., Shimizu, K., Lama, C., Fogh, J., and Wigler, M. Human-Tumor-Derived Cell-Lines Contain Common and Different Transforming Genes. Cell 27(3), 467-476. 1981.

3. Chiu, V. K., Bivona, T., Hach, A., Sajous, J. B., Silletti, J., Wiener, H., Johnson, R. L., Cox, A. D., and Philips, M. R. Ras signalling on the endoplasmic reticulum and the Golgi. Nature Cell Biology 4(5), 343-350. 2002.

4. Burridge, K. and Wennerberg, K. Rho and Rac take center stage. Cell 116(2), 167-179. 23-1-2004.

5. Randazzo, P. A., Nie, Z., Miura, K., and Hsu, V. W. Molecular aspects of the cellular activities of ADP-ribosylation factors. Sci.STKE. 2000(59), RE1. 21-11-2000.

6. Stryer, L. and Bourne, H. R. G proteins: a family of signal transducers. Annu.Rev.Cell Biol. 2, 391-419. 1986.

7. Weis, K. Regulating access to the genome: nucleocytoplasmic transport throughout the cell cycle. Cell 112(4), 441-451. 21-2-2003.

8. Zerial, M. and McBride, H. Rab proteins as membrane organizers. Nat.Rev.Mol.Cell Biol. 2(2), 107-117. 2001.

9. Bourne, H. R., Sanders, D. A., and Mccormick, F. The Gtpase Superfamily - Conserved Structure and Molecular Mechanism. Nature 349(6305), 117-127. 10-1-1991.

10. Geyer, M., Herrmann, C., Wohlgemuth, S., Wittinghofer, A., and Kalbitzer, H. R. Structure of the Ras-binding domain of RalGEF and implications for Ras binding and signalling. Nat.Struct.Biol. 4(9), 694-699. 1997.

11. Bourne, H. R., Sanders, D. A., and Mccormick, F. The GTPase superfamily: a conserved switch for diverse cell functions. Nature 348(6297), 125-132. 8-11-1990.

12. Simon, I., Zerial, M., and Goody, R. S. Kinetics of interaction of Rab5 and Rab7 with nucleotides and magnesium ions. J.Biol.Chem. 271(34), 20470-20478. 23-8-1996.

13. Novick, P., Field, C., and Schekman, R. Identification of 23 complementation groups required for post-translational events in the yeast secretory pathway. Cell 21(1), 205-215. 1980.

14. Walworth, N. C., Goud, B., Kabcenell, A. K., and Novick, P. J. Mutational analysis of SEC4 suggests a cyclical mechanism for the regulation of vesicular traffic. EMBO J. 8(6), 1685-1693. 1989.

15. Gallwitz, D., Donath, C., and Sander, C. A yeast gene encoding a protein homologous to the human c-has/bas proto-oncogene product. Nature 306(5944), 704-707. 15-12-1983.

16. Schmitt, H. D., Wagner, P., Pfaff, E., and Gallwitz, D. The ras-related YPT1 gene product in yeast: a GTP-binding protein that might be involved in microtubule organization. Cell 47(3), 401-412. 7-11-1986.

17. Touchot, N., Chardin, P., and Tavitian, A. Four additional members of the ras gene superfamily isolated by an oligonucleotide strategy: molecular cloning of YPT-related cDNAs from a rat brain library. Proc.Natl.Acad.Sci.U.S.A 84(23), 8210-8214. 1987.

18. Bock, J. B., Matern, H. T., Peden, A. A., and Scheller, R. H. A genomic perspective on membrane compartment organization. Nature 409(6822), 839-841. 15-2-2001.

19. Brown, M. S. and Goldstein, J. L. Protein prenylation. Mad bet for Rab. Nature 366(6450), 14-15. 4-11-1993.

20. Armstrong, S. A., Seabra, M. C., Sudhof, T. C., Goldstein, J. L., and Brown, M. S. cDNA cloning and expression of the alpha and beta subunits of rat Rab geranylgeranyl transferase. J.Biol.Chem. 268(16), 12221-12229. 5-6-1993.

21. Zhang, H., Seabra, M. C., and Deisenhofer, J. Crystal structure of Rab geranylgeranyltransferase at 2.0 A resolution. Structure.Fold.Des 8(3), 241-251. 15-3-2000.

22. Casey, P. J. and Seabra, M. C. Protein prenyltransferases. J.Biol.Chem. 271(10), 5289-5292. 8-3-1996.

23. Casey, P. J., Solski, P. A., Der, C. J., and Buss, J. E. p21ras is modified by a farnesyl isoprenoid. Proc.Natl.Acad.Sci.U.S.A 86(21), 8323-8327. 1989.

24. Farnsworth, C. C., Seabra, M. C., Ericsson, L. H., Gelb, M. H., and Glomset, J. A. Rab geranylgeranyl transferase catalyzes the geranylgeranylation of adjacent cysteines in the small GTPases Rab1A, Rab3A, and Rab5A. Proc.Natl.Acad.Sci.U.S.A 91(25), 11963-11967. 6-12-1994.

25. Khosravi-Far, R., Lutz, R. J., Cox, A. D., Conroy, L., Bourne, J. R., Sinensky, M., Balch, W. E., Buss, J. E., and Der, C. J. Isoprenoid modification of rab proteins terminating in CC or CXC motifs. Proc.Natl.Acad.Sci.U.S.A 88(14), 6264-6268. 15-7-1991.

26. Bailly, E., McCaffrey, M., Touchot, N., Zahraoui, A., Goud, B., and Bornens, M. Phosphorylation of two small GTP-binding proteins of the Rab family by p34cdc2. Nature 350(6320), 715-718. 25-4-1991.

27. van der, Sluijs P., Hull, M., Huber, L. A., Male, P., Goud, B., and Mellman, I. Reversible phosphorylation--dephosphorylation determines the localization of rab4 during the cell cycle. EMBO J. 11(12), 4379-4389. 1992.

28. Giner, J. L. and Rando, R. R. Novel methyltransferase activity modifying the carboxy terminal bis(geranylgeranyl)-Cys-Ala-Cys structure of small GTP-binding proteins. Biochemistry 33(50), 15116-15123. 20-12-1994.

29. Andres, D. A., Seabra, M. C., Brown, M. S., Armstrong, S. A., Smeland, T. E., Cremers, F. P., and Goldstein, J. L. cDNA cloning of component A of Rab geranylgeranyl transferase and demonstration of its role as a Rab escort protein. Cell 73(6), 1091-1099. 18-6-1993.

30. Seabra, M. C., Goldstein, J. L., Sudhof, T. C., and Brown, M. S. Rab geranylgeranyl transferase. A multisubunit enzyme that prenylates GTP-binding proteins terminating in Cys-X-Cys or Cys-Cys. J.Biol.Chem. 267(20), 14497-14503. 15-7-1992.

31. Alexandrov, K., Simon, I., Iakovenko, A., Holz, B., Goody, R. S., and Scheidig, A. J. Moderate discrimination of REP-1 between Rab7 x GDP and Rab7 x GTP arises from a difference of an order of magnitude in dissociation rates. FEBS Lett. 425(3), 460-464. 3-4-1998.

32. Seabra, M. C. Nucleotide dependence of Rab geranylgeranylation. Rab escort protein interacts preferentially with GDP-bound Rab. J.Biol.Chem. 271(24), 14398-14404. 14-6-1996.

33. Goody, R. S., Rak, A., and Alexandrov, K. The structural and mechanistic basis for recycling of Rab proteins between membrane compartments. Cell Mol.Life Sci. 62(15), 1657-1670. 2005.

34. Alexandrov, K., Simon, I., Yurchenko, V., Iakovenko, A., Rostkova, E., Scheidig, A. J., and Goody, R. S. Characterization of the ternary complex between Rab7, REP-1 and Rab geranylgeranyl transferase. Eur.J.Biochem. 265(1), 160-170. 1-10-1999.

35. Shen, F. and Seabra, M. C. Mechanism of digeranylgeranylation of Rab proteins. Formation of a complex between monogeranylgeranyl-Rab and Rab escort protein. J.Biol.Chem. 271(7), 3692-3698. 16-2-1996.

36. Thoma, N. H., Niculae, A., Goody, R. S., and Alexandrov, K. Double prenylation by RabGGTase can proceed without dissociation of the mono-prenylated intermediate. J.Biol.Chem. 276(52), 48631-48636. 28-12-2001.

37. Alexandrov, K., Horiuchi, H., Steele-Mortimer, O., Seabra, M. C., and Zerial, M. Rab escort protein-1 is a multifunctional protein that accompanies newly prenylated rab proteins to their target membranes. EMBO J. 13(22), 5262-5273. 15-11-1994.

38. Thoma, N. H., Iakovenko, A., Kalinin, A., Waldmann, H., Goody, R. S., and Alexandrov, K. Allosteric regulation of substrate binding and product release in geranylgeranyltransferase type II. Biochemistry 40(1), 268-274. 9-1-2001.

39. Boguski, M. S. and McCormick, F. Proteins regulating Ras and its relatives. Nature 366(6456), 643-654. 16-12-1993.

40. Klebe, C., Prinz, H., Wittinghofer, A., and Goody, R. S. The kinetic mechanism of Ran--nucleotide exchange catalyzed by RCC1. Biochemistry 34(39), 12543-12552. 3-10-1995.

41. Moya, M., Roberts, D., and Novick, P. DSS4-1 is a dominant suppressor of sec4-8 that encodes a nucleotide exchange protein that aids Sec4p function. Nature 361(6411), 460-463. 4-2-1993.

42. Rossman, K. L., Der, C. J., and Sondek, J. GEF means go: turning on RHO GTPases with guanine nucleotide-exchange factors. Nat.Rev.Mol.Cell Biol. 6(2), 167-180. 2005.

43. Wada, M., Nakanishi, H., Satoh, A., Hirano, H., Obaishi, H., Matsuura, Y., and Takai, Y. Isolation and characterization of a GDP/GTP exchange protein specific for the Rab3 subfamily small G proteins. J.Biol.Chem. 272(7), 3875-3878. 14-2-1997.

44. Lippe, R., Miaczynska, M., Rybin, V., Runge, A., and Zerial, M. Functional synergy between Rab5 effector Rabaptin-5 and exchange factor Rabex-5 when physically associated in a complex. Mol.Biol.Cell 12(7), 2219-2228. 2001.

45. Wurmser, A. E., Sato, T. K., and Emr, S. D. New component of the vacuolar class C-Vps complex couples nucleotide exchange on the Ypt7 GTPase to SNARE-dependent docking and fusion. J.Cell Biol. 151(3), 551-562. 30-10-2000.

46. Mccormick, F. Going for the GAP. Current Biology 8(19), R673-R674. 24-9-1998.

47. Albert, S. and Gallwitz, D. Two new members of a family of Ypt/Rab GTPase activating proteins. Promiscuity of substrate recognition. J.Biol.Chem. 274(47), 33186-33189. 19-11-1999.

48. Cuif, M. H., Possmayer, F., Zander, H., Bordes, N., Jollivet, F., Couedel-Court, Janoueix-Lerosey, I., Langsley, G., Bornens, M., and Goud, B. Characterization of GAPCenA, a GTPase activating protein for Rab6, part of which associates with the centrosome. EMBO J. 18(7), 1772-1782. 1-4-1999.

49. Haas, A. K., Fuchs, E., Kopajtich, R., and Barr, F. A. A GTPase-activating protein controls Rab5 function in endocytic trafficking. Nat.Cell Biol. 7(9), 887-893. 2005.

50. Bernards, A. GAPs galore! A survey of putative Ras superfamily GTPase activating proteins in man and Drosophila. Biochim.Biophys.Acta 1603(2), 47-82. 17-3-2003.

51. Rybin, V., Ullrich, O., Rubino, M., Alexandrov, K., Simon, I., Seabra, M. C., Goody, R., and Zerial, M. GTPase activity of Rab5 acts as a timer for endocytic membrane fusion. Nature 383(6597), 266-269. 19-9-1996.

52. Schalk, I., Zeng, K., Wu, S. K., Stura, E. A., Matteson, J., Huang, M., Tandon, A., Wilson, I. A., and Balch, W. E. Structure and mutational analysis of Rab GDP-dissociation inhibitor. Nature 381(6577), 42-48. 2-5-1996.

53. Olofsson, B. Rho guanine dissociation inhibitors: pivotal molecules in cellular signalling. Cell Signal. 11(8), 545-554. 1999.

54. Garrett, M. D., Zahner, J. E., Cheney, C. M., and Novick, P. J. GDI1 encodes a GDP dissociation inhibitor that plays an essential role in the yeast secretory pathway. EMBO J. 13(7), 1718-1728. 1-4-1994.

55. Nishimura, N., Nakamura, H., Takai, Y., and Sano, K. Molecular cloning and characterization of two rab GDI species from rat brain: brain-specific and ubiquitous types. J.Biol.Chem. 269(19), 14191-14198. 13-5-1994.

56. Shisheva, A., Buxton, J., and Czech, M. P. Differential intracellular localizations of GDP dissociation inhibitor isoforms. Insulin-dependent redistribution of GDP dissociation inhibitor-2 in 3T3-L1 adipocytes. J.Biol.Chem. 269(39), 23865-23868. 30-9-1994.

57. Erdman, R. A. and Maltese, W. A. Different Rab GTPases associate preferentially with alpha or beta GDP-dissociation inhibitors. Biochem.Biophys.Res.Commun. 282(1), 4-9. 23-3-2001.

58. Shisheva, A., Chinni, S. R., and DeMarco, C. General role of GDP dissociation inhibitor 2 in membrane release of Rab proteins: modulations of its functional interactions by in vitro and in vivo structural modifications. Biochemistry 38(36), 11711-11721. 7-9-1999.

59. Shapiro, A. D. and Pfeffer, S. R. Quantitative analysis of the interactions between prenyl Rab9, GDP dissociation inhibitor-alpha, and guanine nucleotides. J.Biol.Chem. 270(19), 11085-11090. 12-5-1995.

60. Luan, P., Balch, W. E., Emr, S. D., and Burd, C. G. Molecular dissection of guanine nucleotide dissociation inhibitor function in vivo. Rab-independent binding to membranes and role of Rab recycling factors. J.Biol.Chem. 274(21), 14806-14817. 21-5-1999.

61. Goody, R. S., Rak, A., and Alexandrov, K. The structural and mechanistic basis for recycling of Rab proteins between membrane compartments. Cell Mol.Life Sci. 62(15), 1657-1670. 2005.

62. Ullrich, O., Horiuchi, H., Bucci, C., and Zerial, M. Membrane association of Rab5 mediated by GDP-dissociation inhibitor and accompanied by GDP/GTP exchange. Nature 368(6467), 157-160. 10-3-1994.

63. Dirac-Svejstrup, A. B., Sumizawa, T., and Pfeffer, S. R. Identification of a GDI displacement factor that releases endosomal Rab GTPases from Rab-GDI. EMBO J. 16(3), 465-472. 3-2-1997.

64. Sivars, U., Aivazian, D., and Pfeffer, S. R. Yip3 catalyses the dissociation of endosomal Rab-GDI complexes. Nature 425(6960), 856-859. 23-10-2003.

65. Calero, M. and Collins, R. N. Saccharomyces cerevisiae Pra1p/Yip3p interacts with Yip1p and Rab proteins. Biochem.Biophys.Res.Commun. 290(2), 676-681. 18-1-2002.

66. Yang, X., Matern, H. T., and Gallwitz, D. Specific binding to a novel and essential Golgi membrane protein (Yip1p) functionally links the transport GTPases Ypt1p and Ypt31p. EMBO J. 17(17), 4954-4963. 1-9-1998.

67. Barrowman, J., Wang, W., Zhang, Y., and Ferro-Novick, S. The Yip1p.Yif1p complex is required for the fusion competence of endoplasmic reticulum-derived vesicles. J.Biol.Chem. 278(22), 19878-19884. 30-5-2003.

68. Jurnak, F. Structure of the GDP domain of EF-Tu and location of the amino acids homologous to ras oncogene proteins. Science 230(4721), 32-36. 4-10-1985.

69. Pai, E. F., Kabsch, W., Krengel, U., Holmes, K. C., John, J., and Wittinghofer, A. Structure of the guanine-nucleotide-binding domain of the Ha-ras oncogene product p21 in the triphosphate conformation. Nature 341(6239), 209-214. 21-9-1989.

70. Sondek, J., Lambright, D. G., Noel, J. P., Hamm, H. E., and Sigler, P. B. GTPase mechanism of Gproteins from the 1.7-A crystal structure of transducin alpha-GDP-AIF-4. Nature 372(6503), 276-279. 17-11-1994.

71. Kjeldgaard, M., Nyborg, J., and Clark, B. F. C. Protein motifs .10. The GTP binding motif: Variations on a theme. Faseb Journal 10(12), 1347-1368. 1996.

72. Milburn, M. V., Tong, L., Devos, A. M., Brunger, A., Yamaizumi, Z., Nishimura, S., and Kim, S. H. Molecular switch for signal transduction: structural differences between active and inactive forms of protooncogenic ras proteins. Science 247(4945), 939-945. 23-2-1990.

73. Schlichting, I., Almo, S. C., Rapp, G., Wilson, K., Petratos, K., Lentfer, A., Wittinghofer, A., Kabsch, W., Pai, E. F., Petsko, G. A., and . Time-resolved X-ray crystallographic study of the conformational change in Ha-Ras p21 protein on GTP hydrolysis. Nature 345(6273), 309-315. 24-5-1990.

74. Valencia, A., Chardin, P., Wittinghofer, A., and Sander, C. The ras protein family: evolutionary tree and role of conserved amino acids. Biochemistry 30(19), 4637-4648. 14-5-1991.

75. Neal, S. E., Eccleston, J. F., and Webb, M. R. Hydrolysis of GTP by p21NRAS, the NRAS protooncogene product, is accompanied by a conformational change in the wild-type protein: use of a single fluorescent probe at the catalytic site. Proc.Natl.Acad.Sci.U.S.A 87(9), 3562-3565. 1990.

76. Richardson, C. J., Jones, S., Litt, R. J., and Segev, N. GTP hydrolysis is not important for Ypt1 GTPase function in vesicular transport. Mol.Cell Biol. 18(2), 827-838. 1998.

77. Pereira-Leal, J. B. and Seabra, M. C. The mammalian Rab family of small GTPases: definition of family and subfamily sequence motifs suggests a mechanism for functional specificity in the Ras superfamily. J.Mol.Biol. 301(4), 1077-1087. 25-8-2000.

78. Ostermeier, C. and Brunger, A. T. Structural basis of Rab effector specificity: crystal structure of the small G protein Rab3A complexed with the effector domain of rabphilin-3A. Cell 96(3), 363-374. 5-2-1999.

79. Takai, Y., Sasaki, T., and Matozaki, T. Small GTP-binding proteins. Physiol Rev. 81(1), 153-208. 2001.

80. Valencia, A., Chardin, P., Wittinghofer, A., and Sander, C. The ras protein family: evolutionary tree and role of conserved amino acids. Biochemistry 30(19), 4637-4648. 14-5-1991.

81. Merithew, E., Hatherly, S., Dumas, J. J., Lawe, D. C., Heller-Harrison, R., and Lambright, D. G. Structural plasticity of an invariant hydrophobic triad in the switch regions of Rab GTPases is a determinant of effector recognition. J.Biol.Chem. 276(17), 13982-13988. 27-4-2001.

82. McNew, J. A., Weber, T., Parlati, F., Johnston, R. J., Melia, T. J., Sollner, T. H., and Rothman, J. E. Close is not enough: SNARE-dependent membrane fusion requires an active mechanism that transduces force to membrane anchors. J.Cell Biol. 150(1), 105-117. 10-7-2000.

83. Weber, T., Zemelman, B. V., McNew, J. A., Westermann, B., Gmachl, M., Parlati, F., Sollner, T. H., and Rothman, J. E. SNAREpins: minimal machinery for membrane fusion. Cell 92(6), 759-772. 20-3-1998.

84. Pfeffer, S. R. Transport-vesicle targeting: tethers before SNAREs. Nat.Cell Biol. 1(1), E17-E22. 1999.

85. Segev, N. Ypt/rab gtpases: regulators of protein trafficking. Sci.STKE. 2001(100), RE11. 18-9-2001.

86. Fasshauer, D., Antonin, W., Margittai, M., Pabst, S., and Jahn, R. Mixed and non-cognate SNARE complexes. Characterization of assembly and biophysical properties. J.Biol.Chem. 274(22), 15440-15446. 28-5-1999.

87. McLauchlan, H., Newell, J., Morrice, N., Osborne, A., West, M., and Smythe, E. A novel role for Rab5-GDI in ligand sequestration into clathrin-coated pits. Curr.Biol. 8(1), 34-45. 1-1-1998.

88. Carroll, K. S., Hanna, J., Simon, I., Krise, J., Barbero, P., and Pfeffer, S. R. Role of Rab9 GTPase in facilitating receptor recruitment by TIP47. Science 292(5520), 1373-1376. 18-5-2001.

89. Mammoto, A., Sasaki, T., Kim, Y., and Takai, Y. Physical and functional interaction of rabphilin-11 with mammalian Sec13 protein. Implication in vesicle trafficking. J.Biol.Chem. 275(18), 13167-13170. 5-5-2000.

90. Bloom, G. S. and Goldstein, L. S. Cruising along microtubule highways: how membranes move through the secretory pathway. J.Cell Biol. 140(6), 1277-1280. 23-3-1998.

91. Fukuda, M., Kuroda, T. S., and Mikoshiba, K. Slac2-a/melanophilin, the missing link between Rab27 and myosin Va: implications of a tripartite protein complex for melanosome transport. J.Biol.Chem. 277(14), 12432-12436. 5-4-2002.

92. Bahadoran, P., Aberdam, E., Mantoux, F., Busca, R., Bille, K., Yalman, N., Saint-Basile, G., Casaroli-Marano, R., Ortonne, J. P., and Ballotti, R. Rab27a: A key to melanosome transport in human melanocytes. J.Cell Biol. 152(4), 843-850. 19-2-2001.

93. Hume, A. N., Collinson, L. M., Rapak, A., Gomes, A. Q., Hopkins, C. R., and Seabra, M. C. Rab27a regulates the peripheral distribution of melanosomes in melanocytes. J.Cell Biol. 152(4), 795-808. 19-2-2001.

94. Bahadoran, P., Busca, R., Chiaverini, C., Westbroek, W., Lambert, J., Bille, K., Valony, G., Fukuda, M., Naeyaert, J. M., Ortonne, J. P., and Ballotti, R. Characterization of the molecular defects in Rab27a, caused by RAB27A missense mutations found in patients with Griscelli syndrome. J.Biol.Chem. 278(13), 11386-11392. 28-3-2003.

95. Menasche, G., Pastural, E., Feldmann, J., Certain, S., Ersoy, F., Dupuis, S., Wulffraat, N., Bianchi, D., Fischer, A., Le Deist, F., and de Saint, Basile G. Mutations in RAB27A cause Griscelli syndrome associated with haemophagocytic syndrome. Nat.Genet. 25(2), 173-176. 2000.

96. Pastural, E., Barrat, F. J., Dufourcq-Lagelouse, R., Certain, S., Sanal, O., Jabado, N., Seger, R., Griscelli, C., Fischer, A., and de Saint, Basile G. Griscelli disease maps to chromosome 15q21 and is associated

with mutations in the myosin-Va gene. Nat.Genet. 16(3), 289-292. 1997.

97. Griscelli, C., Durandy, A., Guy-Grand, D., Daguillard, F., Herzog, C., and Prunieras, M. A syndrome associating partial albinism and immunodeficiency. Am.J.Med. 65(4), 691-702. 1978.

98. Christoforidis, S., McBride, H. M., Burgoyne, R. D., and Zerial, M. The Rab5 effector EEA1 is a core component of endosome docking. Nature 397(6720), 621-625. 18-2-1999.

99. Christoforidis, S., Miaczynska, M., Ashman, K., Wilm, M., Zhao, L., Yip, S. C., Waterfield, M. D., Backer, J. M., and Zerial, M. Phosphatidylinositol-3-OH kinases are Rab5 effectors. Nat.Cell Biol. 1(4), 249-252. 1999.

100. Gaullier, J. M., Gillooly, D., Simonsen, A., and Stenmark, H. Regulation of endocytic membrane traffic by phosphatidylinositol 3-phosphate. Biochem.Soc.Trans. 27(4), 666-670. 1999.

101. Cao, X., Ballew, N., and Barlowe, C. Initial docking of ER-derived vesicles requires Uso1p and Ypt1p but is independent of SNARE proteins. EMBO J. 17(8), 2156-2165. 15-4-1998.

102. Whyte, J. R. and Munro, S. Vesicle tethering complexes in membrane traffic. J.Cell Sci. 115(Pt 13), 2627-2637. 1-7-2002.

103. Sannerud, R., Saraste, J., and Goud, B. Retrograde traffic in the biosynthetic-secretory route: pathways and machinery. Current Opinion in Cell Biology 15(4), 438-445. 2003.

104. Barbero, P., Bittova, L., and Pfeffer, S. R. Visualization of Rab9-mediated vesicle transport from endosomes to the trans-Golgi in living cells. J.Cell Biol. 156(3), 511-518. 4-2-2002.

105. Wilcke, M., Johannes, L., Galli, T., Mayau, V., Goud, B., and Salamero, J. Rab11 regulates the compartmentalization of early endosomes required for efficient transport from early endosomes to the trans-golgi network. J.Cell Biol. 151(6), 1207-1220. 11-12-2000.

106. Mallard, F., Tang, B. L., Galli, T., Tenza, D., Saint-Pol, A., Yue, X., Antony, C., Hong, W., Goud, B., and Johannes, L. Early/recycling endosomes-to-TGN transport involves two SNARE complexes and a Rab6 isoform. J.Cell Biol. 156(4), 653-664. 18-2-2002.

107. Conibear, E., Cleck, J. N., and Stevens, T. H. Vps51p mediates the association of the GARP (Vps52/53/54) complex with the late Golgi t-SNARE Tlg1p. Mol.Biol.Cell 14(4), 1610-1623. 2003.

108. Siniossoglou, S. and Pelham, H. R. An effector of Ypt6p binds the SNARE Tlg1p and mediates selective fusion of vesicles with late Golgi membranes. EMBO J. 20(21), 5991-5998. 1-11-2001.

109. Hoe, M. H., Slusarewicz, P., Misteli, T., Watson, R., and Warren, G. Evidence for recycling of the resident medial/trans Golgi enzyme, N-acetylglucosaminyltransferase I, in ldlD cells. J.Biol.Chem. 270(42), 25057-25063. 20-10-1995.

110. Suvorova, E. S., Duden, R., and Lupashin, V. V. The Sec34/Sec35p complex, a Ypt1p effector required for retrograde intra-Golgi trafficking, interacts with Golgi SNAREs and COPI vesicle coat proteins. J.Cell Biol. 157(4), 631-643. 13-5-2002.

111. Ungar, D., Oka, T., Brittle, E. E., Vasile, E., Lupashin, V. V., Chatterton, J. E., Heuser, J. E., Krieger, M., and Waters, M. G. Characterization of a mammalian Golgi-localized protein complex, COG, that is required for normal Golgi morphology and function. J.Cell Biol. 157(3), 405-415. 29-4-2002.

112. Nickel, W., Brugger, B., and Wieland, F. T. Vesicular transport: the core machinery of COPI recruitment and budding. J.Cell Sci. 115(Pt 16), 3235-3240. 15-8-2002.

113. Girod, A., Storrie, B., Simpson, J. C., Johannes, L., Goud, B., Roberts, L. M., Lord, J. M., Nilsson, T., and Pepperkok, R. Evidence for a COP-I-independent transport route from the Golgi complex to the endoplasmic reticulum. Nat.Cell Biol. 1(7), 423-430. 1999.

114. White, J., Johannes, L., Mallard, F., Girod, A., Grill, S., Reinsch, S., Keller, P., Tzschaschel, B., Echard, A., Goud, B., and Stelzer, E. H. Rab6 coordinates a novel Golgi to ER retrograde transport pathway in live cells. J.Cell Biol. 147(4), 743-760. 15-11-1999.

115. Martinez, O., Antony, C., Pehau-Arnaudet, G., Berger, E. G., Salamero, J., and Goud, B. GTP-bound forms of rab6 induce the redistribution of Golgi proteins into the endoplasmic reticulum. Proc.Natl.Acad.Sci.U.S.A 94(5), 1828-1833. 4-3-1997.

116. Echard, A., Jollivet, F., Martinez, O., Lacapere, J. J., Rousselet, A., Janoueix-Lerosey, I., and Goud, B. Interaction of a Golgi-associated kinesin-like protein with Rab6. Science 279(5350), 580-585. 23-1-1998.

117. Hill, E., Clarke, M., and Barr, F. A. The Rab6-binding kinesin, Rab6-KIFL, is required for cytokinesis. EMBO J. 19(21), 5711-5719. 1-11-2000.

118. Neef, R., Preisinger, C., Sutcliffe, J., Kopajtich, R., Nigg, E. A., Mayer, T. U., and Barr, F. A. Phosphorylation of mitotic kinesin-like protein 2 by polo-like kinase 1 is required for cytokinesis. J.Cell Biol. 162(5), 863-875. 1-9-2003.

119. Matanis, T., Akhmanova, A., Wulf, P., Del Nery, E., Weide, T., Stepanova, T., Galjart, N., Grosveld, F., Goud, B., De Zeeuw, C. I., Barnekow, A., and Hoogenraad, C. C. Bicaudal-D regulates COPI-independent Golgi-ER transport by recruiting the dynein-dynactin motor complex. Nat.Cell Biol. 4(12), 986-992. 2002.

120. Short, B., Preisinger, C., Schaletzky, J., Kopajtich, R., and Barr, F. A. The Rab6 GTPase regulates recruitment of the dynactin complex to Golgi membranes. Curr.Biol. 12(20), 1792-1795. 15-10-2002.

121. Hoogenraad, C. C., Akhmanova, A., Howell, S. A., Dortland, B. R., De Zeeuw, C. I., Willemsen, R., Visser, P., Grosveld, F., and Galjart, N. Mammalian Golgi-associated Bicaudal-D2 functions in the dynein-dynactin pathway by interacting with these complexes. EMBO J. 20(15), 4041-4054. 1-8-2001.

122. Stenmark, H., Vitale, G., Ullrich, O., and Zerial, M. Rabaptin-5 is a direct effector of the small GTPase Rab5 in endocytic membrane fusion. Cell 83(3), 423-432. 3-11-1995.

123. Miaczynska, M., Christoforidis, S., Giner, A., Shevchenko, A., Uttenweiler-Joseph, S., Habermann, B., Wilm, M., Parton, R. G., and Zerial, M. APPL proteins link Rab5 to nuclear signal transduction via an endosomal compartment. Cell 116(3), 445-456. 6-2-2004.

124. Vitale, G., Rybin, V., Christoforidis, S., Thornqvist, P., McCaffrey, M., Stenmark, H., and Zerial, M. Distinct Rab-binding domains mediate the interaction of Rabaptin-5 with GTP-bound Rab4 and Rab5. EMBO J. 17(7), 1941-1951. 1-4-1998.

125. Mattera, R., Arighi, C. N., Lodge, R., Zerial, M., and Bonifacino, J. S. Divalent interaction of the GGAs with the Rabaptin-5-Rabex-5 complex. EMBO J. 22(1), 78-88. 2-1-2003.

126. Hirokawa, N., Noda, Y., and Okada, Y. Kinesin and dynein superfamily proteins in organelle transport and cell division. Curr.Opin.Cell Biol. 10(1), 60-73. 1998.

127. Schroer, T. A., Bingham, J. B., and Gill, S. R. Actin-related protein 1 and cytoplasmic dynein-based motility - what's the connection? Trends Cell Biol. 6(6), 212-215. 1996.

128. Karcher, R. L., Deacon, S. W., and Gelfand, V. I. Motor-cargo interactions: the key to transport specificity. Trends Cell Biol. 12(1), 21-27. 2002.

129. Zahraoui, A., Touchot, N., Chardin, P., and Tavitian, A. The human Rab genes encode a family of GTP-binding proteins related to yeast YPT1 and SEC4 products involved in secretion. J.Biol.Chem. 264(21), 12394-12401. 25-7-1989.

130. Opdam, F. J., Echard, A., Croes, H. J., van den Hurk, J. A., van de Vorstenbosch, R. A., Ginsel, L. A., Goud, B., and Fransen, J. A. The small GTPase Rab6B, a novel Rab6 subfamily member, is cell-type specifically expressed and localised to the Golgi apparatus. J.Cell Sci. 113 (Pt 15), 2725-2735. 2000.

131. Martinez, O., Antony, C., Pehau-Arnaudet, G., Berger, E. G., Salamero, J., and Goud, B. GTP-bound forms of rab6 induce the redistribution of

Golgi proteins into the endoplasmic reticulum. Proc.Natl.Acad.Sci.U.S.A 94(5), 1828-1833. 4-3-1997.

132. Strom, M., Vollmer, P., Tan, T. J., and Gallwitz, D. A Yeast Gtpase-Activating Protein That Interacts Specifically with A Member of the Ypt/Rab Family. Nature 361(6414), 736-739. 25-2-1993.

133. de Castro, F. A., Ward, G. E., Jambou, R., Attal, G., Mayau, V., Jaureguiberry, G., Braun-Breton, C., Chakrabarti, D., and Langsley, G. Identification of a family of Rab G-proteins in Plasmodium falciparum and a detailed characterisation of pfrab6. Mol.Biochem.Parasitol. 80(1), 77-88. 1996.

134. Chattopadhyay, D., Langsley, G., Carson, M., Recacha, R., DeLucas, L., and Smith, C. Structure of the nucleotide-binding domain of Plasmodium falciparum rab6 in the GDP-bound form. Acta Crystallogr.D.Biol.Crystallogr. 56 (Pt 8), 937-944. 2000.

135. Echard, A., Opdam, F. J., de Leeuw, H. J., Jollivet, F., Savelkoul, P., Hendriks, W., Voorberg, J., Goud, B., and Fransen, J. A. Alternative splicing of the human Rab6A gene generates two close but functionally different isoforms. Mol.Biol.Cell 11(11), 3819-3833. 2000.

136. Goud, B., Zahraoui, A., Tavitian, A., and Saraste, J. Small GTP-binding protein associated with Golgi cisternae. Nature 345(6275), 553-556. 7-6-1990.

137. Garcia-Saez, I., Tcherniuk, S., and Kozielski, F. The structure of human neuronal Rab6B in the active and inactive form. Acta Crystallogr.D Biol.Crystallogr. 62(Pt 7), 725-733. 2006.

138. Young, J., Stauber, T., del Nery, E., Vernos, I., Pepperkok, R., and Nilsson, T. Regulation of microtubule-dependent recycling at the trans-Golgi network by Rab6A and Rab6A'. Mol.Biol.Cell 16(1), 162-177. 2005.

139. Valsdottir, R., Hashimoto, H., Ashman, K., Koda, T., Storrie, B., and Nilsson, T. Identification of rabaptin-5, rabex-5, and GM130 as putative effectors of rab33b, a regulator of retrograde traffic between the Golgi apparatus and ER. FEBS Lett. 508(2), 201-209. 16-11-2001.

140. Del Nery, E., Miserey-Lenkei, S., Falguieres, T., Nizak, C., Johannes, L., Perez, F., and Goud, B. Rab6A and Rab6A' GTPases play non-overlapping roles in membrane trafficking. Traffic 7(4), 394-407. 2006.

141. Franke, W. W., Kartenbeck, J., Krien, S., VanderWoude, W. J., Scheer, U., and Morre, D. J. Inter- and intracisternal elements of the Golgi apparatus. A system of membrane-to-membrane cross-links. Z.Zellforsch.Mikrosk.Anat. 132(3), 365-380. 1972.

142. Cluett, E. B. and Brown, W. J. Adhesion of Golgi cisternae by proteinaceous interactions: intercisternal bridges as putative adhesive structures. J.Cell Sci. 103 (Pt 3), 773-784. 1992.

143. Slusarewicz, P., Nilsson, T., Hui, N., Watson, R., and Warren, G. Isolation of a matrix that binds medial Golgi enzymes. J.Cell Biol. 124(4), 405-413. 1994.

144. Short, B., Haas, A., and Barr, F. A. Golgins and GTPases, giving identity and structure to the Golgi apparatus. Biochim.Biophys.Acta 1744(3), 383-395. 10-7-2005.

145. Nakamura, N., Rabouille, C., Watson, R., Nilsson, T., Hui, N., Slusarewicz, P., Kreis, T. E., and Warren, G. Characterization of a cis-Golgi matrix protein, GM130. J.Cell Biol. 131(6 Pt 2), 1715-1726. 1995.

146. Suter, B., Romberg, L. M., and Steward, R. Bicaudal-D, a Drosophila gene involved in developmental asymmetry: localized transcript accumulation in ovaries and sequence similarity to myosin heavy chain tail domains. Genes Dev. 3(12A), 1957-1968. 1989.

147. Matanis, T., Akhmanova, A., Wulf, P., Del Nery, E., Weide, T., Stepanova, T., Galjart, N., Grosveld, F., Goud, B., De Zeeuw, C. I., Barnekow, A., and Hoogenraad, C. C. Bicaudal-D regulates COPI-independent Golgi-ER transport by recruiting the dynein-dynactin motor complex. Nat.Cell Biol. 4(12), 986-992. 2002.

148. Fuchs, E., Short, B., and Barr, F. A. Assay and properties of rab6 interaction with dynein-dynactin complexes. Methods Enzymol. 403, 607-618. 2005.

149. Deacon, S. W., Serpinskaya, A. S., Vaughan, P. S., Lopez, Fanarraga M., Vernos, I., Vaughan, K. T., and Gelfand, V. I. Dynactin is required for bidirectional organelle transport. J.Cell Biol. 160(3), 297-301. 3-2-2003.

150. Neudauer, C. L., Joberty, G., and Macara, I. G. PIST: a novel PDZ/coiled-coil domain binding partner for the rho-family GTPase TC10. Biochem.Biophys.Res.Commun. 280(2), 541-547. 19-1-2001.

151. Charest, A., Lane, K., McMahon, K., and Housman, D. E. Association of a novel PDZ domain-containing peripheral Golgi protein with the Q-SNARE (Q-soluble N-ethylmaleimide-sensitive fusion protein (NSF) attachment protein receptor) protein syntaxin 6. J.Biol.Chem. 276(31), 29456-29465. 3-8-2001.

152. Hassel, B., Schreff, M., Stube, E. M., Blaich, U., and Schumacher, S. CALEB/NGC interacts with the Golgi-associated protein PIST. J.Biol.Chem. 278(41), 40136-40143. 10-10-2003.

153. Yao, R., Maeda, T., Takada, S., and Noda, T. Identification of a PDZ domain containing Golgi protein, GOPC, as an interaction partner of frizzled. Biochem.Biophys.Res.Commun. 286(4), 771-778. 31-8-2001.

154. Gentzsch, M., Cui, L., Mengos, A., Chang, X. B., Chen, J. H., and Riordan, J. R. The PDZ-binding chloride channel ClC-3B localizes to the Golgi and associates with cystic fibrosis transmembrane conductance

regulator-interacting PDZ proteins. J.Biol.Chem. 278(8), 6440-6449. 21-2-2003.

155. Wente, W., Stroh, T., Beaudet, A., Richter, D., and Kreienkamp, H. J. Interactions with PDZ domain proteins PIST/GOPC and PDZK1 regulate intracellular sorting of the somatostatin receptor subtype 5. J.Biol.Chem. 280(37), 32419-32425. 16-9-2005.

156. Ito, H., Iwamoto, I., Morishita, R., Nozawa, Y., Asano, T., and Nagata, K. Identification of a PDZ protein, PIST, as a binding partner for Rho effector Rhotekin: biochemical and cell-biological characterization of Rhotekin-PIST interaction. Biochem.J. 397(3), 389-398. 1-8-2006.

157. Pauling, L. and Corey, R. B. Compound helical configurations of polypeptide chains: structure of proteins of the alpha-keratin type. Nature 171(4341), 59-61. 10-1-1953.

158. Landschulz, W. H., Johnson, P. F., and McKnight, S. L. The leucine zipper: a hypothetical structure common to a new class of DNA binding proteins. Science 240(4860), 1759-1764. 24-6-1988.

159. Lupas, A. Coiled coils: new structures and new functions. Trends Biochem.Sci. 21(10), 375-382. 1996.

160. Stetefeld, J., Jenny, M., Schulthess, T., Landwehr, R., Engel, J., and Kammerer, R. A. Crystal structure of a naturally occurring parallel right-handed coiled coil tetramer. Nat.Struct.Biol. 7(9), 772-776. 2000.

161. Arndt, K. M., Pelletier, J. N., Muller, K. M., Pluckthun, A., and Alber, T. Comparison of in vivo selection and rational design of heterodimeric coiled coils. Structure 10(9), 1235-1248. 2002.

162. Akey, D. L., Malashkevich, V. N., and Kim, P. S. Buried polar residues in coiled-coil interfaces. Biochemistry 40(21), 6352-6360. 29-5-2001.

163. O'Shea, E. K., Lumb, K. J., and Kim, P. S. Peptide 'Velcro': design of a heterodimeric coiled coil. Curr.Biol. 3(10), 658-667. 1-10-1993.

164. Crick, F. C. H. The packing of á-helices: simple coiled coils. Acta Crystallographica 6, 689-697. 1-1-1953.

165. Cohen, C. and Parry, D. A. Alpha-helical coiled coils: more facts and better predictions. Science 263(5146), 488-489. 28-1-1994.

166. Mason, J. M. and Arndt, K. M. Coiled coil domains: stability, specificity, and biological implications. Chembiochem. 5(2), 170-176. 6-2-2004.

167. Steinmetz, M. O., Stock, A., Schulthess, T., Landwehr, R., Lustig, A., Faix, J., Gerisch, G., Aebi, U., and Kammerer, R. A. A distinct 14 residue site triggers coiled-coil formation in cortexillin I. EMBO J. 17(7), 1883-1891. 1-4-1998.

168. Zhu, G., Zhai, P., Liu, J., Terzyan, S., Li, G., and Zhang, X. C. Structural basis of Rab5-Rabaptin5 interaction in endocytosis. Nat.Struct.Mol.Biol. 11(10), 975-983. 2004.

169. Eathiraj, S., Mishra, A., Prekeris, R., and Lambright, D. G. Structural Basis for Rab11-mediated Recruitment of FIP3 to Recycling Endosomes. J.Mol.Biol. 26-8-2006.

170. Matanis, T., Akhmanova, A., Wulf, P., Del Nery, E., Weide, T., Stepanova, T., Galjart, N., Grosveld, F., Goud, B., De Zeeuw, C. I., Barnekow, A., and Hoogenraad, C. C. Bicaudal-D regulates COPI-independent Golgi-ER transport by recruiting the dynein-dynactin motor complex. Nat.Cell Biol. 4(12), 986-992. 2002.

171. Kumar, S., Zhou, Y., and Plamann, M. Dynactin-membrane interaction is regulated by the C-terminal domains of p150(Glued). EMBO Rep. 2(10), 939-944. 2001.

172. Altschul, S. F., Madden, T. L., Schaffer, A. A., Zhang, J., Zhang, Z., Miller, W., and Lipman, D. J. Gapped BLAST and PSI-BLAST: a new generation of protein database search programs. Nucleic Acids Res. 25(17), 3389-3402. 1-9-1997.

173. Higgins, D. G. and Sharp, P. M. CLUSTAL: a package for performing multiple sequence alignment on a microcomputer. Gene 73(1), 237-244. 15-12-1988.

174. Gasteiger, E., Gattiker, A., Hoogland, C., Ivanyi, I., Appel, R. D., and Bairoch, A. ExPASy: The proteomics server for in-depth protein knowledge and analysis. Nucleic Acids Res. 31(13), 3784-3788. 1-7-2003.

175. Corpet, F. Multiple sequence alignment with hierarchical clustering. Nucleic Acids Res. 16(22), 10881-10890. 25-11-1988.

176. Wolf, E., Kim, P. S., and Berger, B. MultiCoil: a program for predicting two- and three-stranded coiled coils. Protein Sci. 6(6), 1179-1189. 1997.

177. Berger, B., Wilson, D. B., Wolf, E., Tonchev, T., Milla, M., and Kim, P. S. Predicting coiled coils by use of pairwise residue correlations. Proc.Natl.Acad.Sci.U.S.A 92(18), 8259-8263. 29-8-1995.

178. Berman, H. M., Westbrook, J., Feng, Z., Gilliland, G., Bhat, T. N., Weissig, H., Shindyalov, I. N., and Bourne, P. E. The Protein Data Bank. Nucleic Acids Res. 28(1), 235-242. 1-1-2000.

179. Studier, F. W., Rosenberg, A. H., Dunn, J. J., and Dubendorff, J. W. Use of T7 RNA polymerase to direct expression of cloned genes. Methods Enzymol. 185, 60-89. 1990.

180. Kalinin, A., Thoma, N. H., Iakovenko, A., Heinemann, I., Rostkova, E., Constantinescu, A. T., and Alexandrov, K. Expression of mammalian geranylgeranyltransferase type-II in Escherichia coli and its

application for in vitro prenylation of Rab proteins. Protein Expr.Purif. 22(1), 84-91. 2001.

181. Sorensen, H. P., Sperling-Petersen, H. U., and Mortensen, K. K. A favorable solubility partner for the recombinant expression of streptavidin. Protein Expr.Purif. 32(2), 252-259. 2003.

182. Mullis, K., Faloona, F., Scharf, S., Saiki, R., Horn, G., and Erlich, H. Specific enzymatic amplification of DNA in vitro: the polymerase chain reaction. 1986. Biotechnology 24, 17-27. 1992.

183. Tung, W. L. and Chow, K. C. A modified medium for efficient electrotransformation of E. coli. Trends Genet. 11(4), 128-129. 1995.

184. Laemmli, U. K. Cleavage of structural proteins during the assembly of the head of bacteriophage T4. Nature 227(5259), 680-685. 15-8-1970.

185. Bradford, M. M. A rapid and sensitive method for the quantitation of microgram quantities of protein utilizing the principle of protein-dye binding. Anal.Biochem. 72, 248-254. 7-5-1976.

186. Gasteiger, E., Gattiker, A., Hoogland, C., Ivanyi, I., Appel, R. D., and Bairoch, A. ExPASy: The proteomics server for in-depth protein knowledge and analysis. Nucleic Acids Res. 31(13), 3784-3788. 1-7-2003.

187. Cohen, S. L. and Chait, B. T. Mass spectrometry of whole proteins eluted from sodium dodecyl sulfate-polyacrylamide gel electrophoresis gels. Anal.Biochem. 247(2), 257-267. 1-5-1997.

188. Smith, D. B. and Johnson, K. S. Single-step purification of polypeptides expressed in Escherichia coli as fusions with glutathione S-transferase. Gene 67(1), 31-40. 15-7-1988.

189. Tucker, J., Sczakiel, G., Feuerstein, J., John, J., Goody, R. S., and Wittinghofer, A. Expression of p21 proteins in Escherichia coli and stereochemistry of the nucleotide-binding site. EMBO J. 5(6), 1351-1358. 1986.

190. Fatania, H. R., Matthews, B., and Dalziel, K. On the mechanism of NADP+-linked isocitrate dehydrogenase from heart mitochondria. I. The kinetics of dissociation of NADPH from its enzyme complex. Proc.R.Soc.Lond B Biol.Sci. 214(1196), 369-387. 22-2-1982.

191. Wiseman, T., Williston, S., Brandts, J. F., and Lin, L. N. Rapid measurement of binding constants and heats of binding using a new titration calorimeter. Anal.Biochem. 179(1), 131-137. 15-5-1989.

192. Rossmann, M. G. The molecular replacement method. Acta Crystallogr.A 46 (Pt 2), 73-82. 1-2-1990.

193. Navaza, J. Implementation of molecular replacement in AMoRe. Acta Crystallogr.D.Biol.Crystallogr.2001.Oct.;57.(Pt.10):1367.-72.Epub.2001.Sep.21. 57, 1367-1372. 2001.

194. Sali, A. and Blundell, T. L. Comparative protein modelling by satisfaction of spatial restraints. J.Mol.Biol. 234, 779-815. 5-12-1993.

195. Brunger, A. T., Adams, P. D., Clore, G. M., DeLano, W. L., Gros, P., Grosse-Kunstleve, R. W., Jiang, J. S., Kuszewski, J., Nilges, M., Pannu, N. S., Read, R. J., Rice, L. M., Simonson, T., and Warren, G. L. Crystallography & NMR system: A new software suite for macromolecular structure determination. Acta Crystallogr.D.Biol.Crystallogr. 54 (Pt 5), 905-921. 1-9-1998.

196. Murshudov, G. N., Vagin, A. A., and Dodson, E. J. Refinement of macromolecular structures by the maximum-likelihood method. Acta Crystallogr.D.Biol.Crystallogr. 53, 240-255. 1-5-1997.

197. Bloch, F. Nuclear induction. Physical Review (70), 460-474. 1946.

198. Purcell, E. M. and Torrey, E. C. Resonance absorption by nuclear magnetic moments in a solid. Physical Review (69), 37-38. 1946.

199. Breeze, A. L. Isotope-filtered NMR methods for the study of bimolecular structure and interactions. Progress in Nuclear Magnetic Resonance Spectroscopy (36), 323-372. 17-12-1999.

200. Paduch, M., Jelen, F., and Otlewski, J. Structure of small G proteins and their regulators. Acta Biochim.Pol. 48(4), 829-850. 2001.

201. Brachvogel, V., Neu, M., and Metcalf, P. Rab7: crystallization of intact and C-terminal truncated constructs complexed with GDP and GppNHp. Proteins 27(2), 210-212. 1997.

202. John, J., Schlichting, I., Schiltz, E., Rosch, P., and Wittinghofer, A. C-terminal truncation of p21H preserves crucial kinetic and structural properties. J.Biol.Chem. 264(22), 13086-13092. 5-8-1989.

203. Chattopadhyay, D., Smith, C. D., Barchue, J., and Langsley, G. Plasmodium falciparum rab6 GTPase: expression, purification, crystallization and preliminary crystallographic studies. Acta Crystallogr.D.Biol.Crystallogr. 56 (Pt 8), 1017-1019. 2000.

204. Neal, S. E., Eccleston, J. F., and Webb, M. R. Hydrolysis of GTP by p21NRAS, the NRAS protooncogene product, is accompanied by a conformational change in the wild-type protein: use of a single fluorescent probe at the catalytic site. Proc.Natl.Acad.Sci.U.S.A 87(9), 3562-3565. 1990.

205. Der, C. J., Finkel, T., and Cooper, G. M. Biological and biochemical properties of human rasH genes mutated at codon 61. Cell 44(1), 167-176. 17-1-1986.

206. Christoforidis, S. and Zerial, M. Purification and identification of novel Rab effectors using affinity chromatography. Methods 20(4), 403-410. 2000.

207. Esters, H., Alexandrov, K., Iakovenko, A., Ivanova, T., Thoma, N., Rybin, V., Zerial, M., Scheidig, A. J., and Goody, R. S. Vps9, Rabex-5 and DSS4: proteins with weak but distinct nucleotide-exchange activities for Rab proteins. J.Mol.Biol. 310(1), 141-156. 29-6-2001.

208. Itzen, A., Pylypenko, O., Goody, R. S., Alexandrov, K., and Rak, A. Nucleotide exchange via local protein unfolding--structure of Rab8 in complex with MSS4. EMBO J. 25(7), 1445-1455. 5-4-2006.

209. Huber, S. K. and Scheidig, A. J. High resolution crystal structures of human Rab4a in its active and inactive conformations. FEBS Lett. 579(13), 2821-2829. 23-5-2005.

210. Kikuchi, A., Yamashita, T., Kawata, M., Yamamoto, K., Ikeda, K., Tanimoto, T., and Takai, Y. Purification and characterization of a novel GTP-binding protein with a molecular weight of 24,000 from bovine brain membranes. J.Biol.Chem. 263(6), 2897-2904. 25-2-1988.

211. Kikuchi, A., Yamashita, T., Kawata, M., Yamamoto, K., Ikeda, K., Tanimoto, T., and Takai, Y. Purification and characterization of a novel GTP-binding protein with a molecular weight of 24,000 from bovine brain membranes. J.Biol.Chem. 263(6), 2897-2904. 25-2-1988.

212. Esters, H., Alexandrov, K., Constantinescu, A. T., Goody, R. S., and Scheidig, A. J. High-resolution crystal structure of S. cerevisiae Ypt51(DeltaC15)-GppNHp, a small GTP-binding protein involved in regulation of endocytosis. J.Mol.Biol. 298(1), 111-121. 21-4-2000.

213. Will, E. and Gallwitz, D. Biochemical characterization of Gyp6p, a Ypt/Rab-specific GTPase-activating protein from yeast. J.Biol.Chem. 276(15), 12135-12139. 13-4-2001.

214. Kabsch, W. AUTOMATIC PROCESSING OF ROTATION DIFFRACTION DATA FROM CRYSTALS OF INITIALLY UNKNOWN SYMMETRY AND CELL CONSTANTS. Journal of Applied Crystallography 26, 795-800. 1993.

215. Dumas, J. J., Zhu, Z., Connolly, J. L., and Lambright, D. G. Structural basis of activation and GTP hydrolysis in Rab proteins. Structure.Fold.Des 7(4), 413-423. 15-4-1999.

216. Scheffzek, K., Klebe, C., Fritz-Wolf, K., Kabsch, W., and Wittinghofer, A. Crystal structure of the nuclear Ras-related protein Ran in its GDP-bound form. Nature 374(6520), 378-381. 23-3-1995.

217. Zhu, G. Y., Liu, J., Terzyan, S., Zhai, P., Li, G. P., and Zhang, X. C. High resolution crystal structures of human Rab5a and five mutants with substitutions in the catalytically important phosphate-binding loop. Journal of Biological Chemistry 278(4), 2452-2460. 24-1-2003.

218. Rak, A., Pylypenko, O., Niculae, A., Pyatkov, K., Goody, R. S., and Alexandrov, K. Structure of the Rab7:REP-1 complex: insights into the mechanism of Rab prenylation and choroideremia disease. Cell 117(6), 749-760. 11-6-2004.

219. Brunger, A. T., Adams, P. D., Clore, G. M., DeLano, W. L., Gros, P., Grosse-Kunstleve, R. W., Jiang, J. S., Kuszewski, J., Nilges, M., Pannu, N. S., Read, R. J., Rice, L. M., Simonson, T., and Warren, G. L. Crystallography & NMR system: A new software suite for macromolecular structure determination. Acta Crystallogr.D.Biol.Crystallogr. 54 (Pt 5), 905-921. 1-9-1998.

220. Murshudov, G. N., Vagin, A. A., and Dodson, E. J. Refinement of macromolecular structures by the maximum-likelihood method. Acta Crystallogr.D.Biol.Crystallogr. 53, 240-255. 1-5-1997.

221. Pai, E. F., Kabsch, W., Krengel, U., Holmes, K. C., John, J., and Wittinghofer, A. Structure of the guanine-nucleotide-binding domain of the Ha-ras oncogene product p21 in the triphosphate conformation. Nature 341(6239), 209-214. 21-9-1989.

222. Zhong, J. M., Chen-Hwang, M. C., and Hwang, Y. W. Switching nucleotide specificity of Ha-Ras p21 by a single amino acid substitution at aspartate 119. J.Biol.Chem. 270(17), 10002-10007. 28-4-1995.

223. Saraste, M., Sibbald, P. R., and Wittinghofer, A. The P-loop--a common motif in ATP- and GTP-binding proteins. Trends Biochem.Sci. 15(11), 430-434. 1990.

224. Prive, G. G., Milburn, M. V., Tong, L., de Vos, A. M., Yamaizumi, Z., Nishimura, S., and Kim, S. H. X-ray crystal structures of transforming p21 ras mutants suggest a transition-state stabilization mechanism for GTP hydrolysis. Proc.Natl.Acad.Sci.U.S.A 89(8), 3649-3653. 15-4-1992.

225. Gideon, P., John, J., Frech, M., Lautwein, A., Clark, R., Scheffler, J. E., and Wittinghofer, A. Mutational and kinetic analyses of the GTPase-activating protein (GAP)-p21 interaction: the C-terminal domain of GAP is not sufficient for full activity. Mol.Cell Biol. 12(5), 2050-2056. 1992.

226. Erdman, R. A., Shellenberger, K. E., Overmeyer, J. H., and Maltese, W. A. Rab24 is an atypical member of the Rab GTPase family. Deficient GTPase activity, GDP dissociation inhibitor interaction, and prenylation of Rab24 expressed in cultured cells. J.Biol.Chem. 275(6), 3848-3856. 11-2-2000.

227. Colicelli, J. Human RAS superfamily proteins and related GTPases. Sci.STKE.2004.Sep.14;2004.(250.):RE13. 2004, RE13. 14-9-2004.

228. Yu, Y. D., Li, S., Xu, X., Li, Y., Guan, K. L., Arnold, E., and Ding, J. P. Structural basis for the unique biological function of small GTPase

RHEB. Journal of Biological Chemistry 280(17), 17093-17100. 29-4-2005.

229. Albert, S. and Gallwitz, D. Two new members of a family of Ypt/Rab GTPase activating proteins - Promiscuity of substrate recognition. Journal of Biological Chemistry 274(47), 33186-33189. 19-11-1999.

230. Terzyan, S., Zhu, G., Li, G., and Zhang, X. C. Refinement of the structure of human Rab5a GTPase domain at 1.05 A resolution. Acta Crystallogr.D Biol.Crystallogr. 60(Pt 1), 54-60. 2004.

231. Eathiraj, S., Pan, X., Ritacco, C., and Lambright, D. G. Structural basis of family-wide Rab GTPase recognition by rabenosyn-5. Nature 436(7049), 415-419. 21-7-2005.

232. Merithew, E., Hatherly, S., Dumas, J. J., Lawe, D. C., Heller-Harrison, R., and Lambright, D. G. Structural plasticity of an invariant hydrophobic triad in the switch regions of Rab GTPases is a determinant of effector recognition. J.Biol.Chem. 276(17), 13982-13988. 27-4-2001.

233. Gruenberg, J. and Maxfield, F. R. Membrane-Transport in the Endocytic Pathway. Current Opinion in Cell Biology 7(4), 552-563. 1995.

234. Feng, Y., Press, B., and Wandingerness, A. Rab-7 - An Important Regulator of Late Endocytic Membrane Traffic. Journal of Cell Biology 131(6), 1435-1452. 1995.

235. Saneto, R. P., Awasthi, Y. C., and Srivastava, S. K. Interrelationship between cationic and anionic forms of glutathione S-transferases of bovine ocular lens. Biochem.J. 191(1), 11-20. 1-10-1980.

236. Stein, M. P., Dong, J., and Wandinger-Ness, A. Rab proteins and endocytic trafficking: potential targets for therapeutic intervention. Adv.Drug Deliv.Rev. 55(11), 1421-1437. 14-11-2003.

237. Short, B., Haas, A., and Barr, F. A. Golgins and GTPases, giving identity and structure to the Golgi apparatus. Biochim.Biophys.Acta 1744(3), 383-395. 10-7-2005.

238. Guo, Y., Kammerer, R. A., and Engel, J. The unusually stable coiled-coil domain of COMP exhibits cold and heat denaturation in 4-6 M guanidinium chloride. Biophys.Chem. 85(2-3), 179-186. 15-7-2000.

239. Cohen, S. L. and Chait, B. T. Mass spectrometry of whole proteins eluted from sodium dodecyl sulfate-polyacrylamide gel electrophoresis gels. Anal.Biochem. 247(2), 257-267. 1-5-1997.

240. Stura, E. A., Nemerow, G. R., and Wilson, I. A. Strategies in the Crystallization of Glycoproteins and Protein Complexes. Journal of Crystal Growth 122(1-4), 273-285. 1992.

241. Lupas, A. Prediction and analysis of coiled-coil structures. Methods Enzymol. 266, 513-525. 1996.

242. Akey, D. L., Malashkevich, V. N., and Kim, P. S. Buried polar residues in coiled-coil interfaces. Biochemistry 40(21), 6352-6360. 29-5-2001.

243. Arndt, K. M., Pelletier, J. N., Muller, K. M., Pluckthun, A., and Alber, T. Comparison of in vivo selection and rational design of heterodimeric coiled coils. Structure 10(9), 1235-1248. 2002.

244. Huber, S. K. Kristallographische und biophysikalische Untersuchung der kleinen GTPase Rab4a und ihres Effectors Rabaptin-5. 1-158. 2003. Max-Planck-Institute of Molecular Physiology.

245. Wiseman, T., Williston, S., Brandts, J. F., and Lin, L. N. Rapid measurement of binding constants and heats of binding using a new titration calorimeter. Anal.Biochem. 179(1), 131-137. 15-5-1989.

246. Indyk, L. and Fisher, H. F. Theoretical aspects of isothermal titration calorimetry. Methods Enzymol. 295, 350-364. 1998.

247. Eathiraj, S., Mishra, A., Prekeris, R., and Lambright, D. G. Structural Basis for Rab11-mediated Recruitment of FIP3 to Recycling Endosomes. J.Mol.Biol. 26-8-2006.

248. Kishida, S., Shirataki, H., Sasaki, T., Kato, M., Kaibuchi, K., and Takai, Y. Rab3A GTPase-activating protein-inhibiting activity of Rabphilin-3A, a putative Rab3A target protein. J.Biol.Chem. 268(30), 22259-22261. 25-10-1993.

249. Rybin, V., Ullrich, O., Rubino, M., Alexandrov, K., Simon, I., Seabra, M. C., Goody, R., and Zerial, M. GTPase activity of Rab5 acts as a timer for endocytic membrane fusion. Nature 383(6597), 266-269. 19-9-1996.

250. Nagelkerken, B., Van Anken, E., van Raak, M., Gerez, L., Mohrmann, K., Van Uden, N., Holthuizen, J., Pelkmans, L., and van der, Sluijs P. Rabaptin4, a novel effector of the small GTPase rab4a, is recruited to perinuclear recycling vesicles. Biochem.J. 346 Pt 3, 593-601. 15-3-2000.

7 ACKNOWLEDGEMENTS

Mein Dank gilt:

Prof. Dr. Roger S. Goody (Max-Planck-Institut für molekulare Physiologie, Abteilung Physikalische Biochemie) für die freundliche Aufnahme in seine Abteilung, die gute Unterstützung und das fortlaufende Interesse an meiner Arbeit.

Prof. Dr. Roland Winter (Universität Dortmund, Institut für Physikalische Chemie I) für die Übernahme des Zweitgutachtens.

Dr. Kirill Alexandrov für die Überlassung eines sehr interessanten und anspruchsvollen Projekts. Seine uneingeschränkte Unterstützung, sowie die gewährten großen wissenschaftlichen Freiräume waren stets das Fundament zum Gelingen dieser Arbeit.

Dr. Olena Pylypenko und Dr. Alexey Rak für die Einführung in die Methoden der Kristallisation und Strukturanalyse, sowie die erfolgreiche Zusammenarbeit.

Dr. Francis Barr (Max-Planck-Institut für Biochemie, Martinsried) für die Kooperation und die zur Verfügung gestellten DNA Template der Effektor Proteine.

Natalie Bleimling und Petra Herde für zahlreichen Ratschläge, Tipps und Tricks bei der täglichen Laborarbeit und den umfangreichen apparativen Methoden.

Dr. Christine Delon für die konstruktive Diskussion und Vorschläge zum Manuskript dieser Arbeit.

Dr. Mathias Geyer für die zur Verfügung gestellte Messzeit und die Diskussion der Ergebnisse der NMR-Spektroskopischen Untersuchungen.

Meinen ehemaligen und aktuellen Kollegen und Freunden verschiedener Arbeitsgruppen der Abteilung (Aymelt, André, Ion, Susanna, Natasha, Natalia) für die stets anregende und unterstützende Arbeitatmosphäre.

Nicht zuletzt und in besonderer Weise gilt mein Dank meiner Familie und meinen Freunden ohne deren vorbehaltlosen Rückhalt die Verwirklichung dieser Arbeit nicht möglich gewesen wäre.

8 EIDESSTATTLICHE ERKLÄRUNG

Hiermit versichere ich an Eides statt, dass ich die vorliegende Arbeit selbständig und nur mit den angegebenen Hilfsmitteln angefertigt habe.

Dortmund, den

_____

Tim Bergbrede